

PHOTOCOPY

①

AD-A227 931

ATMOSPHERIC BOUNDARY LAYER GROUP  
TECHNICAL REPORT

OFFICE OF NAVAL RESEARCH CONTRACT N00014-89-J-1660

THE VERTICAL STRUCTURE OF  
THE MARINE ATMOSPHERIC BOUNDARY LAYER  
ACROSS A SEA SURFACE TEMPERATURE FRONT.

By  
Christopher G. Herbst

Department of Meteorology  
Florida State University  
Tallahassee, Florida 32306-3034

DTIC  
SELECTED  
OCT 24 1990  
S D

DISTRIBUTION STATEMENT A  
Approved for public release  
Distribution Unlimited



July, 1990

## Foreword

This report is the M. S. thesis of Christopher G. Herbster. It is one of several investigations which we have made into the structure of the marine atmospheric boundary layer (MABL) in the vicinity of an oceanic sea surface temperature (SST) front. This thesis uses data obtained by the NCAR Electra and the NRL-P3 aircraft on February 14 and 16, 1986 during the Frontal Air-Sea Interaction Experiment (FASINEX). These days had northerly winds in the region which gave an unstable transition at the front (flow from over cold water to over warm water). Flight patterns used on these days had several levels, thus enabling examination of the vertical structure of the MABL.

A boxcar technique was previously developed by Crescenti (1988) and used by him to examine horizontal changes in near-surface turbulent variances, fluxes and other covariances in the region of the FASINEX SST front. In this work the boxcar technique is applied here for the first time to show vertical structure of turbulent statistics. A Hilbert transform is also used to extend Crescenti's boxcar technique to enable computation of boxcar coherence and phase angle.

This study shows that turbulent statistics at all levels within the MABL are very rapidly modified as the air flows across the SST front. The location of the changes in statistics shifts slightly downwind as one goes to higher levels in the MABL and the zone in which the changes take place become slightly wider. One striking feature of the results is that regions of enhanced or suppressed vertical turbulent transport often extend vertically through the MABL. We believe that these are convective elements. These elements have lifetimes at least as long as the 2 plus hours required to complete the flight patterns.

Together with Crescenti's work, this thesis, shows that the MABL is strongly affected by the SST front. Several features of the MABL boxcar statistics agree with expectations based on previous studies using traditional techniques. Other features are seen that are only possible to examine using this technique. These have therefore not been previously noticed. Because the boxcar technique is new, we expect that our ability to interpret the results in terms of the structure of turbulence within the layer will improve as more experience is obtained by applying the technique to other data sets. Analysis is further restricted by limitations in the vertical resolution of the FASINEX flight patterns and by shortcomings of the NRL-P3 instrument performance.

Steven A. Stage  
Associate Professor  
Department of Meteorology  
Florida State University

ATMOSPHERIC BOUNDARY LAYER GROUP  
TECHNICAL REPORT

OFFICE OF NAVAL RESEARCH CONTRACT N00014-89-J-1660

THE VERTICAL STRUCTURE OF  
THE MARINE ATMOSPHERIC BOUNDARY LAYER  
ACROSS A SEA SURFACE TEMPERATURE FRONT.<sup>1</sup>

By  
Christopher G. Herbster

Department of Meteorology  
Florida State University  
Tallahassee, Florida 32306-3034



Accession No.	
NTIS GRA&I	J
DTIC TAB	U
Unannounced	U
Justification	
By <i>per call</i>	
Distribution	
Availability Codes	
Dist	Avail and/or Statement
<i>A-1</i>	

July, 1990

STATEMENT "A" per Dr. Robert Abbey  
ONR/Code 1122MM  
TELECON 10/19/90

VG

-----  
1. This is FASINEX contribution number 99.

THE VERTICAL STRUCTURE OF  
THE MARINE ATMOSPHERIC BOUNDARY LAYER  
ACROSS A SEA SURFACE TEMPERATURE FRONT.

Christopher G. Herbster, M.S.  
The Florida State University, 1990

Major Professor: Steven A. Stage, Ph.D.

The response of the lower marine atmospheric boundary layer to a sharp change in sea-surface temperature was studied in the Frontal Air-Sea Interaction Experiment (FASINEX) with ships and aircraft instrumented for turbulence measurements. The synoptic conditions on the 14th and 16th of February, 1986 presented the opportunity to study the vertical structure of the turbulence for the case of a North wind, blowing from the cold to warm side of the front. A moving boxcar averaging technique (after Crescenti, 1988) was used to determine the turbulent statistics and fluxes for the meteorological variables, and their associated changes, as the air made the transition from the cold to warm side of the front.

The data for this study were obtained from two aircraft, the NCAR Electra and NRL-P3, equipped for turbulence measurements in the atmosphere. The flight tracks for the two days were designed to investigate somewhat different aspects of the marine atmospheric boundary layer, concentrating on either the vertical structure

alone (14 February) or on both the vertical and horizontal structure (16 February) in the vicinity of an oceanic temperature front.

The depth of the atmospheric boundary layer was found to be approximately 200 m deeper over the warm water than was found over the cold water. The potential temperature was found to respond very rapidly to the underlying warm water throughout the entire depth of the boundary layer. The increase in temperature was found to occur over a slightly broader region as the altitude was increased.

The vertical heat flux for each of the two days showed a pronounced increase over the warm water. While each day showed this general trend, there were distinct differences for the two days. The heat flux for the 14th showed two organized convective cells in the immediate vicinity of the front; one of which showed evidence of penetration into the inversion layer. This type of organized convection was not found on the 16th.

An analysis of the vertical momentum transfer, or stress, showed a nearly quadrature relationship between the horizontal and vertical velocity fluctuations. The phase relationship between these two variables was found to be more complicated than was found for the heat flux. Regions in the lower boundary layer in which the stress was found to be negative were found to coincide, in general, with regions which had about a  $45^\circ$  phase relationship between the two variables.

The variances of the meteorological variables were found, in general, to increase across the front over the warmer water. Both the vertical velocity and temperature fields showed a vertical structure which was in good agreement with previous boundary layer experiments. For both of these variables the maximum values for the variances were found to lie in the region between 30 and 60% of the depth of the boundary layer.

## ACKNOWLEDGMENTS

This work was made possible by a grant from the Marine Meteorology Program of the U. S. Office of Naval Research. FASINEX, a cooperative effort by many scientists and technical staff, was funded by several agencies including ONR, NASA, NSF, and NOAA. We would especially like to acknowledge the contributions of the flight crews of the NCAR Electra and the NRL-P3. Without their efforts we could not have obtained this data and returned safely to study it.

## TABLE OF CONTENTS

LIST OF TABLES .....	x
LIST OF FIGURES .....	xi
Chapter 1 Introduction .....	1
1.1 Background .....	1
1.2 Motivation .....	4
1.3 Scientific Objectives .....	9
1.4 Scientific Plan .....	10
1.5 FASINEX Results - An Overview .....	11
Chapter 2 The Data Sets .....	13
2.1 Raw Data .....	13
2.2 Variables .....	14
2.3 Post Flight Data Processing .....	15
2.4 Data Quality .....	16
2.5 Data Corrections .....	16
2.5.1 Horizontal Wind Field Correction .....	16
2.5.2 Specific Humidity Correction .....	18

2.5.3 Sea Surface Temperature Correction .....	19
2.6 The Aircraft Flight Tracks .....	20
2.6.1 FASINEX Flight Box .....	21
2.6.2 The Vertical Stack .....	23
2.6.3 Determination of Frontal Offset .....	24
2.6.4 Rotation of the Wind Coordinate System .....	26
Chapter 3 The Analysis Technique .....	29
3.1 Statistical Methods .....	30
3.1.1 Crescenti, 1988 .....	30
3.1.2 Boxcar Averaging Technique .....	32
3.2 The Hilbert Transform .....	35
3.3 Calculation of Coherence and Phase Angle .....	37
Chapter 4 Case one: 14 February, 1986 .....	40
4.1 Synoptic Forcing in the Region .....	40
4.2 The Vertical Structure From Aircraft Profiles .....	41
4.2.1 The North Side .....	41
4.2.2 The South Side .....	44
4.3 Results from Boxcar Statistics .....	46
4.3.1 Boxcar Means for Potential Temperature .....	48
4.3.2 The Vertical Heat Flux .....	50

4.3.3	Boxcar Variance for Potential Temperature .....	61
4.3.4	Boxcar Variance for Vertical Velocity .....	63
4.3.5	The Vertical Momentum Flux .....	66
4.3.6	The Horizontal Velocity Variances .....	79
4.3.7	Vector Winds .....	82
4.4	Summary for February 14 .....	85
Chapter 5	Case two: 16 February, 1986 .....	87
5.1	Synoptic Forcing in the Region .....	87
5.2	The Vertical Structure .....	88
5.2.1	The North Side .....	88
5.2.2	The South Side .....	91
5.3	Results from Boxcar Statistics .....	93
5.3.1	Boxcar Means for Potential Temperature .....	95
5.3.2	The Vertical Heat Flux .....	98
5.3.3	Boxcar Variance for Potential Temperature .....	110
5.3.4	Boxcar Variance for Vertical Velocity .....	113
5.3.5	The Vertical Momentum Flux .....	116
5.3.6	The Horizontal Velocity Variances .....	127
5.3.7	Vector Winds .....	130
5.4	Summary for February 14 and 16 .....	132

Chapter 6 Summary and Conclusions .....	137
Appendix A .....	147
Appendix B: Synoptic Maps.....	154
References .....	158

## LIST OF TABLES

Table 2.1 Variables .....	14
Table A.1 Summary of NRL-P3 Flights .....	147
Table A.2 NRL-P3 Flight Legs - 14 FEB 86 .....	148
Table A.3 NRL-P3 Flight Legs - 16 FEB 86.....	149
Table A.4 NRL-P3 Profile Times - 14 FEB 86 .....	150
Table A.5 NRL-P3 Profile Times - 16 FEB 86 .....	151
Table A.6 NRL-P3 SST Frontal Offsets - 14 FEB 86 .....	152
Table A.7 NRL-P3 SST Frontal Offsets - 16 FEB 86 .....	152
Table A.8 NCAR Electra SST Frontal Offsets - 16 FEB 86 .....	153
Table A.9 NCAR Electra SST Frontal Offsets - 17 FEB 86 .....	153
Table A.10 NCAR Electra SST Frontal Offsets - 18 FEB 86 .....	153

## LIST OF FIGURES

Figure 1.1 3-D Representation of FASINEX SST Front .....	3
Figure 1.2 Area for FASINEX Intensive Phase .....	8
Figure 2.1 FASINEX Flight Box from 16 FEB 86 .....	23
Figure 2.2 NRL-P3 Flight Tracks from 14 FEB 86 .....	25
Figure 2.3 SST (°C) Before Offset from 14 FEB 86 .....	27
Figure 2.4 SST (°C) After Offset from 14 FEB 86 .....	28
Figure 4.1 (a-h) North Profiles - 14 FEB 86 .....	42
Figure 4.2 (a-d) - South Profiles 14 FEB 86 .....	45
Figure 4.3 SST (°C) from 14 FEB 86 (Track 4 omitted) .....	47
Figure 4.4 Potential temperature (K) - 14 FEB 86 (Track 4 omitted) .....	49
Figure 4.5 Boxcar Covariance (W-Theta) (Kms <sup>-2</sup> ) - 14 FEB 86 .....	51
Figure 4.6 Boxcar Correlation (W-Theta) - 14 FEB 86 .....	53
Figure 4.7 Boxcar Coherence (W-Theta) - 14 FEB 86 .....	55
Figure 4.8 Boxcar Phase Angle (W-Theta) - 14 FEB 86 .....	57
Figure 4.9 Phase Angle PDF for (W-Theta) - 14 FEB 86 (a-j) .....	58
Figure 4.10 Boxcar Variance Theta (K <sup>2</sup> ) - 14 FEB 86 .....	62
Figure 4.11 Boxcar Variance Vertical Velocity (m <sup>2</sup> s <sup>-2</sup> ) - 14 FEB 86 .....	65

Figure 4.12 Boxcar Covariance (U-W) ( $m^2s^{-2}$ ) - 14 FEB 86 .....	68
Figure 4.13 Boxcar Correlation (U-W) - 14 FEB 86 .....	71
Figure 4.14 Boxcar Coherence (U-W) - 14 FEB 86 .....	72
Figure 4.15 Boxcar Phase Angle (U-W) - 14 FEB 86 .....	75
Figure 4.16 Phase Angle PDF for (U-W) - 14 FEB 86 (a-j) .....	76
Figure 4.17 Boxcar Variance U Wind Component ( $m^2s^{-2}$ ) - 14 FEB 86 .....	80
Figure 4.18 Boxcar Variance V Wind Component ( $m^2s^{-2}$ ) - 14 FEB 86 .....	81
Figure 4.19 Vector Winds - 14 FEB 86 .....	84
Figure 5.1 (a-h) North Profiles - 16 FEB 86 .....	89
Figure 5.2 (a-d) South Profiles - 16 FEB 86 .....	92
Figure 5.3 SST ( $^{\circ}C$ ) from 16 FEB 86 .....	94
Figure 5.4 Potential temperature (K) - 16 FEB 86 .....	97
Figure 5.5 Boxcar Covariance (W-Theta) ( $Kms^{-2}$ ) - 16 FEB 86 .....	100
Figure 5.6 Boxcar Correlation (W-Theta) - 16 FEB 86 .....	102
Figure 5.7 Boxcar Coherence (W-Theta) - 16 FEB 86 .....	103
Figure 5.8 Boxcar Phase Angle (W-Theta) - 16 FEB 86 .....	106
Figure 5.9 Phase Angle PDF for (W-Theta) - 16 FEB 86 (a-l) .....	107
Figure 5.10 Boxcar Variance Theta ( $K^2$ ) - 16 FEB 86 .....	112
Figure 5.11 Boxcar Variance Vertical Velocity ( $m^2s^{-2}$ ) - 16 FEB 86 .....	115
Figure 5.12 Boxcar Covariance (U-W) ( $m^2s^{-2}$ ) - 16 FEB 86 .....	117

Figure 5.13 Boxcar Correlation (U-W) - 16 FEB 86 .....	119
Figure 5.14 Boxcar Coherence (U-W) - 16 FEB 86 .....	121
Figure 5.15 Boxcar Phase Angle (U-W) - 16 FEB 86 .....	123
Figure 5.16 Phase Angle PDF for (U-W) - 16 FEB 86 (a-l) .....	124
Figure 5.17 Boxcar Variance U Wind Component ( $m^2s^{-2}$ ) - 16 FEB 86 .....	128
Figure 5.18 Boxcar Variance V Wind Component ( $m^2s^{-2}$ ) - 16 FEB 86 .....	129
Figure 5.19 Vector Winds - 16 FEB 86 .....	131
Figure B.1 NMC Surface weather maps for 14 FEB 86 .....	155
Figure B.2 NMC Surface weather maps for 15 FEB 86 .....	156
Figure B.3 NMC Surface weather maps for 16 FEB 86 .....	157

# CHAPTER 1

## INTRODUCTION

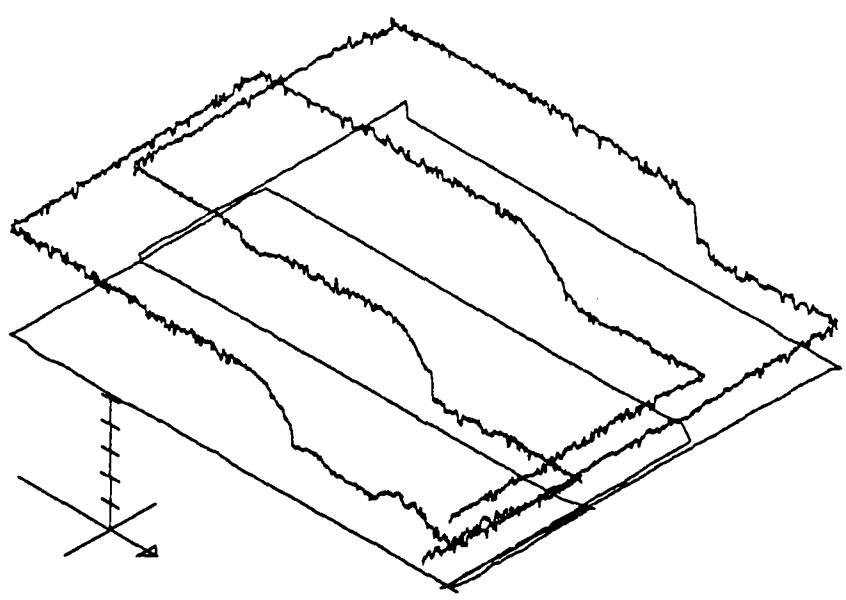
### 1.1 Background

An oceanic sea surface front is most commonly defined as a region in which the density changes very quickly over a relatively short horizontal distance (Cromwell and Reid, 1956). Other properties often change abruptly at a sea surface front in addition to density, among these are temperature, salinity, organic composition, and current velocity. The front is often sinuous in form and is frequently made visible by a region of increased surface wavelets; also there is often an accumulation of surface debris associated with the front. In the subtropical convergence zone, in the Sargasso Sea southwest of Bermuda, sea surface fronts are quite common and may often be located by an accumulation of sargassum weed at the interface between the two different water masses. These interfaces can be quite energetic as is evident through an account of a sea surface front making so much noise that it could be heard from a distance of three miles (Bowman, 1978). It is believed that the noise is generated by the chaotic movement of the small wavelets around the surface front.

Oceanic fronts can be found on all scales at varying intensities, from planetary down to fractions of a meter. Bowman (1978) lists six types of sea surface fronts most commonly found in nature. They are: (1) shallow sea fronts which are found to form in regions around islands, in continental seas and estuaries, around capes, banks, and shoals; (2) plume fronts found at the boundaries of riverine plumes discharging into coastal waters; (3) shelf break fronts which are formed at the boundaries of a shelf and slope waters; (4) fronts located in regions of upwelling; (5) fronts located at, and marking, the edges of major western boundary currents; and (6) planetary scale fronts which are usually associated with convergence of surface Ekman transports, found away from major ocean boundaries. It was this last type of front that was investigated and was the source for the data for this research.

One common thread that these fronts share is that of persistence. These frontal systems can last for days, weeks, or even months despite diffusive tendencies due to the strong horizontal gradients, and surface convergence which is associated with strong vertical convection. Other forces which are important in the formation and maintenance of oceanic fronts include the surface wind stress and the transport of heat and moisture at both the local and global scale.

An example of sea surface temperature variation along the front which was found in this study is shown in figure 1.1 (after Crescenti, 1988). For this figure the cross frontal legs are 100 km long while the overall dimension along the front is 90



Z AXIS MAX =	24.00	Z MAX =	23.62	16 FEB 86
Z AXIS MIN =	19.00	Z MIN =	19.71	SST (C)
Z INC =	1.00			

Figure 1.1 3-D Representation of FASINEX SST Front

km. Thus the spacing between each cross frontal leg is about 30 km. The SST change associated with the front is on the order of  $2^{\circ}\text{C}$  often occurring over a horizontal distance of 10 km or less. Frequently a large percentage of the change occurs over a distance as short as 2 km.

### 1.2 Motivation

Temperature gradients in the ocean have long been known to have an effect on the large scale circulations in both the atmosphere and the ocean. In this study it is the smaller scale of horizontal surface temperature gradients to which our attention is focused. Previous studies of the marine atmospheric boundary layer (MABL) have dealt with the transfer processes between the ocean surface and the MABL. These studies include AMTEX (Air Mass Transformation Experiment, February 1974 and 1975) and GATE (GARP Atlantic Tropical Experiment). The transfer process in the MABL as cold air from Asia moved across the warm Kuroshio Current off the coast of Japan was concentrated on in AMTEX. GATE was conducted near the equator in the Atlantic Ocean in the summer of 1974. During GATE there was little difference between the air and sea temperatures. This is the typical condition over wide areas of the ocean, leaving the MABL neutrally stratified (Stage and Weller, 1985).

From mid-July to mid-September of 1978 the Joint Air Sea Interaction Experiment (JASIN) was conducted. JASIN was the first large scale effort by both meteorologists and oceanographers to work together to further understand the complexities associated with the interface of the atmosphere and the oceans. JASIN was conducted in the North Rockwell Trough, an area of deep water (1000-2000 m) which is several hundred kilometers across, located off the northwest coast of Scotland (Pollard et al. 1983). JASIN was a large project with more than fifty teams of investigators from nine countries participating. They used 14 ships and three aircraft as their movable platforms. Thirty five mooring systems were also deployed to obtain data at many different levels of the ocean and the atmospheric boundary layer (ABL).

There have been many results from JASIN published in the literature, among these are the following: (1) Spatial variability in the SST associated with an oceanic eddy caused mesoscale horizontal variability in the fluxes of momentum and moisture in the MABL; (2) The turbulent structures in the MABL were found to have distinctively different scales on the two sides of the SST feature (Stage and Weller, 1985). The JASIN area had been selected because horizontal variability in the sea surface temperature (SST) was typically quite small. However, during the JASIN intensive period there were more oceanic eddies and fronts than had been expected (Pollard et al., 1983). The occurrence of the SST inhomogeneity has been cited as

an indication that this was a topic worthy of further investigation (Pollard et al. 1983; McWilliams, 1983).

The presence of an increased horizontal variability from what had been expected resulted in some of JASIN's shortcomings. The flight plans, buoy array spacing and ship cruise patterns were not designed to properly explore the horizontal or temporal variability in the ocean that was observed (Stage and Weller, 1985). The aircraft flight tracks were fixed triangles and did not allow for adjustment to accommodate the SST anomaly. However, in spite of these shortcomings it was noticed that there was a response to the varied SST field and that the response by the atmosphere was of the same scale as the inhomogeneity in the SST itself (Guymer et al., 1983). Since the JASIN data would not support the investigation of the MABL's response to the oceanic temperature change, the need for a new study specifically designed to inspect this type of feature became apparent.

The U.S. Office of Naval Research (ONR) sponsored a workshop in February 1983 at the National Center for Atmospheric Research (NCAR) on air-sea interaction. The workshop brought meteorologists and oceanographers together to discuss those areas which were considered to be important and to propose future cooperative field experiments (McWilliams, 1983).

Among the conclusions of the workshop participants was the consensus that a better data set was needed in order to study the effects of variations with spatial

scales less than 200 km and temporal scales less than 12 hours. Also of interest in the area of air-sea interaction was the question of what type of coupled response one fluid would exhibit in the vicinity of a horizontal variation of the other.

It was felt that the best location to conduct an experiment of this nature was either in the Gulf Stream, a Gulf Stream ring or eddy, or an open oceanic temperature front. Among these choices there were advantages and disadvantages of each. The Gulf Stream tends to be a very persistent feature, but there are problems associated with the deployment of moored and unmoored buoys within the Gulf Stream as the velocities of the Gulf Stream are much too great. In contrast, a Gulf Stream ring or eddy might not be a very persistent feature and could also translate through the experiment area too quickly. For these reasons the choice of an open-ocean temperature front seemed to be the most appropriate. From these considerations and the consensus opinion that a better data set was required for detailed analysis came the origin of the Frontal Air Sea Interaction Experiment or FASINEX .

The area chosen for FASINEX is the region bounded by 68-72 deg W and 25-30 deg N (Stage and Weller, 1985), a region with mainly flat bottom topography which is relatively distant from any continental effects (see figure 1.2). The SST front is frequently visible through satellite infrared images (AVHRR - Advanced Very High Resolution Radiometer) during the period from October through May of each year. After May the surface waters in this region warm up to a nearly uniform

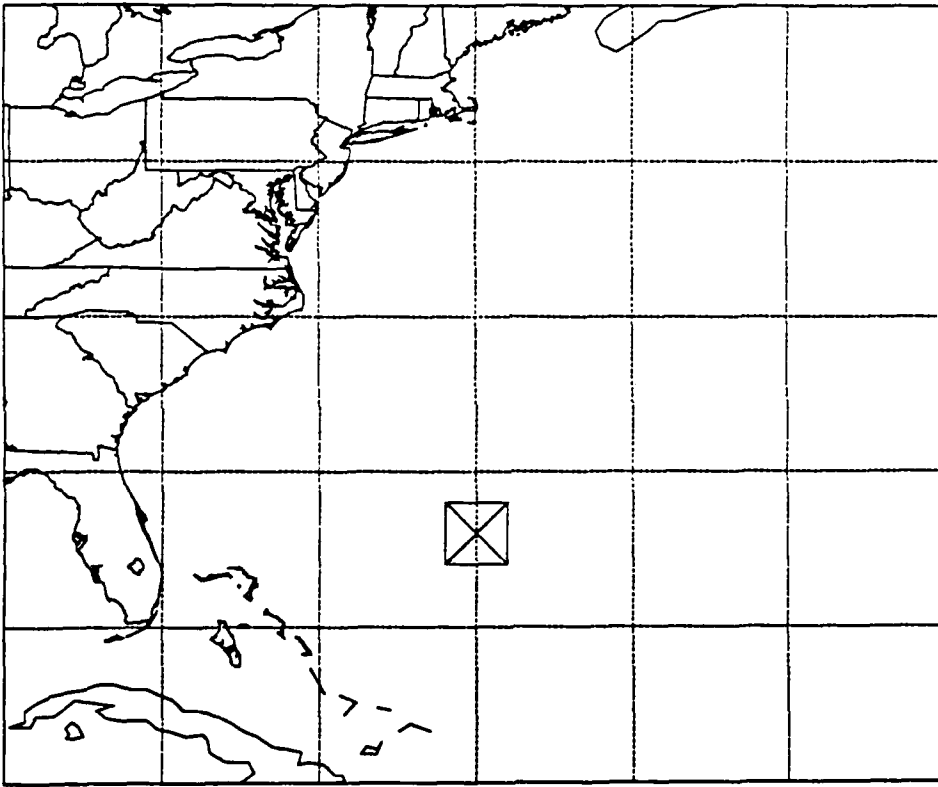


Figure 1.2 Area for FASINEX Intensive Phase

temperature, therefore temperature is a poor indicator, and often cannot be used, for the location of the existing SST fronts (Stage and Weller, 1985). This region was chosen because climatologically the area tends to have large horizontal sea surface temperature gradients, lower sea states and less cloud coverage than areas to the north. This would allow for a better data set and satellite assistance in the determination of the SST front location. The experiment was planned to start in the winter of 1985/1986 and was to continue through July 1986 with an intensive period scheduled for the period spanning the middle of February through the middle of March.

In addition, the region selected tends to have few atmospheric frontal passages. This would allow for a relatively constant horizontally homogeneous atmospheric forcing which is in a nearly steady state with respect to mesoscale time and space scales. The ocean front generally meanders along an east-west axis, and cut off eddies are common (Voorhis, 1969).

### **1.3 Scientific Objectives**

There are eight principal scientific objectives that were established for FASINEX. The objectives of FASINEX that are most relevant to this work include:

- (1) Determine the magnitude of changes in surface stress associated with sea surface temperature (SST) changes across the oceanic front, and investigate different meth-

ods of estimating stresses and fluxes. (2) Determine how the mean structure of the marine atmospheric boundary layer (MABL) changes across the SST front, what adjustment mechanisms exist and how is balance achieved on each side and between the two sides, for momentum, heat, and moisture fluxes.

A much more thorough description of the meteorological and oceanographic objectives for FASINEX has been given by Stage and Weller (1985).

#### 1.4 Scientific Plan

FASINEX was designed with three phases. Phase 1 began in January 1986 when the R/V *Knorr* initiated a series of cruises used to survey the area. After the survey was complete the *Knorr* deployed five surface moorings and four profiling-current-meter (PCM) moorings in a selected area of the front. The placement of this array was aided by satellite imagery and aircraft overflights. This array remained fixed until Phase 3, in June-July 1986, when the *Knorr* returned to retrieve the moorings.

Phase 2 was the intensive period for FASINEX. This period was from mid-February through mid-March of 1986. The intensive period was marked by the concentrated data collection by multiple platforms including: five research aircraft, two research vessels, twelve mooring and PCM's, and satellite imagery. The data

analyzed in this study are from the National Center for Atmospheric Research (NCAR) Electra and Navy Research Laboratory (NRL) P3 aircraft, compiled during the intensive phase. A more complete description of the FASINEX flight plan has been given by Stage and Weller (1986).

Phase 3 was marked by the retrieval of the moored array in the early part of the summer of 1986 by the *Knorr* thus marking the official end of FASINEX.

### 1.5 FASINEX Results - An Overview

FASINEX was the first experiment designed to inspect the role of horizontal SST variability over a horizontal scale of about 100 km and a spatial scale of a few hours. As a result of this effort there is a unique data set containing a wealth of information on these spatial and temporal scales. There has been a considerable contribution to the literature from FASINEX. The total contribution list is quickly approaching 100, composed of conference papers, refereed articles, technical reports and degree theses. The contributions from FASINEX have been varied, ranging in content from a discussion of the data quality for the various platforms (Shaw and Vaucher, 1987), to a catalog of the synoptic conditions (Fellbaum et al., 1988), and an assortment of results of the data using a variety of analysis techniques such as a conditional sampling technique (Khalsa, 1989), two different spectral methods

(Friche et al., 1990) and a moving boxcar technique (Crescenti, 1988).

## CHAPTER 2

### THE DATA SETS

#### 2.1 Raw Data

As mentioned, the data sets for this study were obtained by two turbulence measuring research aircraft. The two data sets have a general similarity to each other, but there are some significant differences between the two. Each aircraft used two different sampling rates; high frequency data were collected at 50 samples per second (sps) while low frequency data were collected at 5 sps. Both the high and low frequency data were filtered during collection to remove frequencies higher than desired. The analog voltage signals from the instruments were converted to digital data signals and were then ingested by an on board computer, and were subsequently written to 1/2 inch magnetic tape. Further discussion of the data acquisition systems has been given by Miller and Friessen (1985).

**2.2 Variables**

The NRL-P3 and the NCAR Electra supplied two similar but distinct data sets. The Electra's data set has been used by a variety of investigators and is generally felt to be quite reliable. In contrast the NRL-P3's data set has some shortcomings which set it apart from the Electra data set. The most notable differences include (1) the lack of a Long Range Navigation (LORAN) system aboard the NRL-P3; (2) the lack of a high frequency humidity sampler aboard the NRL-P3; and (3) the possibility of a biased external ambient temperature measurement due to poor positioning of the temperature probe on the NRL-P3 aircraft's exterior skin (Friehe, personal communication).

A summary of the variables used for analysis of the data is given in Table 2.1.

Table 2.1  
Variables

<u>Name</u>	<u>Description</u>	<u>Units</u>	<u>Rate (sps)</u>	<u>Electra/P3</u>
ALAT	INS Latitude	deg	1	Y/Y
ALON	INS Longitude	deg	1	Y/Y
CLAT	LORAN C Latitude	deg	1	Y/N
CLON	LORAN C Longitude	deg	1	Y/N
HGME	Geometric Radar Altitude	m	1	Y/Y

Table 2.1 (cont.)

Variables

<u>Name</u>	<u>Description</u>	<u>Units</u>	<u>Rate (sps)</u>	<u>Electra/P3</u>
RSTT	Radiometric Sky Temp.	°C	1	N/Y
RSTB	Radiometric Surface Temp.	°C	1	Y/Y
PSFC	Corrected Static Pressure	mb	1	Y/Y
SPHUM	Relative Humidity	%	1	Y/Y
THI	Aircraft True Heading	deg	1	Y/Y
SPHUM (Q)	Specific Humidity	g/kg	1	Y/Y
RSTT	Radiometric Sky Temp.	°C	20	Y/N
ATB/ATF	Ambient Temperature	°C	20	Y/Y
UI	Wind Vector, East Comp.	m/s	20	Y/Y
VI	Wind Vector, North Comp.	m/s	20	Y/Y
WI	Wind Vector, Vertical Comp.	m/s	20	Y/Y
THETA	Potential Temperature	°K	20	Y/Y
VLA (Q)	Lyman Alpha Humidity	g/kg	20	Y/N
<u>Calculated Parameters</u>				
P(fltlv)	Pressure at mean flight level	mb	1	Y/Y
SST	Corrected Sea Surface Temp.	°C	1	Y/Y

**2.3 Post Flight Data Processing**

After the completion of FASINEX, the data tapes were taken to NCAR's Research Aviation Facility (RAF) where a FORTRAN software program called GENPRO was used for final processing of the data. The GENPRO program searched the data for gaps, parity errors, wild points and spikes. The program then re-

placed the spurious values with linearly interpolated values. The high frequency channels (50 sps) were then interpolated to 20 sps while the low frequency data (5 sps) were block averaged to 1 sps. A five point block average was used, with the block centered on the start of each second. For more information on the treatment of the data at the RAF see Miller and Friessen (1985).

## 2.4 Data Quality

In general the data are of high quality. However, because of the somewhat remote location of the FASINEX area the pilots infrequently needed to use high frequency radio to communicate with air traffic controllers, resulting in radio frequency interference (RFI) which sometimes left spurious spikes in one or more of the data channels. Those spikes which were not replaced by GENPRO were replaced with linearly interpolated values as part of our data preparation. For the data sets examined in this study, this problem was not encountered.

## 2.5 Data Corrections

### 2.5.1 Horizontal Wind Field Correction

The winds, which are obtained from an inertial navigation system (INS), are subject to a periodic variation known as the Schuler oscillation (Broxmeyer, 1964).

This oscillation is due directly to the use of the INS for the determination of the winds. All inertial navigation systems are subject to this oscillation which has a period of 84.4 minutes. This is the period of a pendulum of length equal to the Earth's radius. The oscillation has a known period but unknown amplitude and phase; which are prone to change throughout the flight. This variation can result if one of the three accelerometers orthogonally mounted in the INS senses an erroneous acceleration or if the INS platform is not initially level. The latter condition is almost guaranteed to occur as it is essentially impossible to have the platform exactly perpendicular to the local gravity when initializing the system. The former error is one which might be induced when the aircraft undergoes an excessive turn rate, a feature which was common in the flight tracks used for the FASINEX.

The Electra navigation equipment also included a LORAN C, a radio beacon based navigation system. By assuming the LORAN C gave an accurate value for the latitude and longitude we were able to determine the error contained within the INS positions. Following Crescenti (1988), the horizontal wind field for the Electra was corrected for the Schuler oscillation using a cubic spline algorithm and coefficients supplied by Shaw and Vaucher (1987) and Crescenti (1988).

The wind field for the NRL-P3 could not be corrected as there was not a second recording position-indicating instrument on board the aircraft. However, it is judged that, in general, the wind field obtained from the NRL-P3 is reliable owing to

(1) positioning of the INS equipment within the aircraft; (2) relatively small terminal errors which were verified at the end of the flight each day, and (3) consistently small discrepancies during in-flight checks against the aircraft's own inertial and Omega navigation systems (Friehe et al., 1990).

### 2.5.2 Specific Humidity Correction

The NCAR Electra contained two instruments for obtaining atmospheric humidity, one low frequency sampler and one high frequency sampler. The low frequency sampler on both aircraft was a dewpoint hygrometer while the high frequency instrument was a Lyman-alpha hygrometer. The signal obtained from this instrument is returned in volts, which then needed to be converted to g/kg. This instrument, though very reliable over short periods, has an associated error due to long term instrument drift. This error was corrected by loosely constraining the converted Lyman-alpha voltages to converge to the low frequency hygrometer. The necessary algorithm was supplied by Schanot (1987).

The humidity sampler on the NRL-P3 was a low frequency dewpoint hygrometer which proved to be inappropriate for use in determining turbulent fluxes. This instrument was able to supply an estimate of the mean water vapor content in most cases. However, the data record indicates some cases where the instrument appears to have had trouble converging on a value and should not be trusted.

### 2.5.3 Sea Surface Temperature Correction

The SST was determined using a down-looking radiometer. The resulting signal then required correction due to the fact that the ocean surface is not a black-body. The value obtained from the down looking radiometer contained the sum of the radiance emitted from the ocean surface and a component of downwelling infrared radiance which is reflected from the ocean surface. When observations are made in broken cloud conditions, especially cumulus clouds, the downwelling infrared radiation can be quite variable and can produce an error of up to 0.5°C (Lui and Katsaros, 1984; Crescenti, 1988). The radiance must be corrected by subtracting out the reflected signal. Physically this means that the radiance received by the downward looking radiometer on the aircraft is equal to the radiance emitted by the sea plus the radiance emerging from the sea due to the reflected sky radiation.

An algorithm written to correct the SST, using both the upward and downward looking radiometers, was originally supplied by J. Businger and modified by G. Crescenti for use with the FASINEX data. Both aircraft data sets had their SST fields corrected in this manner.

It should also be noted that no correction is made for the atmospheric absorption and emission of radiation which occurs between the surface and the aircraft flight level. An estimate for the effects of the atmospheric layer between the sea

surface and the aircraft on the infrared radiance shows that the error induced due to water vapor differences across the front had a maximum magnitude of  $0.5\text{ C}^\circ$ . This maximum error corresponds to the greatest difference in water vapor content from one side of the front to the other for the maximum path length encountered. This effect is certainly significant and should be taken into account in further studies if the SST estimates are to be used for anything other than placement of the front. It should also be pointed out that while relative sensitivity of the instruments was quite good, the absolute accuracy of the instruments is less certain owing to instrument temperature drift associated with the changing altitude and temperature of the aircraft during the flight.

### 2.6 The Aircraft Flight Tracks

A variety of flight tracks were used by the FASINEX aircraft. When more than one aircraft was present the flight formation generally consisted of the aircraft flying at various altitudes and over the same flight track. In this way the MABL can be sampled at multiple levels in the same horizontal region by the various aircraft at the same time. This formation is not without its own problems as there can be interference from the turbulent airflow associated with the leading aircraft's wings and especially propellers. This interference, or "prop wash" was most noticeable when

the aircraft were allowed to fly too close to each other. For the data we will be looking at there were no apparent manifestations of this problem as the aircraft, when flying together, were spaced quite far apart in the vertical direction.

The most structured flight track used in FASINEX was that of the FASINEX box. This pattern, discussed in more detail in section 2.6.1, was designed to measure the MABL both across the front and parallel to the front on both the cold and warm sides. The pattern also allowed for an evaluation of the stationarity of the turbulence over the entire flight envelope as there were overlapping segments flown at different times.

The second flight pattern we will be discussing is one which lends itself to a vertical inspection of the structure of the MABL in the FASINEX region. This pattern was the vertically orientated radiator or stack. This pattern consisted of a series of cross frontal tracks which are flown at an assortment of altitudes over the same region and is discussed in more detail in section 2.6.2.

### **2.6.1 FASINEX Flight Box**

For the data obtained on 16 February, 1986 both the NCAR Electra and the NRL-P3 flew in a pattern known as the FASINEX box. The pattern was designed to systematically measure the experimental area. The flight track offers a series of straight line legs which have some overlapping segments. The FASINEX flight box

is depicted in figure 2.1. The box is flown in the following order, with turns being made as 270° outside loops: leg 1-2, leg 2-3, leg 3-4, leg 4-1, leg 1-5, leg 5-6, leg 6-7, leg 7-8, and leg 8-1. The Electra flew the pattern at a nominal altitude of 35 m while the NRL-P3 flew the pattern at two different levels. The NRL-P3 flew the box initially, concurrently with the Electra, at a nominal flight level of approximately 945 m. Upon completion of the initial FASINEX flight box, some additional legs were also flown by the P3 alone at 100 m. These legs were leg 1-2, leg 2-3, leg 3-4, and leg 4-1.

The FASINEX box offered four cross frontal legs: leg 2-3, leg 4-1, leg 5-6, and leg 7-8, each 100 km long. The other legs which were parallel to the front comprise the north and south ends of the box to total 90 km.

Tables A.1 through A.7 in Appendix A give the information for NRL-P3 flight tracks for the applicable days. Also provided is a summary of the flights made by the P3 during FASINEX. Flight information for the NCAR Electra is provided in detail in Crescenti (1988). Tables A.8 through A.10 give information for the NCAR Electra which is not available from Crescenti's work.

### **2.6.2 The Vertical Stack**

On 14 February, 1986 the NRL-P3 flew alone in the FASINEX area. The P3 flew a series of tracks across the SST front at a series of altitudes. The altitudes flown, in order, were: track 1, 150 m; track 2, 460 m; track 3, 775 m; track 4, 1800

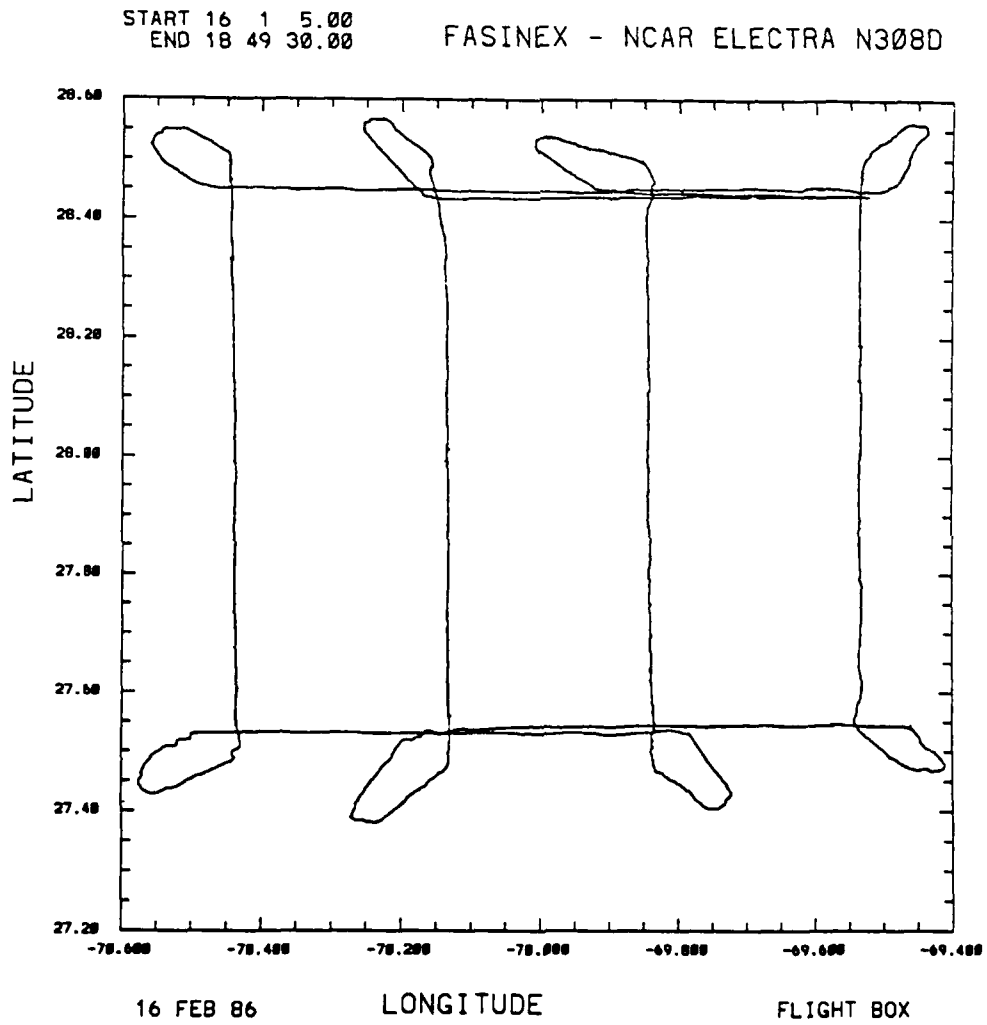


Figure 2.1 FASINEX Flight Box from 16 FEB 86

m; track 5, 100 m, and track 6 at 500 m. The flight tracks, with the exception of track 6, were oriented almost due north-south and approximately perpendicular to the front. Track 6 was oriented roughly northwest-southeast. Figure 2.2 is a map plan of the flight tracks from this day.

Table A.4 in Appendix A gives the start and stop times for each track from the 14<sup>th</sup> of February.

### **2.6.3 Determination of Frontal Offset**

All of the flight legs included in this study are adjusted and plotted in terms of distance from the front with points south of the front denoted by negative values.

For those fronts which exhibit a nearly linear transition region the determination of the frontal offsets was made by finding the midpoint in the temperature change and the midpoint in the transition region and then averaging the two. For those fronts which show a more complicated structure it was necessary to subjectively determine where the "front" should be located. The latter situation was the general case for the front on the 14th with the inclusion of an obvious warm pool of water to the north of the primary frontal region. Figures 2.3 and 2.4 show an example of the SST traces from 14 February before and after being offset, respectively.

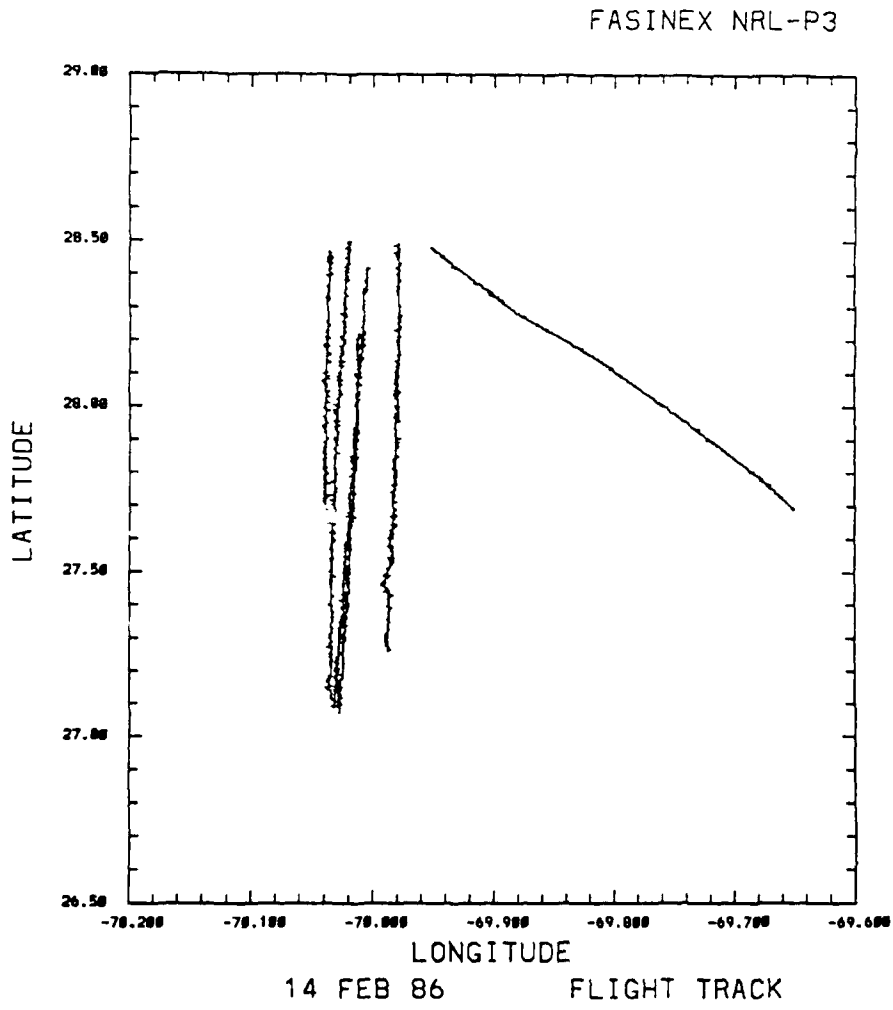


Figure 2.2 NRL-P3 Flight Tracks from 14 FEB 86

#### **2.6.4 Rotation of the Wind Coordinate System**

The coordinate system used for all wind plots and calculations has been rotated such that the U component of the wind is along the mean wind direction for that flight leg.

First the mean eastward (UI) and northward (VI) wind components are determined for each leg or track. From this the mean wind direction is determined. The coordinate system was then realigned along this mean direction. The new coordinate system gives a positive U along the mean wind direction for that leg, and a positive V is oriented normal to and to the left of U, thus establishing a standard right hand coordinate system oriented along the mean wind axis.

FASINEX - NRL-P3

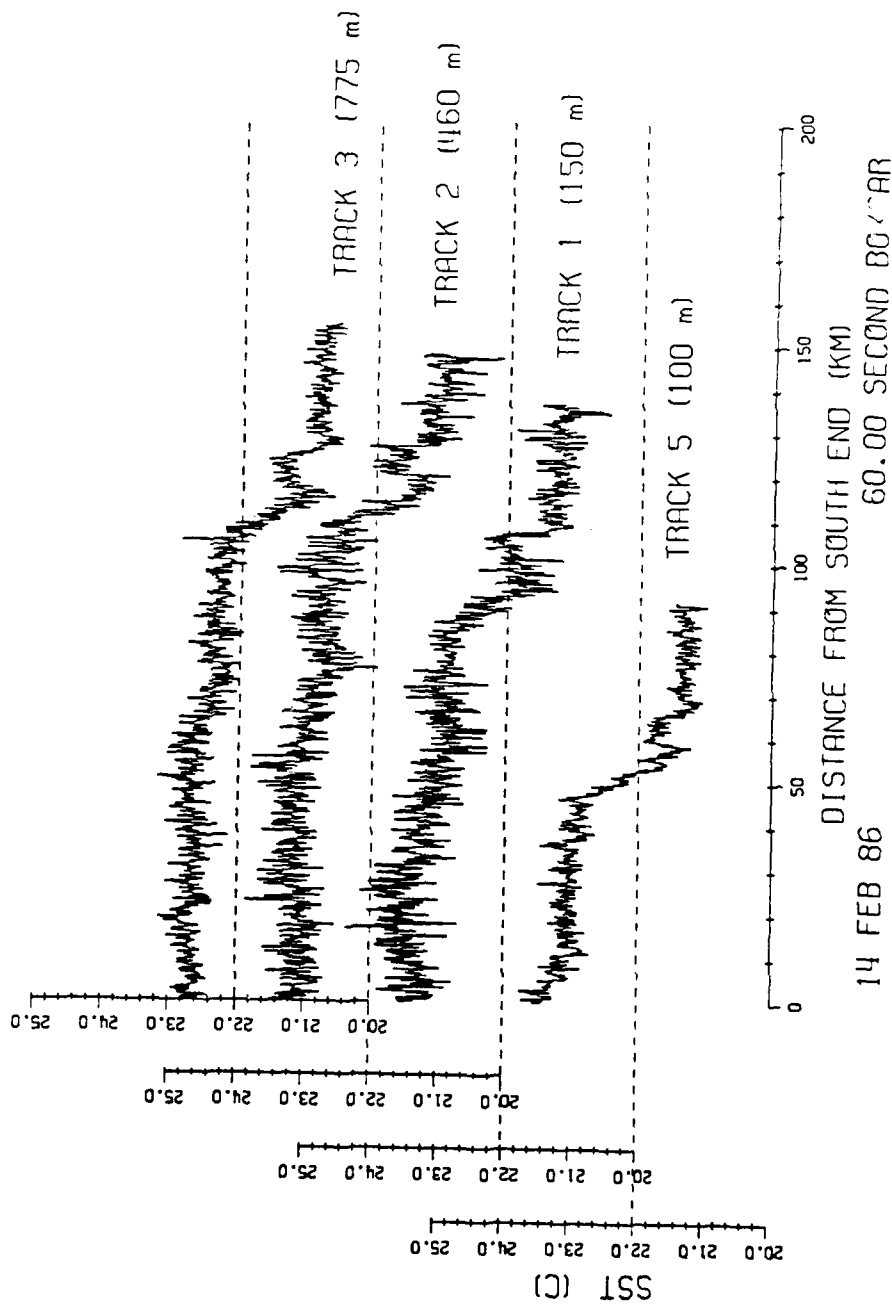


Figure 2.3 SST (°C) Before Offset from 14 FEB 86

FASINEX - NRL-P3

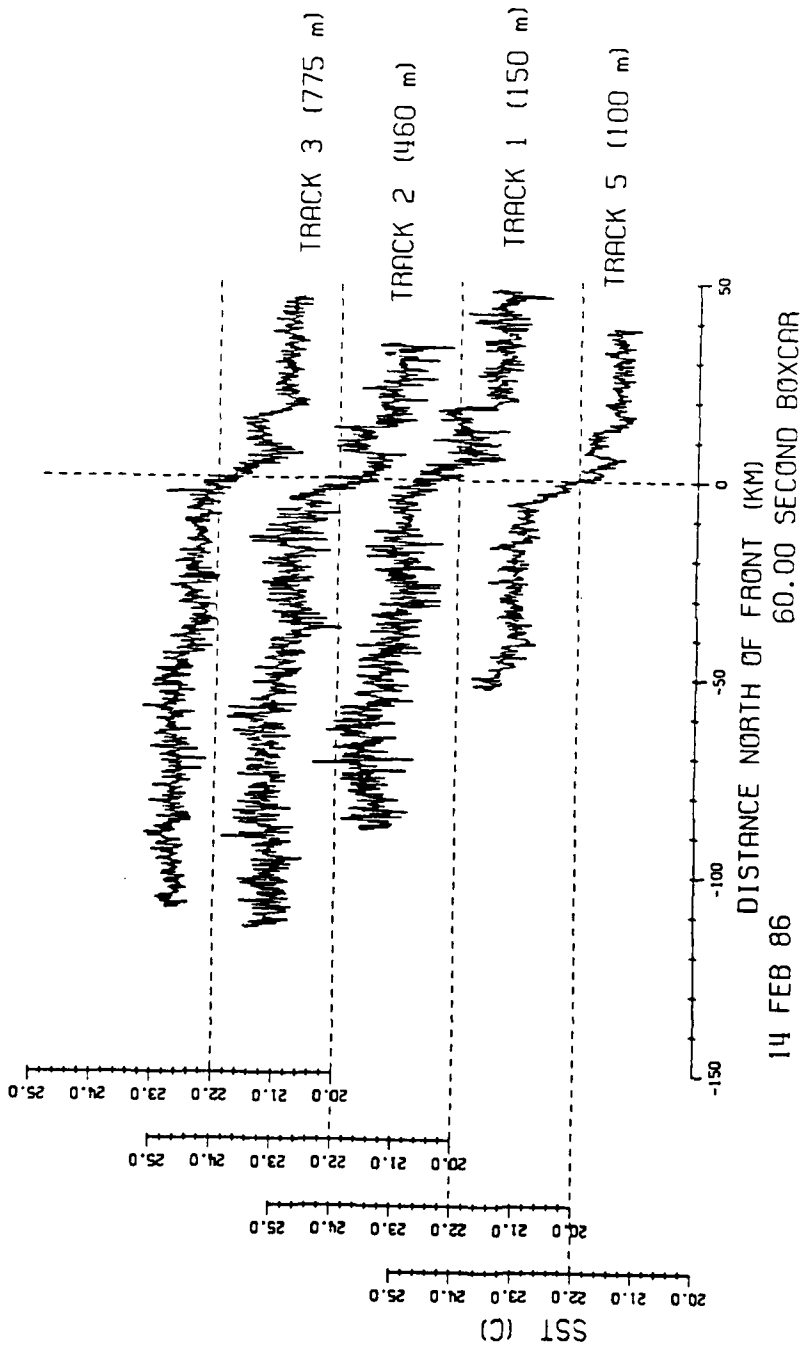


Figure 2.4 SST (°C) After Offset from 14 FEB 86

## CHAPTER 3

### THE ANALYSIS TECHNIQUE

Because of the nature of turbulence, statistical methods need to be used in the description of the turbulent regime. The calculations made require the assumption that there is a "spectral gap." The spectral gap refers to the concept that energy contained within the motions of the atmosphere has distinct temporal and spatial modes. This property of the atmosphere is apparent when one looks at a plot of the spectral density for a variable such as wind speed. In a plot of this type, it is often noticed that there are three distinct peaks in the frequency spectrum. These peaks correspond to the synoptic scale interactions, with time scales in the vicinity of 100 hours, the diurnal cycle, with a time scale of 24 hours, and the energy contained within the microscale eddies, which have a time scale of the order of 10 seconds to about 10 minutes (Stull, 1988).

If we assume that the existence of the spectral gap is real, then we are able to select the appropriate time scale to separate the large scales from the small scales, allowing the separation of the mean characteristics from the turbulent variations contained within the field. The information contained within the mean quantity, or

low frequency data, represents the variations in the field with time scales greater than the time used for averaging. In this way the process of averaging can be thought of as a low pass filter, where the cutoff frequency corresponds to the space and time interval over which the record is averaged. The turbulent quantities are those which have temporal and spatial scales which are shorter than the averaging length. Such turbulent fluctuations are visible in the record as departures from the mean value. This process of separating the mean and turbulent characteristics of a flow, known as Reynold's decomposition, is common in the field of turbulence. This concept is expressed in equation 3.1.

$$U = \bar{U} + u' \quad (3.1)$$

### 3.1 Statistical Methods

#### 3.1.1 Crescenti, 1988

The work presented by Crescenti in 1988 has a particular relevance to the work presented here. Crescenti evaluated two methods of calculating variances and covariances of the meteorological variables. The first method, explained in more detail below, consisted of a moving boxcar average technique, the second was a spectral filtering method. Through his spectral analysis it was determined that there was an indication of a slight decrease in energy, or a "spectral gap", in the frequency

range of 0.0167 Hz. This frequency corresponds to a period of about 60 seconds. This time scale was then used as the averaging length for the moving boxcar method and as a lower cut-off frequency for the spectral method. The results of the two techniques compared favorably with each other and both techniques appeared to show the inhomogeneity of the MABL in the vicinity of the SST front quite well (Crescenti, 1988).

Crescenti went on to do detailed analyses of the lowest level of the MABL for three days during which the synoptic forcing presented a variety of flow regimes, perpendicular to the SST front and along the front. The data set which was used was from the NCAR Electra for the three days included in the 16th through the 18th of February. As will also be seen in this study, the north wind case was shown to have a pronounced adjustment of the turbulent fluctuations in the vicinity of the front. Similar results were found for the south wind case, though the atmosphere became more stable rather than unstable as the air moved across the front. The transition for the wind parallel to the front was much more gradual though an increase in turbulent activity was apparent over the warm water. The results of this work are covered in much greater detail in Crescenti (1988) and Stage et al. (1990) while a comparison between Crescenti's methods and other methods is offered by Friehe et al. (1990).

### 3.1.2 Boxcar Averaging Technique

The boxcar, or moving average, technique is one in which a set length, or mask, of points is averaged together to obtain one value. If we think of the boxcar as moving to the right in time, then to calculate the next boxcar statistic, the left-most point within the boxcar is removed while the next value to the right is added into the boxcar. This procedure is repeated, indexing over all values in the time series. One drawback to this technique is the first boxcar value obtained is located at a distance equal to one half of the boxcar length from the beginning of the series. Similarly the last boxcar value occurs at a point equal to one half of a boxcar from the last value in the series.

Since the boxcar length is determined by time, the number of points contained within a boxcar is a function of both the boxcar length and the sampling rate for the data. That is

$$N = L * S_D \quad (3.2)$$

where  $N$  is the number of points in the boxcar,  $L$  is the length of the boxcar and  $S_D$  is the sampling rate. Thus a high frequency variable averaged with a 60 second boxcar would have 1200 points contained in each boxcar.

The FASINEX aircraft traveled at a speed of approximately 100 m/s, therefore the use of a 60 s boxcar length corresponds to about a 6 km spatial average. This 6 km boxcar length roughly corresponds to the length scale of the SST transi-

tion region. Thus an averaging time of this length helps to maintain much of the detail in the fast responses the variables might exhibit to the front when compared to a longer averaging time. We are also reminded that since the aircraft is in constant motion, the analysis of the data involves both the time and space domains.

Each of the two methods presented by Crescenti had some drawbacks. As mentioned previously, the boxcar method showed that as the boxcar length was increased, more and more of the information at each end of the segment being analyzed was lost due to the smoothing process. Similarly, as the frequency was decreased in the spectral method the periodic properties of the Fast Fourier Transform (FFT) increasingly contaminated the ends of the same segment. Neither method was clearly preferable, though each had its own uses. For a more complete treatment of this topic consult Crescenti (1988).

It was decided that the boxcar method, with the appropriate length boxcar, presented itself in a manner that "showed the turbulent fluctuations" quite well. From the spectral analysis, Crescenti decided that the appropriate boxcar length should be 60 seconds. A boxcar of this length was able to show the rapid transition in the vicinity of the front while removing much of the broader scaled features. A detailed comparison of a series of boxcar lengths and spectral cutoffs has been given by Crescenti (1988).

We will now more formally define the boxcar method and discuss how this technique was used in this study. Let the boxcar mean, or average, for any of the measured variables be defined as

$$\bar{X}(t) = (1/L) \sum_{t'=-L/2}^{t'+L/2} X(t+t') \quad (3.3)$$

where  $L$  is the length of the boxcar as before.

From this definition we can define the covariance between two variables,  $X$  and  $Y$ , as

$$\text{COV}_T(X,Y) = (1/L) \sum_{t'=-L/2}^{t'+L/2} ( [ X(t+t') - \bar{X}(t) ] [ Y(t+t') - \bar{Y}(t) ] ) \quad (3.4)$$

where the subscript  $T$  refers to a non-detrended statistic. Similarly the variance could be defined as above (eq. 3.4) by replacing  $Y$  with  $X$  for  $\text{VAR}(X)_T$  and vice versa.

It is important to notice that  $\bar{X}$  and  $\bar{Y}$  are functions of  $t$  and in this way the covariance is the same as that which would be obtained by breaking the data up into blocks of length  $L$ . This is not the same result as would be obtained if  $X'$  and  $Y'$  were first obtained using a high pass running mean filter and then the boxcar average of their product was taken. The covariance calculated in that manner would have  $t+t'$  as the argument for the means  $\bar{X}$  and  $\bar{Y}$  (Stage and Crescenti, 1988).

We can next define the correlation between  $X$  and  $Y$  as

$$\text{COR}_T(X,Y) = \text{COV}_T(X,Y) / [\text{VAR}_T(X) \text{VAR}_T(Y)]^{0.5}. \quad (3.5)$$

Finally we define the detrended covariance of X and Y as

$$\text{COV}(X,Y) = \text{COV}_T(X,Y) [ 1 - \text{COR}_T(X,t) \text{COR}_T(Y,t) / \text{COR}_T(X,Y) ]. \quad (3.6)$$

A detrended correlation can be defined from COV(X,Y) in the same manner as the non-detrended correlation defined previously. Also the COV as defined above is the same value as would be obtained by taking a block of data centered at time t and calculating the covariance with linearly detrended X and Y (Stage and Crescenti, 1988). That is to say, each boxcar statistic is a linearly detrended value. All of the statistical calculations made in this study use the detrended covariances and correlations.

### **3.2 The Hilbert Transform**

The statistics for the covariance and correlation described above are useful in determining the relationship between two variables which have the same phase relationship. Unfortunately, in meteorology variables are often not in phase with each other and may be in quadrature or at some arbitrary phase relationship. In an effort

to deal with this situation we have made use of the Hilbert transform. An explanation of the Hilbert transform as it relates to this study is offered below.

The use of the Hilbert transform in data analysis is considered an acceptable technique in the determination of the phase and coherence relationships between two real time series (Bendat and Piersol, 1986). The definition most relevant to this study for the Hilbert transform is that of a ( $\Pi/2$ ) phase shift of the original time series. Let  $X_H(f)$  be the Fourier transform of  $X_H(t)$ , that is

$$X_H(f) = F[X_H(t)] = \int_{-\infty}^{\infty} X_H(t) \exp(-i2\Pi ft) dt. \quad (3.7)$$

Conversely,  $X_H(t)$  is the inverse Fourier transform of  $X_H(f)$ . This definition of the Hilbert transform consists of passing  $X(t)$  through a system which leaves the magnitude of  $X(f)$  unchanged, but changes the phase of the variable by  $\Pi/2$ . Since we have taken the FFT of the original time series we are dealing with the variable in a phase domain. We now have the time series in the form of sines and cosine series and, with the linearity of the FFT, the Hilbert transform becomes an algebraic procedure. Simply put, in words, the shift is a positive  $90^\circ$  for positive frequencies and  $-90^\circ$  for all negative frequencies. For a simple time series consisting of a sine wave, the result of the Hilbert transform would be a cosine wave. Similarly the transform of a cosine would be a minus sine. For a complex valued time series the transform

of cosine + i sine should be -sine + i cosine, where i refers to the square root of -1.

### 3.3 Calculation of Coherence and Phase Angle

Using the boxcar procedure discussed in section 3.1.2 to calculate the covariance of two variables, along with an algorithm supplied by Dr. J. Alhquist (personal communication) for the calculation of a Hilbert transform as discussed in the previous section, we are able to calculate the  $COV(X_H, Y)$ , also known as the quadrature. The quadrature gives us an indication of how two variables are related at a 90 degree phase relationship. As mentioned previously, there are times when two variables are varying together in a manner which would not be revealed by the basic statistics, much in the way that the covariance of a sine wave and cosine wave would be zero. This is the type of relationship that we might expect for buoyancy waves in the atmosphere where theta (potential temperature) fluctuations are characteristically 90° out of phase with fluctuations in W, the vertical velocity. In contrast, in turbulence these two variables tend to be either in phase or 180° out of phase (Stull, 1988).

Once we have calculated these two quantities, the covariance and Hilbert covariance, we define the coherence as

$$COH(X, Y) = [ COR(X, Y)^2 + COR(X_H, Y)^2 ]^{1/2} \quad (3.8)$$

where the detrended covariances are used for the calculations (Stage and Herbster, 1989). The final statistic for the boxcar is the detrended phase angle. From the calculations already made we now form the phase angle as

$$\text{Phase}(X,Y) = \text{Tan}^{-1} [ \text{COR}(X_H, Y) / \text{COR}(X,Y) ]. \quad (3.9)$$

The determination of the phase angle for this research has a somewhat complicated meaning. When one describes the phase relationship between two variables the context is usually with respect to time. Due to the nature of the use of a moving aircraft as our measurement platform we must again remember that we are dealing with both a spatial and temporal domain. This concept is particularly important in the calculation of the phase angle between two variables. For the purpose of this study all flight tracks are plotted, and calculated, with respect to the southernmost end of the flight track. For all of our phase angle calculations a reference to a positive phase relationship means that the changes in the first of the two variables lead the changes in the second variable by the given phase while traveling from south to north. In the above notation, if the  $\text{Phase}(X,Y) = 90^\circ$ , then fluctuations in variable  $X$  occur in advance of fluctuations for variable  $Y$  as we travel from south to north in such a way that when  $X$  is changing most rapidly,  $Y$  is changing at its

slowest rate.

We now have a series of statistical operations which will enable us to (1) remove some of the highest frequency energy through the moving boxcar average, (2) provide a linearly detrended statistic for each box car, and (3) describe how two variables are interrelated, both in phase and out, along with an estimate of the phase relationship between the two variables.

As a closing remark we would like to remind the reader that this technique is relatively new when used for the estimation of turbulent quantities. At this point there have only been a few published results from this technique (Crescenti, 1988; Stage and Crescenti, 1989; Stage and Herbster, 1989; Stage et al., 1990; Friehe et al, 1990) and although the results have been quite promising, at times it is not always clear what the physical mechanisms are behind a specific feature in a curve. We do feel that the results from this method show aspects of the turbulent motions which are not apparent from other analysis methods and feel that as this technique becomes more widely used its attributes and limitations will become clearer. For example, one of the attributes of this technique is the fact that it is equivalent to breaking the data up into smaller blocks. This aspect enables us to obtain an estimate for the various statistics which is valid for a particular region along a flight leg. This is particularly important when looking for effects due to inhomogeneities along the flight leg.

## CHAPTER 4

### CASE ONE: 14 FEBRUARY, 1986

#### 4.1 Synoptic Forcing in the Region

The synoptic conditions for the duration of Phase II have been cataloged by Fellbaum et al. (1988). A summary of the conditions for the 14th of February 1986 is contained in the following paragraphs while the appropriate synoptic maps from NMC for the period of interest beginning on the 14th of February are included in Appendix B for reference.

On the 14th of February there was an increase in surface pressure as the subtropical high pressure system common to the region redeveloped after the passage of a cold front on the 13th. The wind shifted direction from the northwest to the northeast and decreased in strength from 12 m/s to 5 m/s. The SST was 2° C to 6° C warmer than the air temperature.

The MABL, defined as the well mixed region in which there is little or no vertical gradient of potential temperature or specific humidity, extended to a height of about 1500 m as measured from ship soundings over the warm water (Fellbaum et

al., 1988). Surface values for theta and Q were 288° K to 290° K and 6 g/kg to 8 g/kg respectively.

## 4.2 The Vertical Structure From Aircraft Profiles

### 4.2.1 The North Side

The boundary layer profiles are available at various times for the 14th of February as the aircraft was flying many legs at different altitudes. As the NRL-P3 moved from one flight level to the next, an ascent or descent profile was obtained for the atmosphere between the two different flight levels. The MABL is perhaps best represented by north profiles 3 (100-500m) and 2 (775-1800m). Profile 3 was obtained after track 5 (100m), while profile 2 was obtained between track 3 and track 4. In this case both profiles were ascent profiles.

Figure 4.1 (a-h) shows the results of the north side ascent profiles. By inspection of the potential temperature, theta (fig. 4.1a-b), one sees that the boundary layer is very well mixed throughout the lowest kilometer to a height of about 1050 m. The wind speed (fig. 4.1c-d) and direction (fig. 4.1e-f) curves reinforce this with a pronounced minimum in speed at about 1050-1100 m and abrupt directional changes in the same region. This minimum in speed at the base of the inversion is in agreement with the results of Stage et al. (1990) and is coincident with an area of

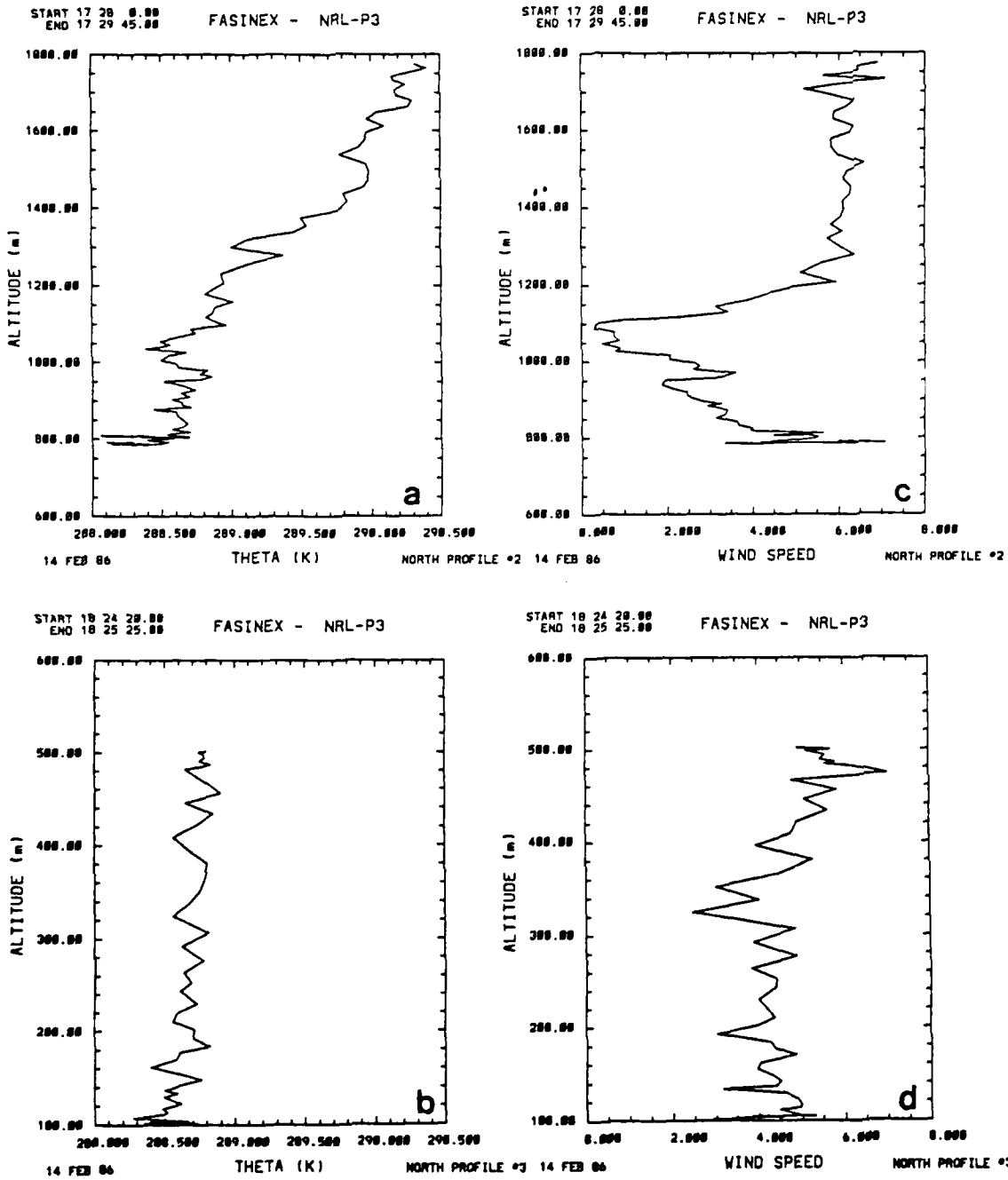


Figure 4.1 (a-h) North Profiles - 14 FEB 86  
(a-b) Potential temperature (K); (c-d) Wind Speed (m/s)

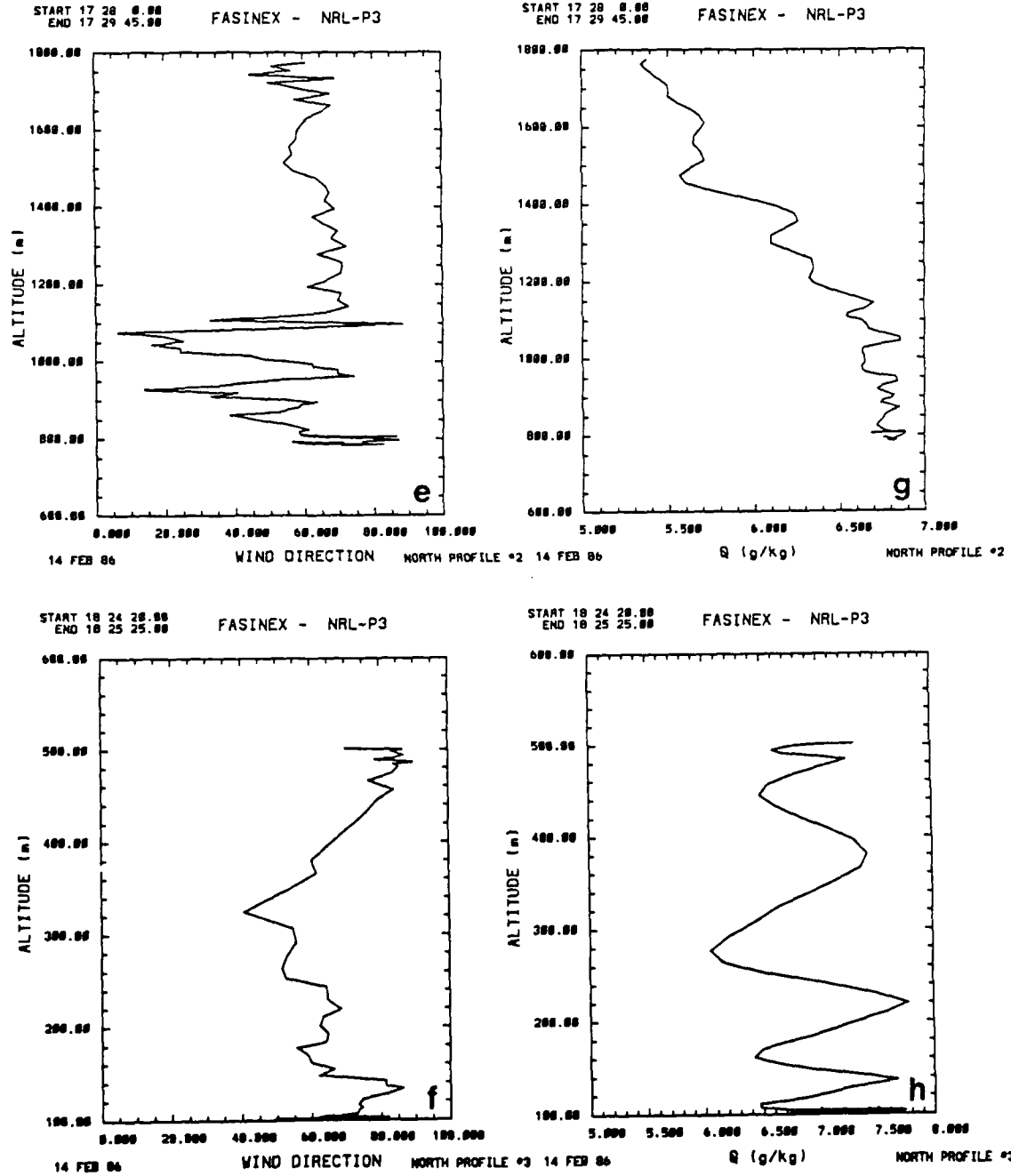


Figure 4.1 (a-h) North Profiles - 14 FEB 86 (cont.)  
 (e-f) Wind Direction; (g-h) Specific Humidity (g/kg)

significant directional shear. The specific humidity,  $Q$  (g/kg), (fig. 4.1g-h) also shows a well mixed layer up through to about 1 km.

#### 4.2.2 The South Side

The south profile for the 14th was recorded while the aircraft was descending from track 4 (1800m) to track 5 (100m). Figure 4.2 (a-d) gives the south profiles for the lowest 1800 m. Again beginning with theta (fig. 4.2a) we see a very well mixed boundary layer up through about 1300 m. Wind speed (fig.4.2b) and direction (fig. 4.2c) do not show as sharp a division as theta, though each does show the region around 800-1300 m to be a significant region of change. Finally,  $Q$  (g/kg) (fig. 4.2d) offers some evidence for the boundary of the mixed layer as the water content is relatively constant up to about 1300 m where there is a rapid increase, followed by a sudden decrease. Given that this profile was obtained during a descent it is likely that this sharp increase was due to an instrumental overshoot as the aircraft descended. In general, for this day the boundary layer shows a much more uniformly mixed composition on the south side than what is found on the north side.

In summary, from the aircraft profiles, we find that the boundary layer is somewhat deeper on the warm side of the front by an amount equal to about two hundred meters. From this analysis it appears that increased surface heating from the underlying warm water helps to deepen the mixed layer south of the SST front.

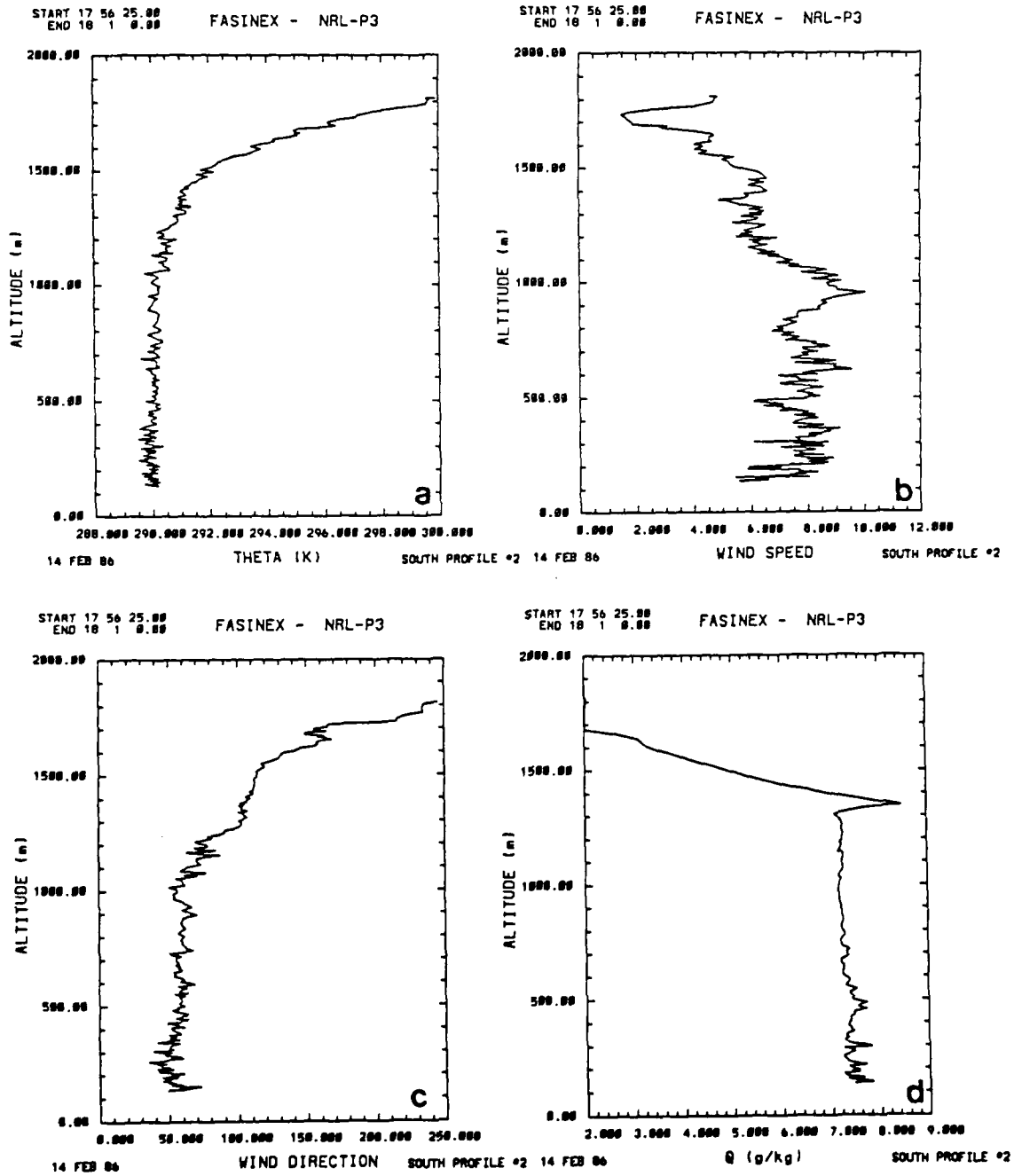


Figure 4.2 (a-d) South Profiles - 14 FEB 86

(a) Potential temp. (K); (b) Wind Speed (m/s); (c) Wind Direction; (d) Specific Humidity (g/kg)

### 4.3 Results from Boxcar Statistics

We now turn our attention to the data obtained during the level flight tracks on the 14th. We must first spend a moment to take a closer look at SST record from this day (fig 4.3). This figure, along with many of the figures to be shown, displays a composite of the various cross frontal legs with the horizontal axis displaying the distance north of the front, as mentioned earlier. Dashed reference lines have been added to the figure to aid in the comparison of the various flight tracks. In general, a vertical dashed line has been placed at the front (distance = 0 km), while horizontal dashed lines have been added either at zero (for covariance and correlation) or at some other value that was chosen for comparison of the various legs.

Returning to figure 4.3, the first item to be pointed out is that track 4 (1800 m) is omitted from the figure because of scale differences. At that level it appears that the radiometer was sensing cloud droplets as the temperature readings are quite cold.

The transition region for the SST is a very complicated feature on this day. The primary transition region is about 10 km wide with an intensity of about 1.5 °C. Just north of the front there is a region of warm water which has about a 0.5 °C jump over a span of ~7 km. South of this warm pool of water the SST returns to essentially the same value it had north of the pool. We will see that this warm pool has an

FASINEX - NRL-P3

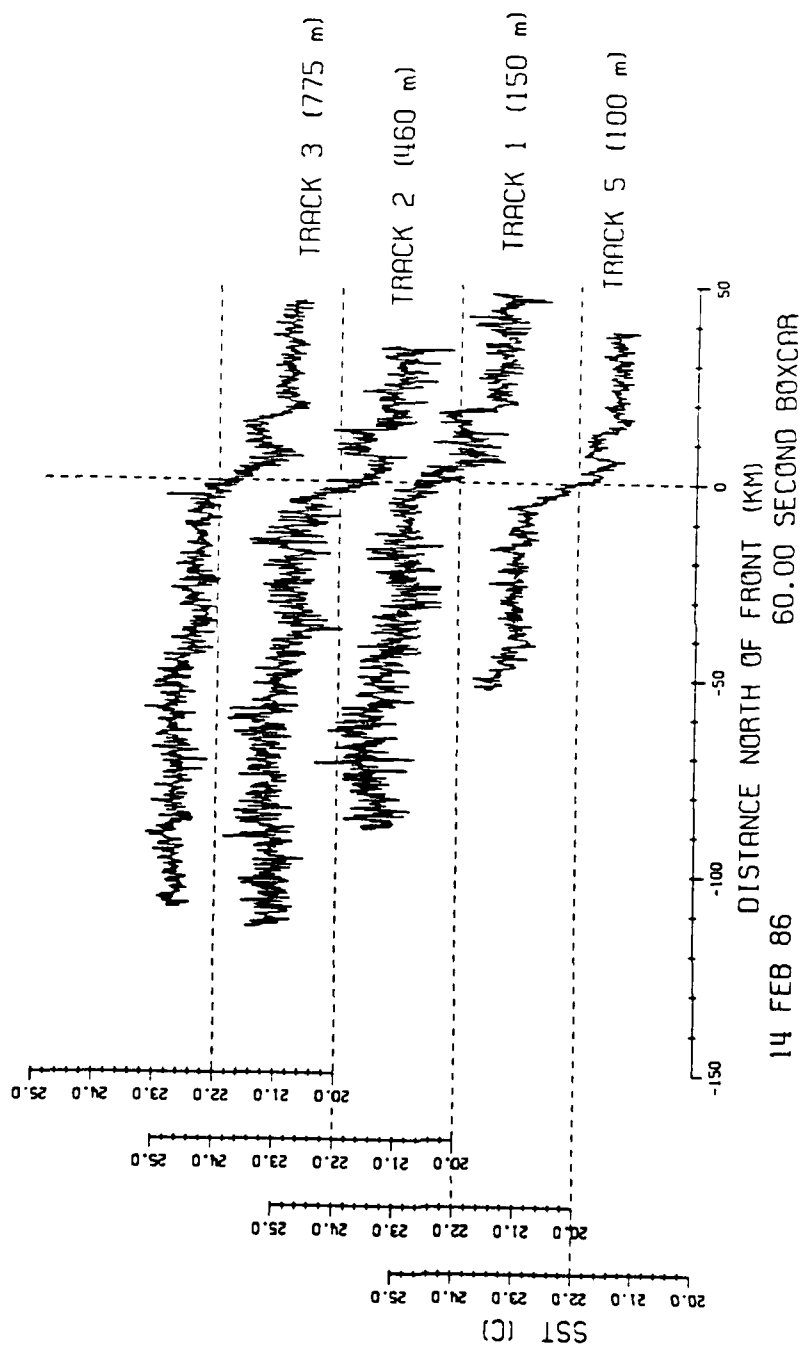


Figure 4.3 SST (°C) from 14 FEB 86 (Track 4 omitted)

effect on the turbulent structure, especially at the lowest levels. South of the front the SST reaches a local maximum at  $\sim$ -25 km and a slight minimum at  $\sim$ -50 km. In general the SST measured from each flight level shows good agreement from one flight track to the next. This is to be expected since the horizontal separation between the various flight tracks is only a few kilometers.

#### 4.3.1 Boxcar Means for Potential Temperature

Theta shows a sharp increase over the warm water at the front on this day, as shown in figure 4.4 (a dashed line is included at 289 K for reference). Track 5 shows a sharp jump in advance of the front concurrent with the warm pool. Track 1 also shows some warming in advance of the front though there is not the same kind of readjustment to the slightly cooler water between the warm pool and the front as is evident for track 5. Tracks 1-3 all increase quite linearly across the front, though each curve shows some degree of complexity in the increase in temperature. There is a decreasing complexity in the structure of the temperature as the altitude increases. Also evident is the apparent 10-20 km lag in the various peaks visible in the three lowest levels. Track 4, again omitted because of scale considerations, shows a fairly uniform temperature across the front, though there is very little fetch over the cold side for this leg.

This figure shows that there is a very rapid adjustment in the air temperature



at the lowest levels. This adjustment, or response, is more gradual as the altitude increases, and is delayed towards the down stream direction increasingly with altitude. This is the type of situation one would expect as the turbulent motions tend to diffuse gradients horizontally as the altitude increases.

#### 4.3.2 The Vertical Heat Flux

Figure 4.5 shows the boxcar covariance (COV) results for W and Theta from the 14th (dashed reference line at 0). For the two lowest levels we find the COV to be positive for almost the entire leg, indicating a transport of heat away from the surface. Both tracks show an increase in COV over the warm water, while track 1 (150 m) shows a more pronounced double peak in the vicinity of the front than does track 5. This pair of, apparently, convective plumes are evident throughout the boundary layer, located directly over the warm pool and the north edge of the front. The 1800 m flight track indicates that one of these plumes even penetrated into the inversion layer over the front as is shown in the figure.

The overall trend from one side to the other is an increase in the upward heat flux for the two lowest tracks over the south side. At 460 m the regions of upward flux are relatively strong ( $\sim 50\text{-}60 \text{ Wm}^{-2}$ ), though there are some regions of downward transport. At 775 m most of the flux is negative except for the convective plumes. However, the values over the warm water are only 30% of the values for

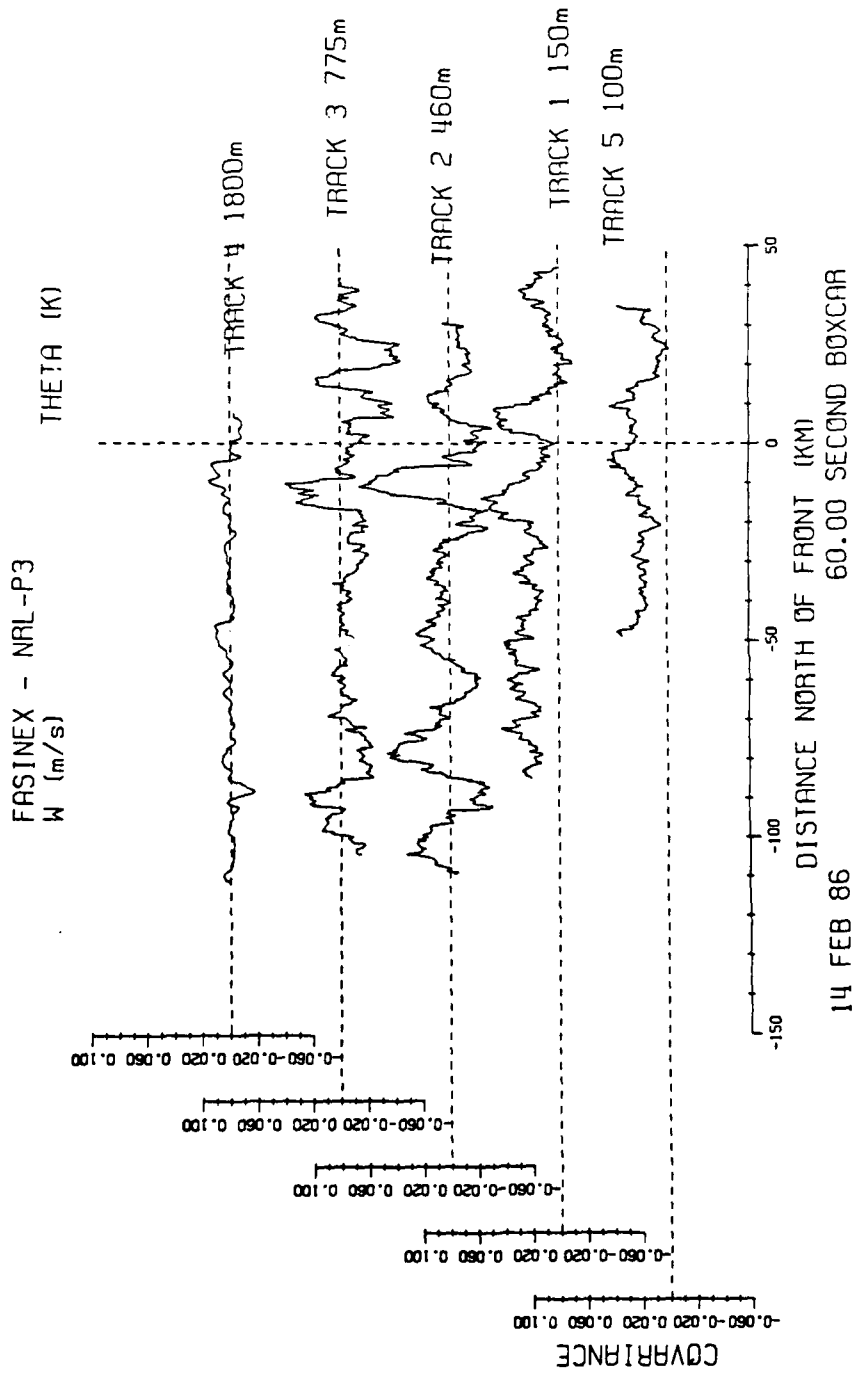


Figure 4.5 Boxcar Covariance (W-Theta) ( $\text{Kms}^{-1}$ ) - 14 FEB 86

the flux over the cold side ( $\sim -4 \text{ Wm}^{-2}$  vs.  $\sim -14.5 \text{ Wm}^{-2}$ ). At 1800 m there is little difference along the track, however, there is little fetch over the north side and it is not possible to make any comparison of the two sides at this level. Despite this, there is little if any heat flux at this level with the exception of a few select features.

The results of the boxcar correlation (COR) calculations (fig 4.6, dashed reference line at 0) shows that  $W$  and  $\theta$ , for turbulence data, are quite well positively correlated in the lowest levels of the BL with a value of  $\sim 0.25$ . This is what we would expect given generally direct circulations (warm air rising / cool air sinking) at these altitudes. Most pronounced are the similarities with the COV. The regions of strong vertical heat flux are also well correlated suggesting a mostly in-phase relationship. At the two middle levels the COR fluctuates slowly with values to either side of zero, especially  $>25 \text{ km}$  south of the front. At 1800 m the COR is somewhat random throughout the entire flight track varying quite quickly in magnitude when compared to the lower levels.

The boxcar coherence (COH) results (fig 4.7, dashed reference line at 0.2) for both the 100 m and 150 m levels shows an increase over the warm water. At 460 m and at 775 m the two variables show evidence of being generally less coherent than at the lower levels. At 460 m there is only a slight net increase in the COH over the warm water. Also, the strong increases seen at the lowest levels are only slight at the middle levels, though they are still visible. At 1800 m, into the inversion

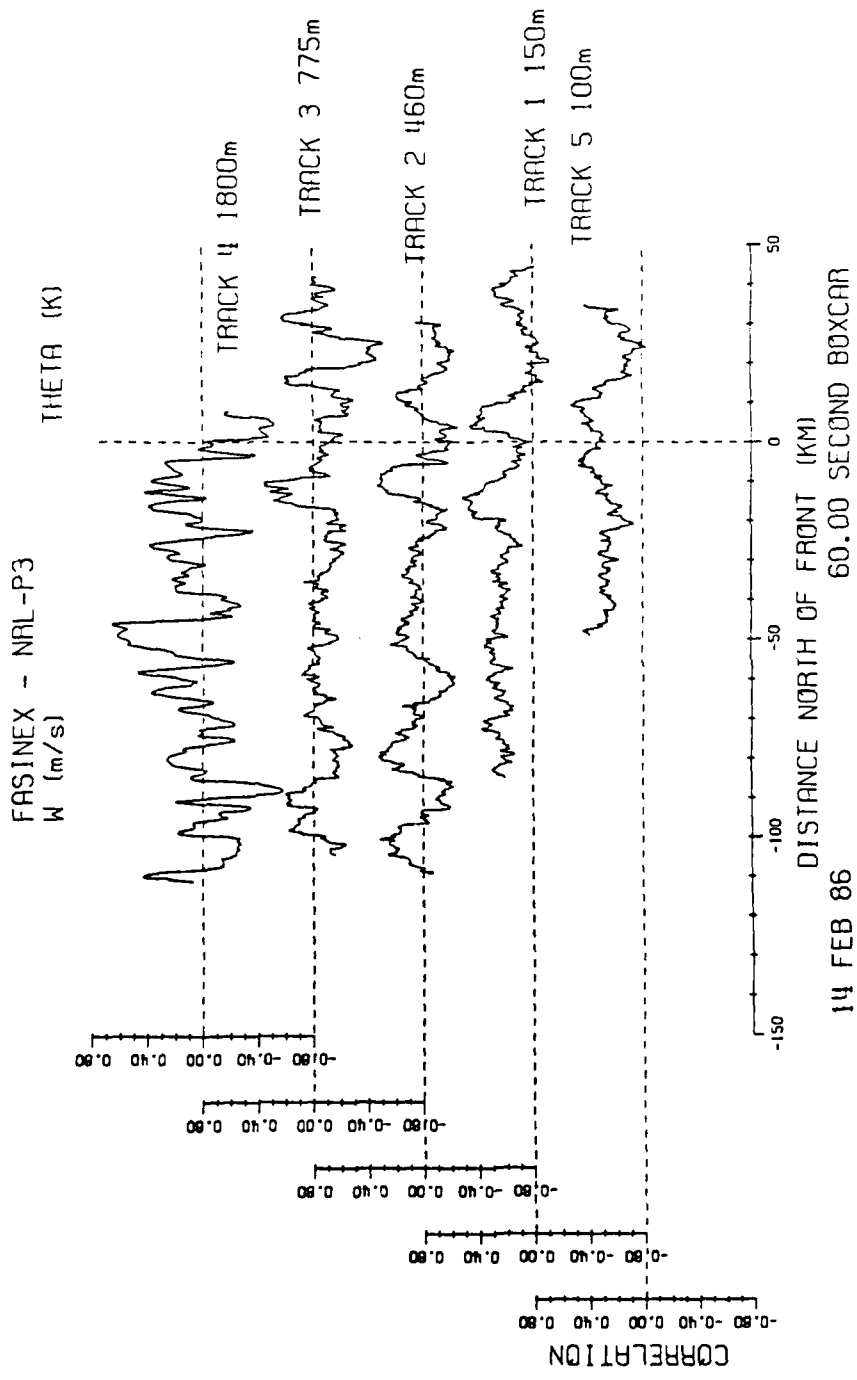


Figure 4.6 Boxcar Correlation (W-Theta) - 14 FEB 86

layer, the COH varies quite rapidly, and it does not have any type of structure to it. The results of the COH calculations show that the turbulent motions of  $W$  and  $\theta$  become more independent of each other as the altitude increases. The high COH values at 1800 m are likely the result of small, similar changes in the two variables,  $W$  and  $\theta$ , which at times give an impression that they are related while at other times show little or no relationship at all.

Figures 4.8 (dashed reference line at  $0^\circ$ ) and 4.9 (a-j) are for the boxcar phase angle (PHASE) calculations. Figure 4.8 shows the actual boxcar values along the leg. Figure 4.9 shows the probability distribution of PHASE binned in five degree blocks, for the north and south sides of each flight level.

At 100 m the PHASE is clustered around  $0^\circ$  on both sides of the front. The distribution of PHASE is narrower over the south side, probably due to the increase in the COV over the warm water. Behavior at 150 m is similar to 100 m except that distribution of the PHASE is much broader at the 150 m level. The 150 m level also shows a region between 15 and 25 km in which the PHASE varies rapidly. This is concurrent with a region in which the COH has very small values. Therefore this is a case of taking the arctan of the ratio of two small numbers ( $\sim 0/\sim 0$ ). When this happens the arctan becomes undefined and there is no phase angle relationship between the two variables. Referring back to fig 4.8, it becomes apparent that the difference between the 100 m and 150 m PHASE distribution can be attributed to

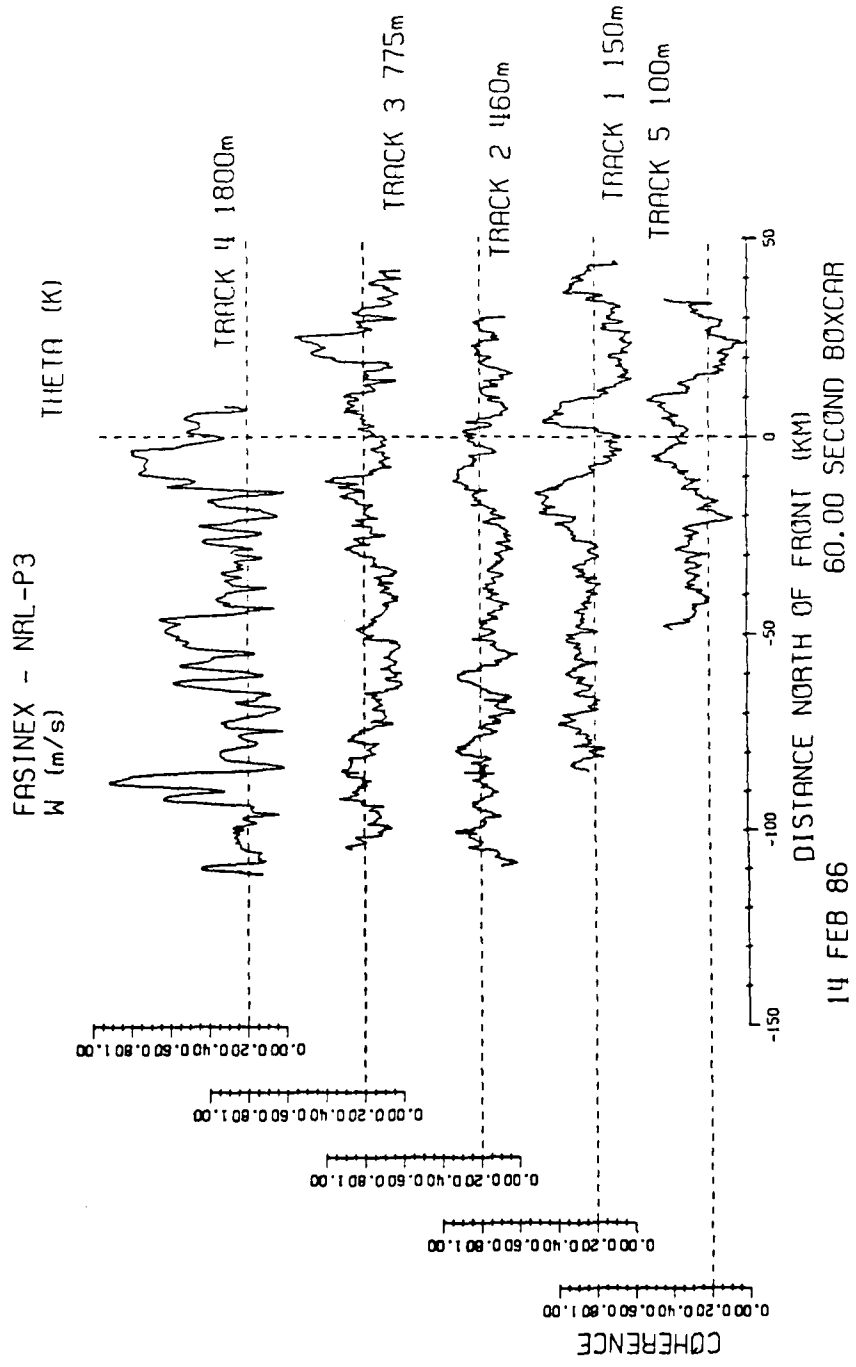


Figure 4.7 Boxcar Coherence (W-Theta) - 14 FEB 86

this region in advance of the front in which the COR and COH both become quite small. Over the warm water the PHASE is again centered near zero with W ranging from  $-30^\circ$  to  $\sim+60^\circ$  with respect to theta.

At 460 m we see that the dominant PHASE relationship is still centered around zero degrees, although it does vary significantly around this value. Over the cold water W tends to lead theta by about  $160^\circ$ , nearly perfectly out of phase. In contrast, south of the front the trend is towards a zero degree relationship, with some evidence of two regions in which W leads by  $\sim 60^\circ$  and by  $\sim 210-240^\circ$ . At 775 m the PHASE relationship is much different from below. At this level we see a strong tendency towards a nearly  $180^\circ$  relationship, though in general there is much more variation at this level than at the lower levels. Above the BL the PHASE relationship has a nearly uniform distribution with only a slight indication of a  $60^\circ$  lag for theta with respect to W. Only a short segment of the flight track at 1800 m is over the cold water and thus there is not a reasonable sample there. Figure 4.9i is only included for completeness.

We can summarize the vertical heat flux for this day as apparently quite responsive to the warm water below. There are two areas of strong convection, both associated with underlying warm water. The relationship between W and theta is quite well correlated, especially at the lowest levels. The two variables are closely in phase at the lowest levels and nearly out of phase in the middle of the BL. In gener-

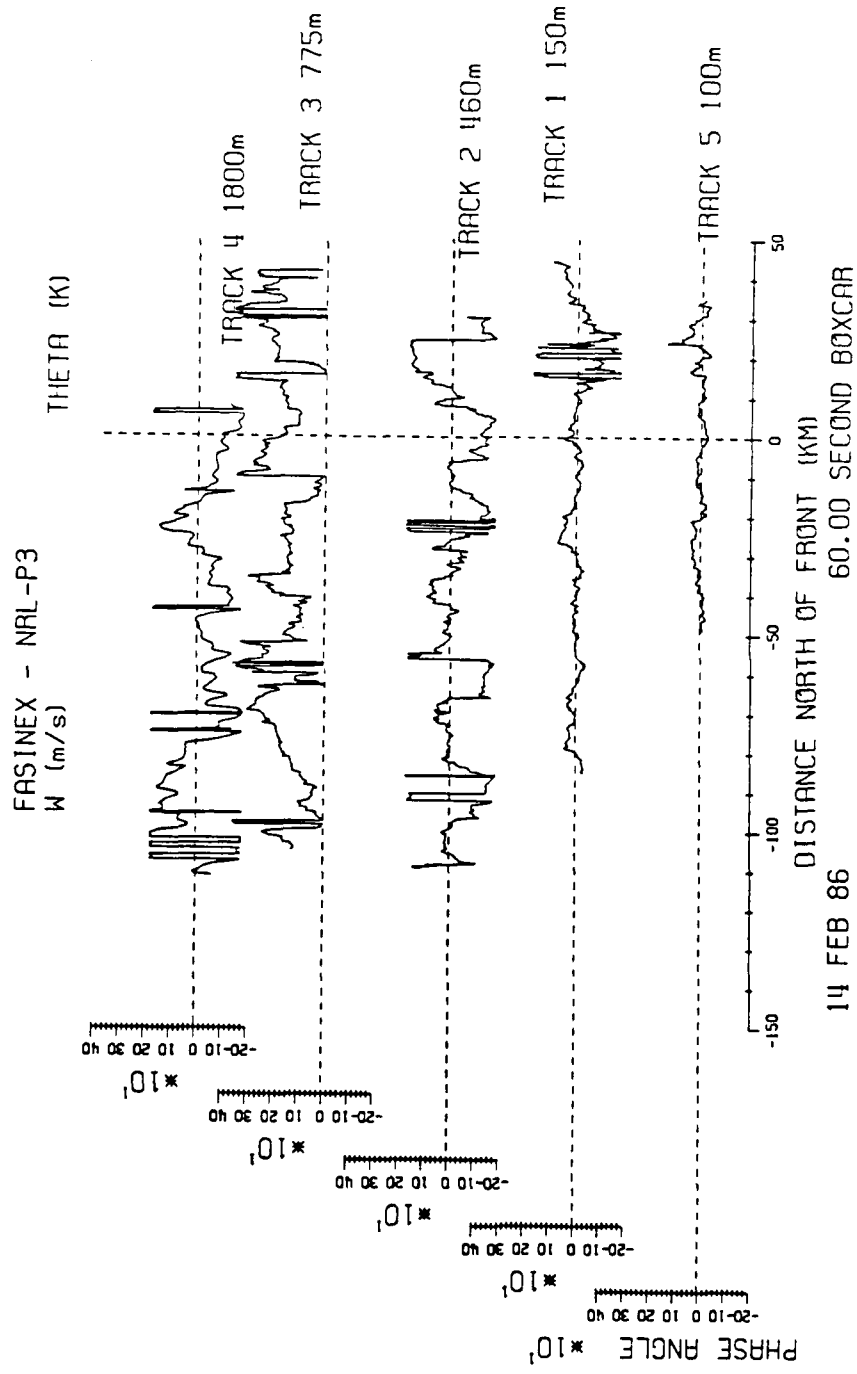
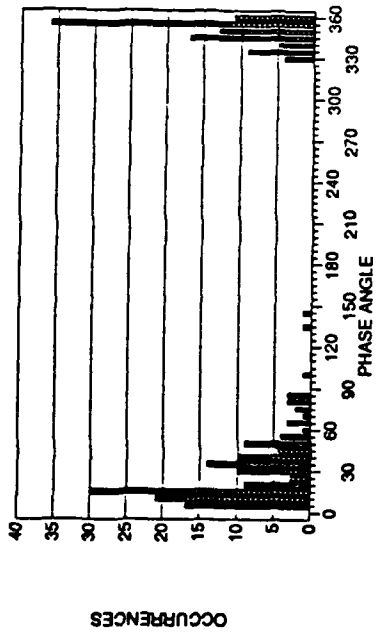


Figure 4.8 Boxcar Phase Angle (W-Theta) - 14 FEB 86

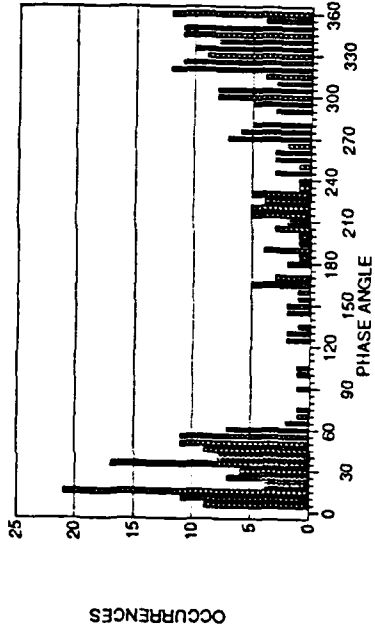
<WT> 14 FEB 86 NRL-P3

TRACK 5 (100 m) North Side



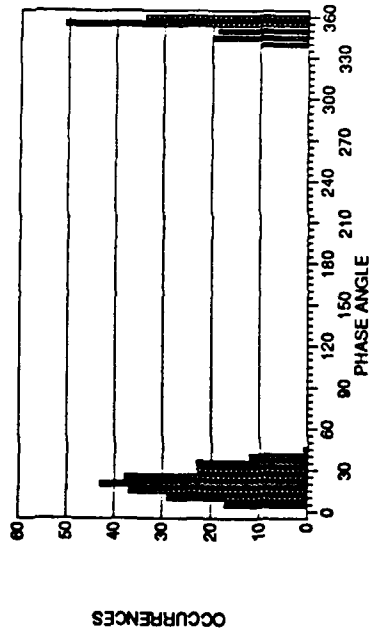
<WT> 14 FEB 86 NRL-P3

TRACK 1 (150 m) North Side



<WT> 14 FEB 86 NRL-P3

TRACK 5 (100 m) South Side



<WT> 14 FEB 86 NRL-P3

TRACK 1 (150 m) South Side

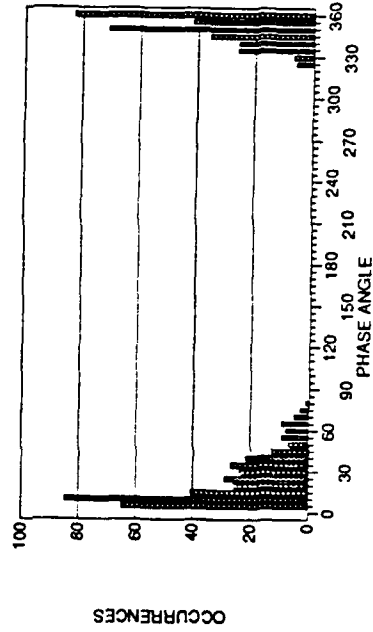
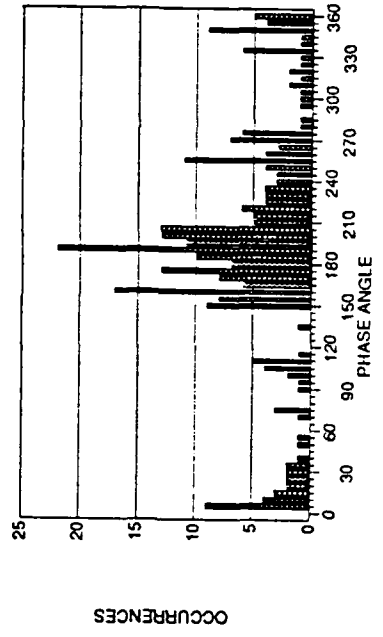


Figure 4.9 Phase Angle PDF for (W-Theta) - 14 FEB 86

(a) Track 5 North Side; (b) Track 5 South Side; (c) Track 1 North Side; (d) Track 1 South Side

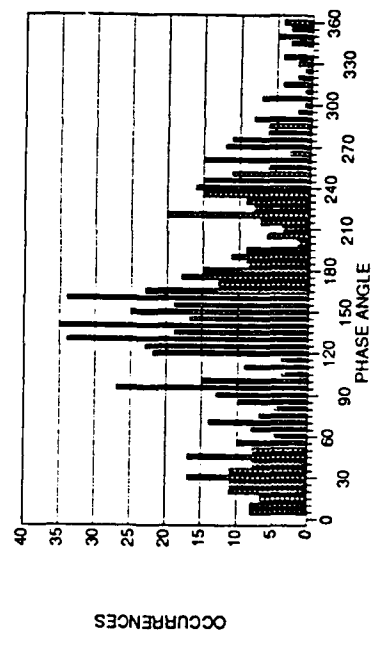
<WT> 14 FEB 86 NRL-P3

TRACK 3 (775 m) North Side



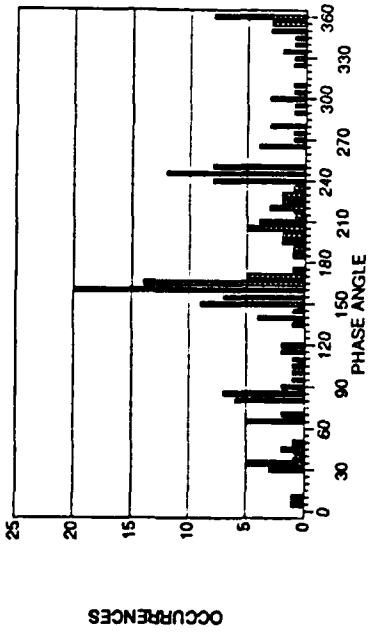
<WT> 14 FEB 86 NRL-P3

TRACK 3 (775 m) South Side



<WT> 14 FEB 86 NRL-P3

TRACK 2 (460 m) North Side



<WT> 14 FEB 86 NRL-P3

TRACK 2 (460 m) South Side

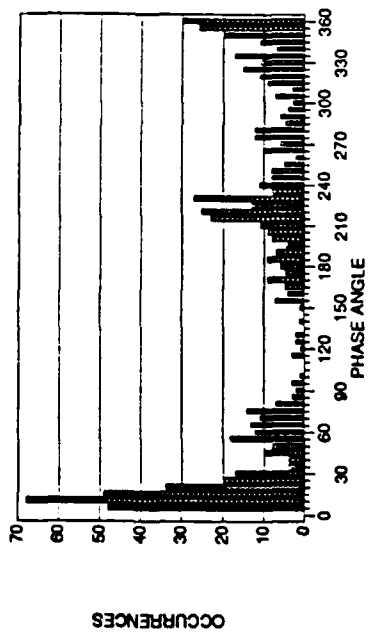
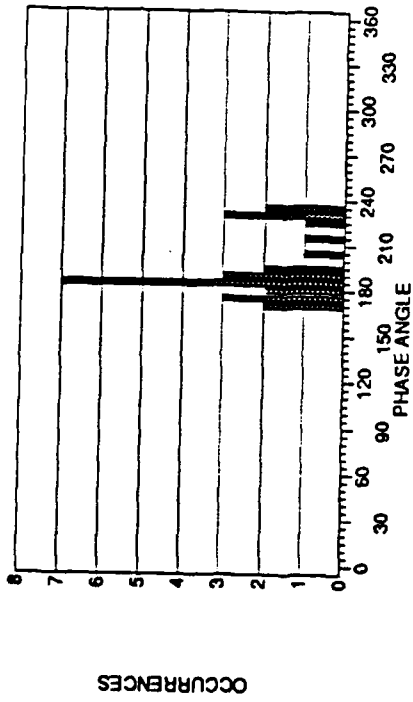


Figure 4.9 Phase Angle PDF for (W-Theta) - 14 FEB 86 (cont.)

(e) Track 2 North Side; (f) Track 2 South Side; (g) Track 3 North Side; (h) Track 3 South Side

<WT> 14 FEB 86 NRL-P3

TRACK 4 (1800 m) North Side



<WT> 14 FEB 86 NRL-P3

TRACK 4 (1800 m) South Side

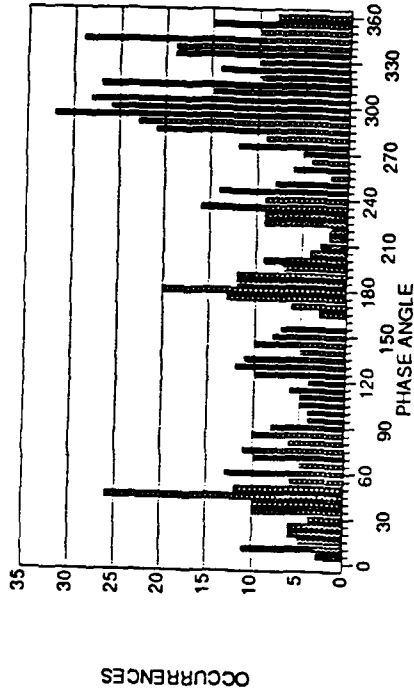


Figure 4.9 Phase Angle PDF for (W-Theta) - 14 FEB 86 (cont.)

(i) Track 4 North Side; (j) Track 4 South Side

al there is a more "in phase" relationship over the warm water when compared to the cold side at any one level within the BL, though this is less noticeable at 775 m. At the top of the BL there is much less uniformity in the phase relationship between  $W$  and  $\theta$ .

#### **4.3.3 Boxcar Variance for Potential Temperature**

Having looked at the vertical heat flux we will now turn our attention to the turbulent fluctuations of the potential temperature. The results for the boxcar variance (VAR) calculations for  $\theta$  are shown in figure 4.10 (dashed reference line at 0.01). As we inspect this figure it becomes quite apparent that the warm pool in advance of the front has an effect on the variance of  $\theta$ . Each of the levels within the BL shows a close connection with the change in SST. At each level there is a pronounced drop in the VAR over the cold water and subsequently a sudden increase in the VAR further to the south. For tracks 1 (150 m) and 3 (775 m) the drop occurs right at the north edge of the warm pool and the increase is directly over the warm pool. At the 100 m level the drop and subsequent increase occurs about 10 km to the north of the north edge of the warm pool. At 460 m the initial drop occurs over the north edge of the warm pool but the VAR remains suppressed until the southern edge of the pool. At this point it is not clear why these differences exist. Just to the south of the front tracks 1-4 all show a region of increased variance. This

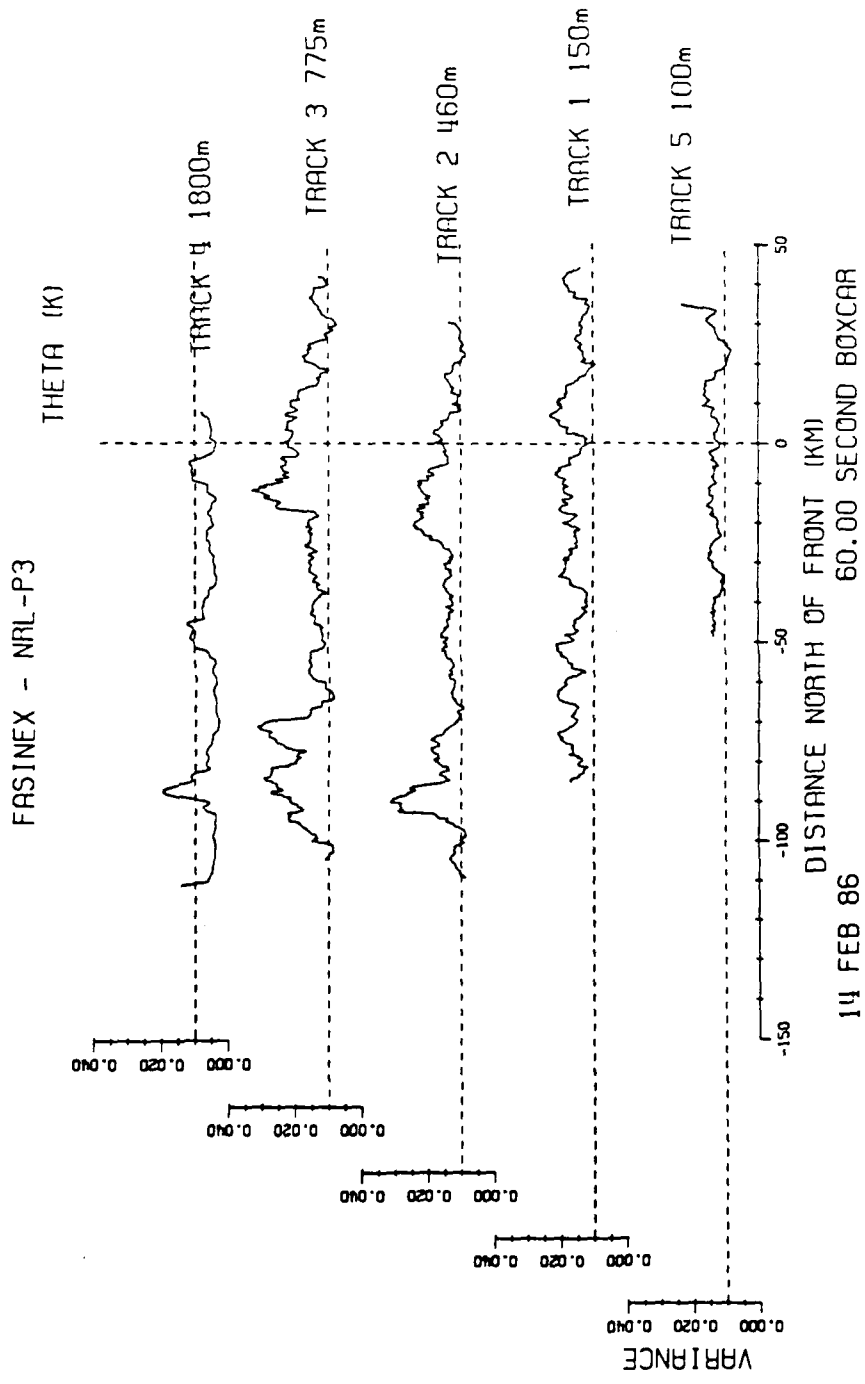


Figure 4.10 Boxcar Variance Theta ( $K^2$ ) - 14 FEB 86

region, which varies slightly in width from level to level, is also concurrent with the southernmost region of increased vertical heat flux associated with the front as was discussed above. The two levels in the middle of the BL (460 m and 775 m) have remarkably similar features suggesting regions of organized convection and an efficient transport of heat in the BL at these levels.

#### 4.3.4 Boxcar Variance for Vertical Velocity

The variance of  $W$  on the 14th is highest in the middle of the boundary layer as exhibited in figure 4.11 (dashed reference line at 0.5). The vertical structure of the variance of the vertical velocity agrees well with previous studies (Stull, 1988, p. 125) which show that the variance of  $W$  usually peaks in the region from  $\sim 30\% Z_i$  to  $\sim 60\% Z_i$ , where  $Z_i$  refers to the height of the inversion layer. Tracks 2 and 3 are at  $Z/Z_i \approx 0.30$  and  $0.50$  respectively. At 100 m, track 5, there is evidence that the warm water has an effect on the variance of  $W$ . The variance of  $W$  for track 5 is much smaller than for tracks 1,2, and 3, but there is a sharp change at the front and the south side averages 30% higher than the north side. This is similar to the results for February 16 (also a north wind day) obtained by Crescenti (1988) and Stage et al. (1990). At 150 m, track 1, the change across the front is much smaller, averaging only a few percent higher on the south side. It is not clear why the difference is as small as it is at this low level.

The highest values for the variance of  $W$  are found at the 460 m flight level.

The variance at this level represents the maximum average value of the five levels, as might be expected for the lower middle of the BL. Again the average variance on the south side is ~30% higher than for the north. At 775 m the variance is decreasing to an average value comparable to track 1, though the fluctuations are somewhat greater at the 775 m level. There is only one apparent connection to the warm water at this level which is a region of increased VAR located between 0 and ~20 km, roughly over, and slightly to the south of, the warm pool. Again we see that the presence of the warm pool has an effect on the bulk of the BL. Both track 2 and 3 show a pronounced increase in the variance of  $W$  in the same area as both the heat flux and variance of  $\theta$  showed increases. This indicates that the warm pool has a significant effect in creating an efficient transport of heat away from the surface and that the increase in the COV of  $W$  and  $\theta$  is due to increases in the variance of both variables. At 1800 m the variance is a full order of magnitude less than that which was found in the BL, again this is much as we would expect at this level located within the lower inversion layer (Stull, 1988). There is the same one feature evident at 1800 m just south of the front which is again concurrent with what was seen for the heat flux and the variance of  $\theta$ . The presence of this feature further supports the assumption that the plume, mentioned above, has penetrated into the inversion layer.

FASINEX - NRL-P3  
W (m/s)

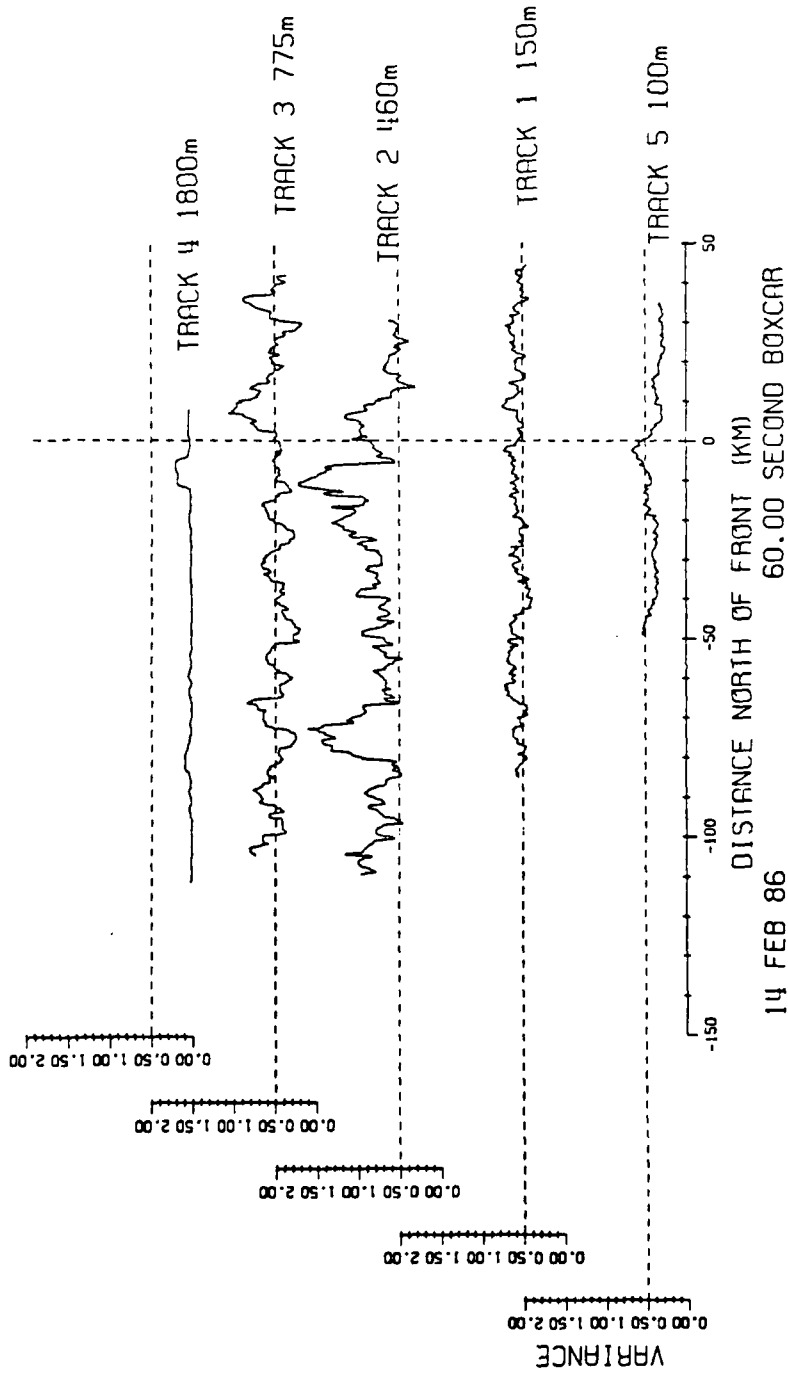


Figure 4.11 Boxcar Variance Vertical Velocity ( $m^2/s^2$ ) - 14 FEB 86

#### 4.3.5 The Vertical Momentum Flux

We now turn to our estimates for the vertical momentum flux. Before beginning the discussion it is appropriate to clarify some of the aspects in the relationship between the covariance, momentum flux, and stress. In classical convective boundary layers we expect the  $COV(UW)$  to be less than zero which indicates transport of faster moving air downward and slower moving air upward. By the usual sign convention this is a downward (negative) momentum transfer and a positive stress. In a convective BL we would expect to see a large negative (positive) covariance (stress) at the surface becoming closer to zero at the top of the BL. The fact that  $COV(UW)$  is generally negative and has the opposite sign as the stress, or momentum transfer, can lead to potential confusion in discussion. In an effort to avoid any potential conflict with this problem, we will try to limit our discussion to the use of the term stress.

Beginning with the covariance ( $COV$ ) for  $UW$  from the 14th (fig 4.12, dashed reference line at 0) there are three distinct patterns. These three patterns or regimes are represented by the surface layer (100 and 150 m levels), the middle BL (460 and 775 m levels), and the flight level at 1800 m into the inversion layer. The general features of these regimes are discussed below.

(1) The first of these regimes involves the two lowest levels which show a

very similar feature at ~10-20 km that is quite well lined up with the warm pool north of the front despite the large difference in time between the two flight tracks. This feature is quite interesting as it is a region of decreased (negative) stress. It is not clear at this point what is responsible for this feature though it does suggest that there are regions within the BL which at times do not conform to the average large-scale expectations. Along with this feature to the north of the front, both of these lower levels show the same general trend of stress values that are somewhat lower than at the middle levels. There is also a noticeable increase in the stress ~30 km south of the front spanning slightly less than 10 km. In general the stress for track 5 (100 m) is lower than track 1 (150 m). It is not clear why this is the case though these legs were separated by slightly more than two hours, thus suggesting changes in the structure of the surface layer in that interval. Friehe et al (1990), using a different analysis technique involving the use of a spectral domain, investigated the north wind case for the 16th at the 30 m flight level and did not find an appreciable difference in the stress across the front. There is no other work at this time which evaluates this day's data from the NRL-P3.

(2) The second regime involves the two middle levels (460 m and 775 m) which also show some similar features with each other, with an indication of about a 5-7 km lag towards the south for the upper level. Track 2 and track 3 both show a broad (~15 km) region of increased stress beginning slightly north of, or at, the front

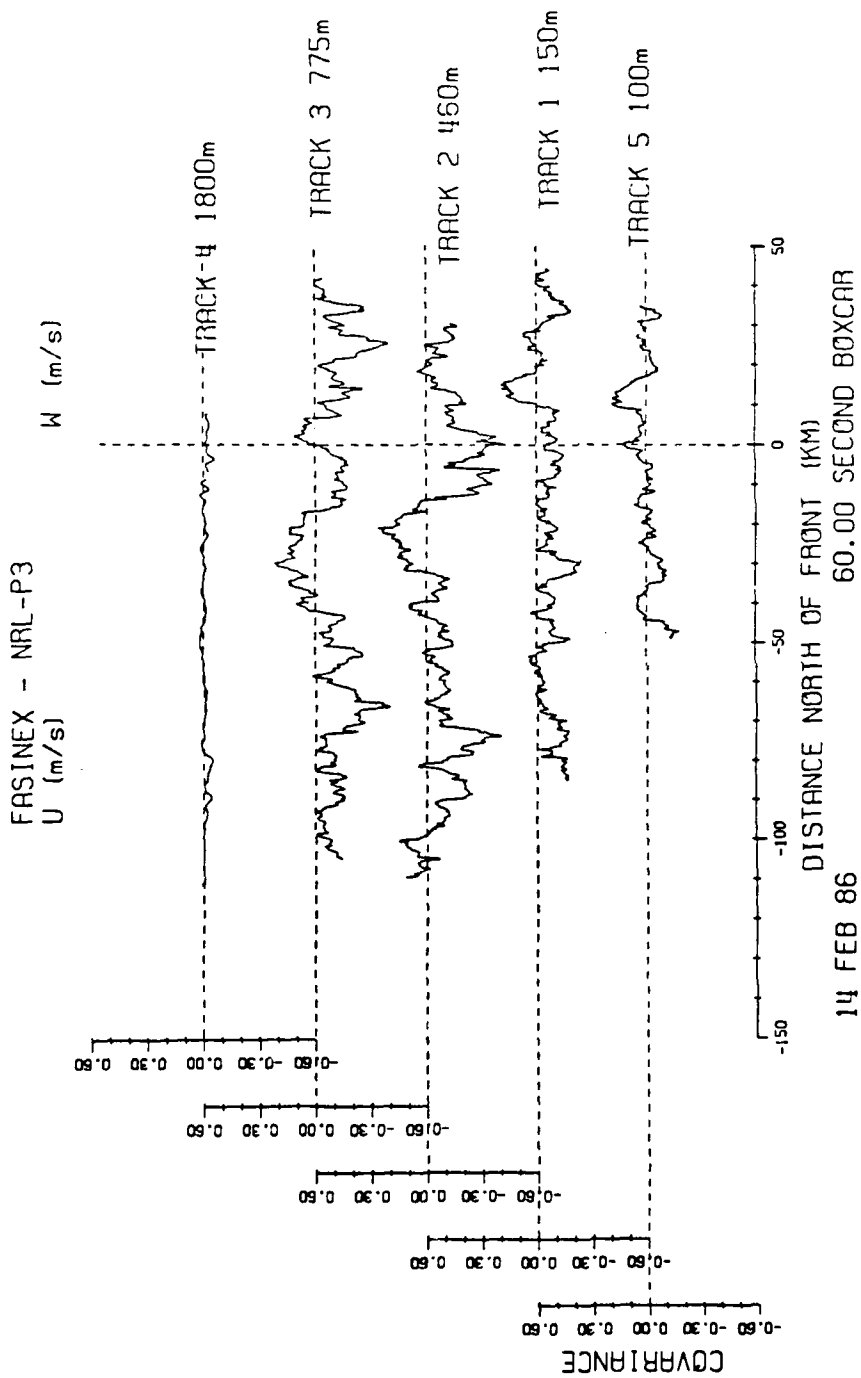


Figure 4.12 Boxcar Covariance (U-W) ( $m^2s^{-2}$ ) - 14 FEB 86

for track 2 and 3 respectively. While track 3 shows the same general feature as at the lower level, it has a somewhat reduced amplitude and a lag of ~6 km. This region is concurrent with the region of increased heat flux mentioned earlier and is representative of a vertical circulation. Just to the south of this high stress region there is another region of reduced stress. Again it is unclear what the mechanism behind these features might be, but these two regions suggest the presence of an updraft/downdraft combination associated with a secondary circulation in the vicinity of the front (Stage and Herbster, 1989). Farther to the south the two legs show little indication of being connected.

(3) Finally, the stress above the BL is very small, on the average an order of magnitude lower than the values found within the BL. Again, this is what we would expect for the vertical momentum flux above the BL (Stull, 1988).

The correlation (COR) for UW (fig 4.13, dashed reference line at 0) shows essentially the same features as did the COV with the exception of the 1800 m level. This indicates that the fluctuations in the stress were caused by similar changes in both the fluctuations in U and the fluctuations in W. Typically the values of the COR range between +/-0.20 within the BL with the absolute value becoming somewhat larger as the flight level increased. At 1800 m the COR varies quite rapidly and with no distinct pattern. This behavior suggests that the fluctuations of these variables at this level, within the inversion layer, are mostly random and

independent of each other.

The coherence (COH) (fig 4.14, dashed reference line at 0.2) between any two levels compares best for tracks 2 and 3, at least in the vicinity of the front. In this region we see the same lag relationship as for the COV. The COH for track 1 through track 3 drops by about 10% when averaged over the warm side of the front compared to the cold side.

The phase angle (PHASE) between U and W for the 5 tracks is shown in figures 4.15 (dashed reference line at  $90^\circ$ ) and 4.16(a-j). In figure 4.15 the discontinuities are mainly the result of the COH going to zero. When this happens there is no phase relationship between the two variables and the PHASE becomes undefined. From fig. 4.15 it is apparent that the two lowest levels have a PHASE relationship in which U leads W by  $\sim 90$ - $100^\circ$  while traveling from south to north. From fig 4.16(a-d) it is apparent that on the south side of the front the relationship is more organized than on the cold side. This is slightly more evident at 100 m than at 150 m. At 100 m there is a distinct difference in the preferred PHASE relationship over the two sides of the front. Most of this difference can be attributed to the region from  $\sim 7$ - $12$  km north of the front where the COH is very low. In this region the phase angle is very erratic as is seen in fig 4.15. Over the warm water both levels show two preferred PHASE relationships as is seen by the double peak structure in fig 4.16 b and d. One peak is located at  $95^\circ$  and the other  $125^\circ$  with a gap at  $110^\circ$ . If this double

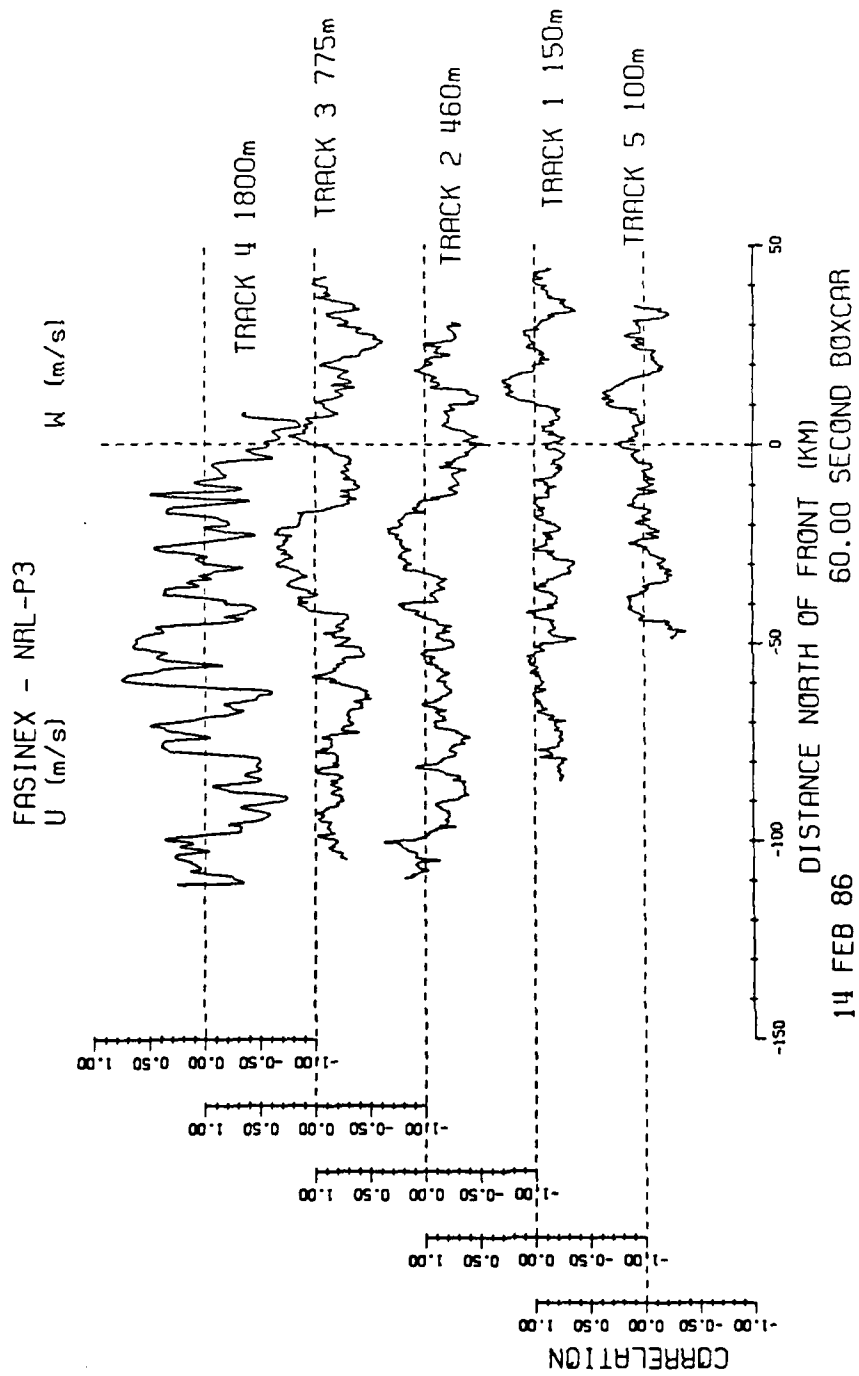


Figure 4.13 Boxcar Correlation (U-W) - 14 FEB 86

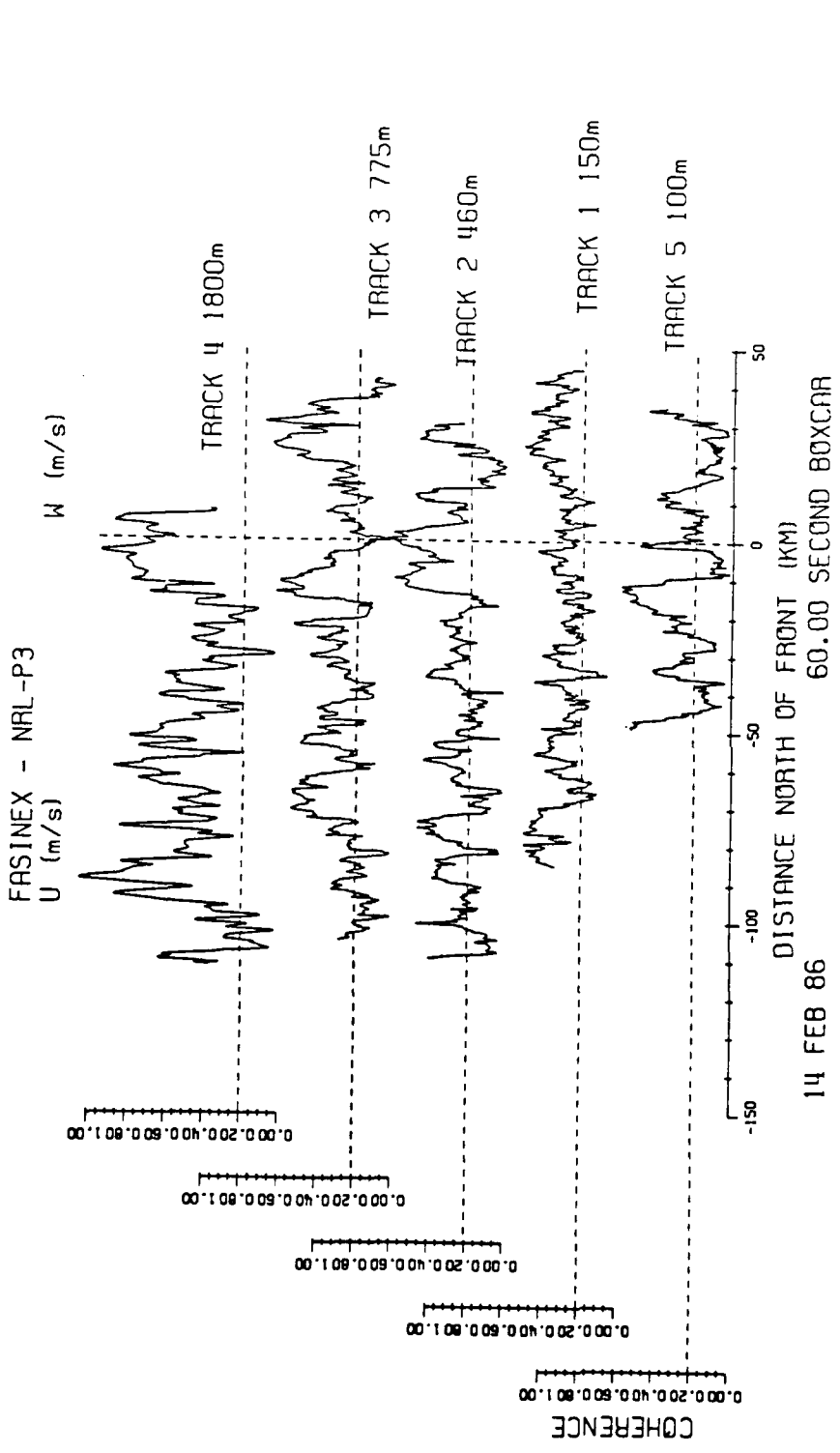


Figure 4.14 Boxcar Coherence (U-W) - 14 FEB 86

peak was seen at only one level it would not be considered significant, but since we see this same structure at both levels it appears to be a real and significant structure. In general, over the warm water U and W are nearly in quadrature, a characteristic quite common for turbulence in the boundary layer (Stull, 1988). At 150 m over the cold water the COH is generally larger than at 100 m and the PHASE is well behaved. The structure of the PHASE distribution from the North and South sides is quite similar. Aside from the less pronounced double peak/gap structure, there is a significant occurrence in the  $45^\circ$  range. This  $45^\circ$  range corresponds exactly to the region of negative stress seen in the COV north of the front between  $\sim 10$  and  $20$  km (see fig 4.12 and 4.15).

At 460 m (fig 4.16e-f) there is a broader distribution of the phase angle over the warm side, though the primary PHASE relationship shows U, while traveling from south to north, leading W by  $\sim 125^\circ$ . Also represented is a cluster around  $180^\circ$  and another around  $45^\circ$ . An inspection of the region where the stress was observed to be negative at this level ( $\sim 15$ - $32$  km south of the front) shows that the PHASE relationship jumped from  $45^\circ$  to  $\sim -25^\circ$  ( $335^\circ$ ) and back to  $45^\circ$ . At 775 m the distribution of PHASE is broader than at the lower levels. This indicates that the turbulent motions are somewhat less organized than at the lower levels. At this level there are a few preferred PHASE relationships south of the front. One in which U leads by  $\sim 120^\circ$  and another with a range of  $\sim 180^\circ$ - $\sim 240^\circ$ . This latter group may

have some structure within itself though we can not be sure from just this one observation. An interesting feature to the south of the front at this level is the lack of occurrences in the vicinity of  $90^\circ$ . While north of the front there are essentially no occurrences outside of the range of  $80^\circ$ - $260^\circ$ , south of the front we find a significant number of occurrences outside of this range. In particular, the region between -15 km and -40 km, where the stress was observed to be negative (fig 4.12), the PHASE varies around  $\pm 45^\circ$ . This is the same type of PHASE relationship as was seen for tracks 1 and 2 where the stress behaved similarly. In each case of the four levels in the BL, where the COV showed a region of negative stress the PHASE relationship was closer to zero than over the rest of the leg and tended towards values in the vicinity of  $\pm 45^\circ$ . Thus at these points, the two variables are not in quadrature but are in more nearly in phase.

A brief inspection of the PHASE for the 1800 m level (fig 4.16i-j) shows that the relationship between U and W within the inversion layer are quite disorganized. This agrees well with the conclusions obtained from the COR and COH (fig 4.13 and fig 4.14) for this level. The one interesting feature to point out is the lack of very many occurrences in the vicinity of  $180^\circ$ . This sharply contrasts the few occurrences which are from over the cold water which are all located within  $\pm 10^\circ$  of  $170^\circ$ . At this point there is no explanation for this type of behavior, and given the relative amplitude for the COV when compared to the lower levels this may not be signifi-

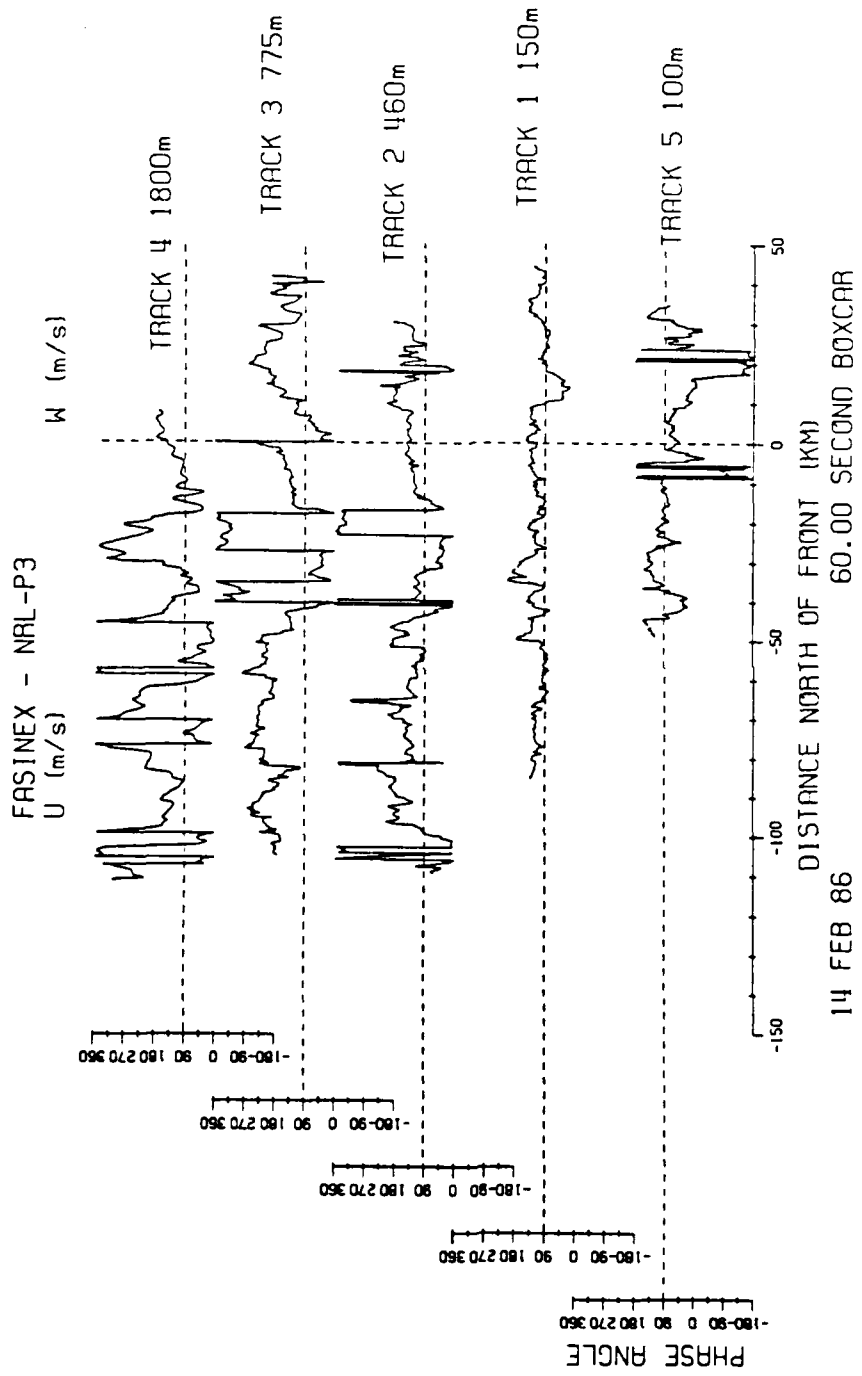
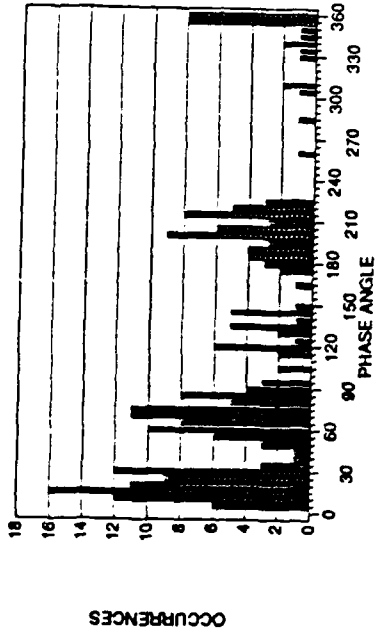


Figure 4.15 Boxcar Phase Angle (U-W) - 14 FEB 86

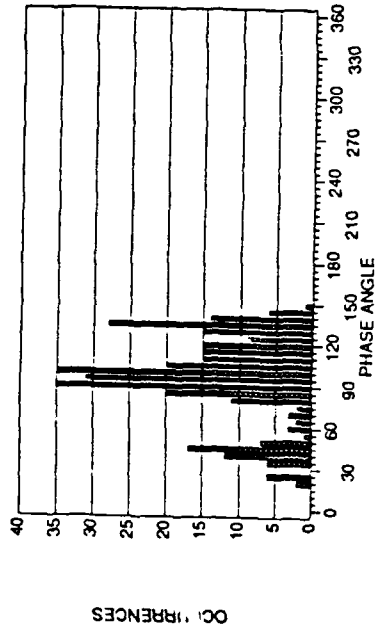
<UW> 14 FEB 86 NRL-P3

TRACK 5 (100 m) North Side



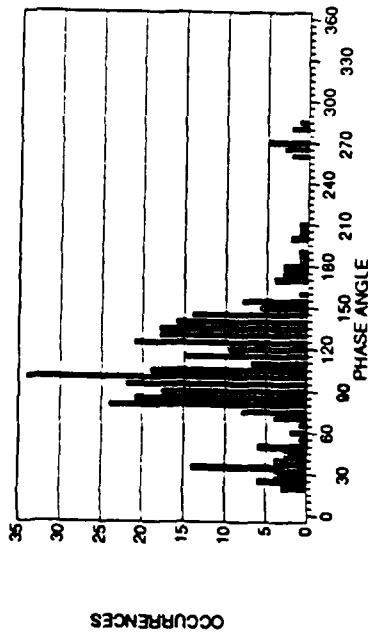
<UW> 14 FEB 86 NRL-P3

TRACK 1 (150 m) North Side



<UW> 14 FEB 86 NRL-P3

TRACK 5 (100 m) South Side



<UW> 14 FEB 86 NRL-P3

TRACK 1 (150 m) South Side

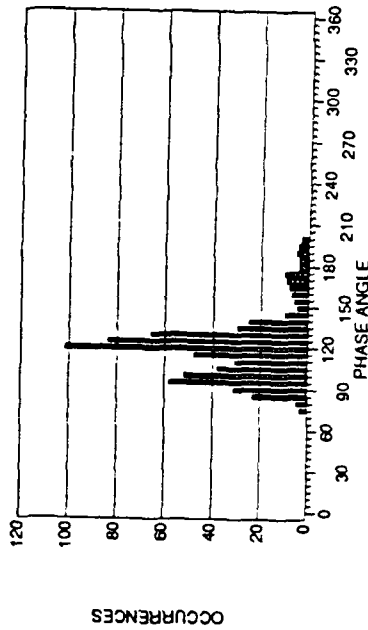
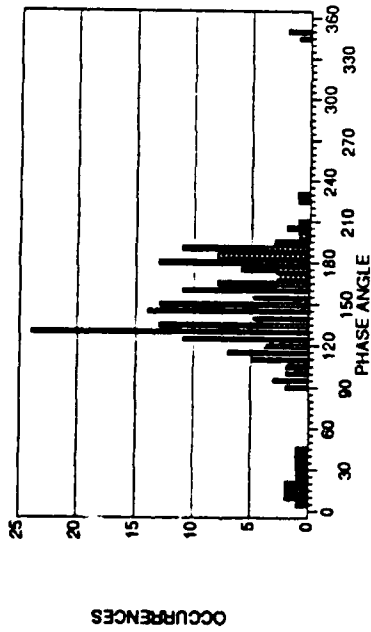


Figure 4.16 Phase Angle PDF for (U-W) - 14 FEB 86  
(a) Track 5 North Side; (b) Track 5 South Side; (c) Track 1 North Side; (d) Track 1 South Side

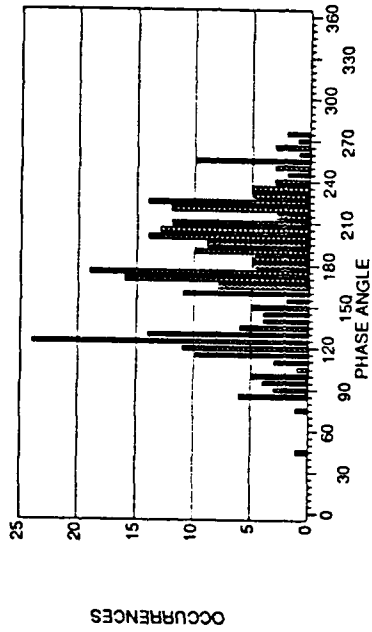
<UW> 14 FEB 86 NRL-P3

TRACK 2 (460 m) North Side



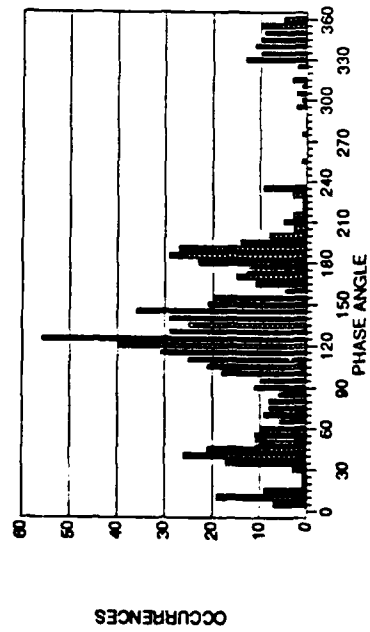
<UW> 14 FEB 86 NRL-P3

TRACK 3 (775 m) North Side



<UW> 14 FEB 86 NRL-P3

TRACK 2 (460 m) South Side



<UW> 14 FEB 86 NRL-P3

TRACK 3 (775 m) South Side

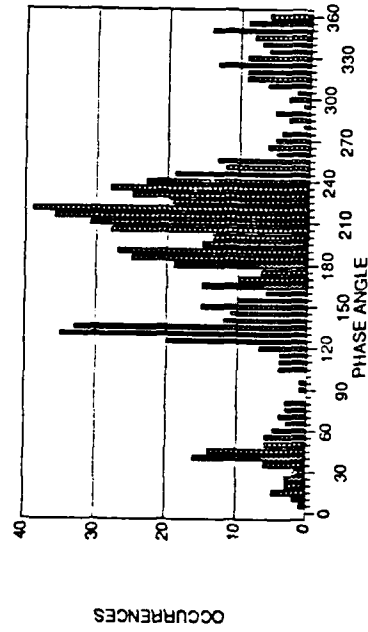
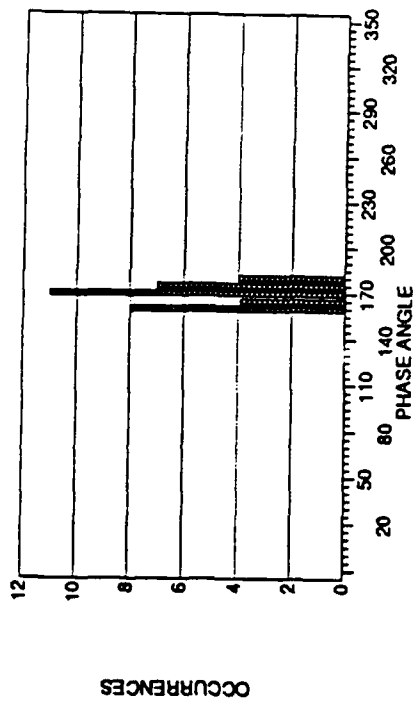


Figure 4.16 Phase Angle PDF for (U-W) - 14 FEB 86 (cont.)

(e) Track 2 North Side; (f) Track 2 South Side; (g) Track 3 North Side; (h) Track 3 South Side

<UW> 14 FEB 86 NRL-P3

TRACK 4 (1800 m) North Side



<UW> 14 FEB 86 NRL-P3

TRACK 4 (1800 m) South Side

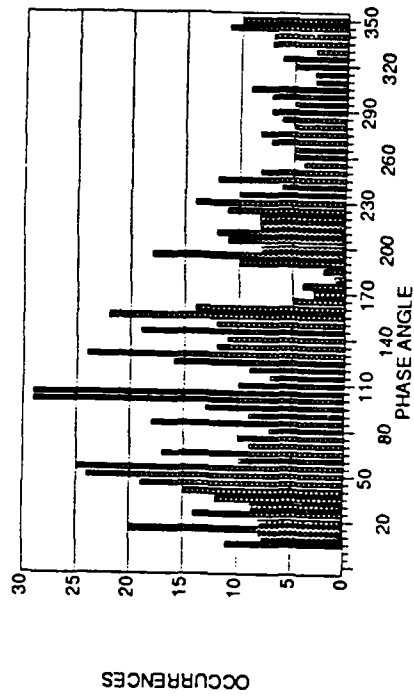


Figure 4.16 Phase Angle PDF for (U-W) - 14 FEB 86 (cont.)

(i) Track 4 North Side; (j) Track 4 South Side;

cant.

#### **4.3.6 The Horizontal Velocity Variances**

Our next topic will be the horizontal component of turbulent kinetic energy (TKE) which can be estimated from the sum of the variances of U and V. Figures 4.17 and 4.18 show the results of the boxcar variances for these two variables from the 14th. Both figures are plotted with the same scales for easier comparison and a reference line has been arbitrarily drawn at  $0.60 \text{ m}^2\text{s}^{-2}$ . From these two figures we see that the amplitudes for both VAR U and VAR V are quite similar, especially in the middle of the BL. At the lowest level, 100 m, the VAR of V is more energetic the VAR of U. One similarity between tracks 1, 2 and 3 is a general increase in the TKE well south of the front. Other than these basic features it is difficult to make any clear connections to the front at each of the levels.

A further comparison of the TKE including the variance of W (figure 4.11) shows that on this day the turbulence was somewhat three dimensionally isotropic. This three dimensional isotropy is what one might expect in a convective environment.

FASINEX - NRL-P3  
U (m/s)

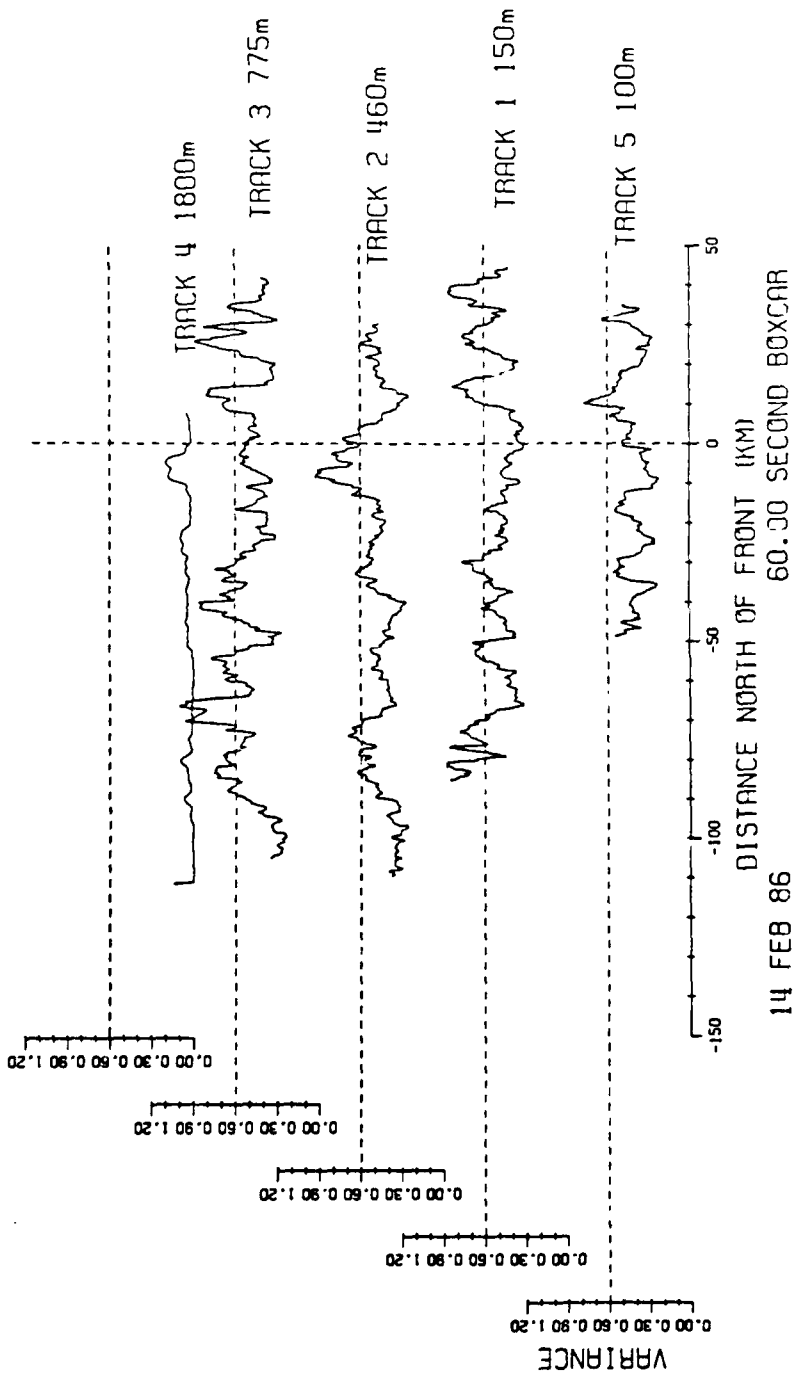


Figure 4.17 Boxcar Variance U Wind Component ( $m^2s^{-2}$ ) - 14 FEB 86

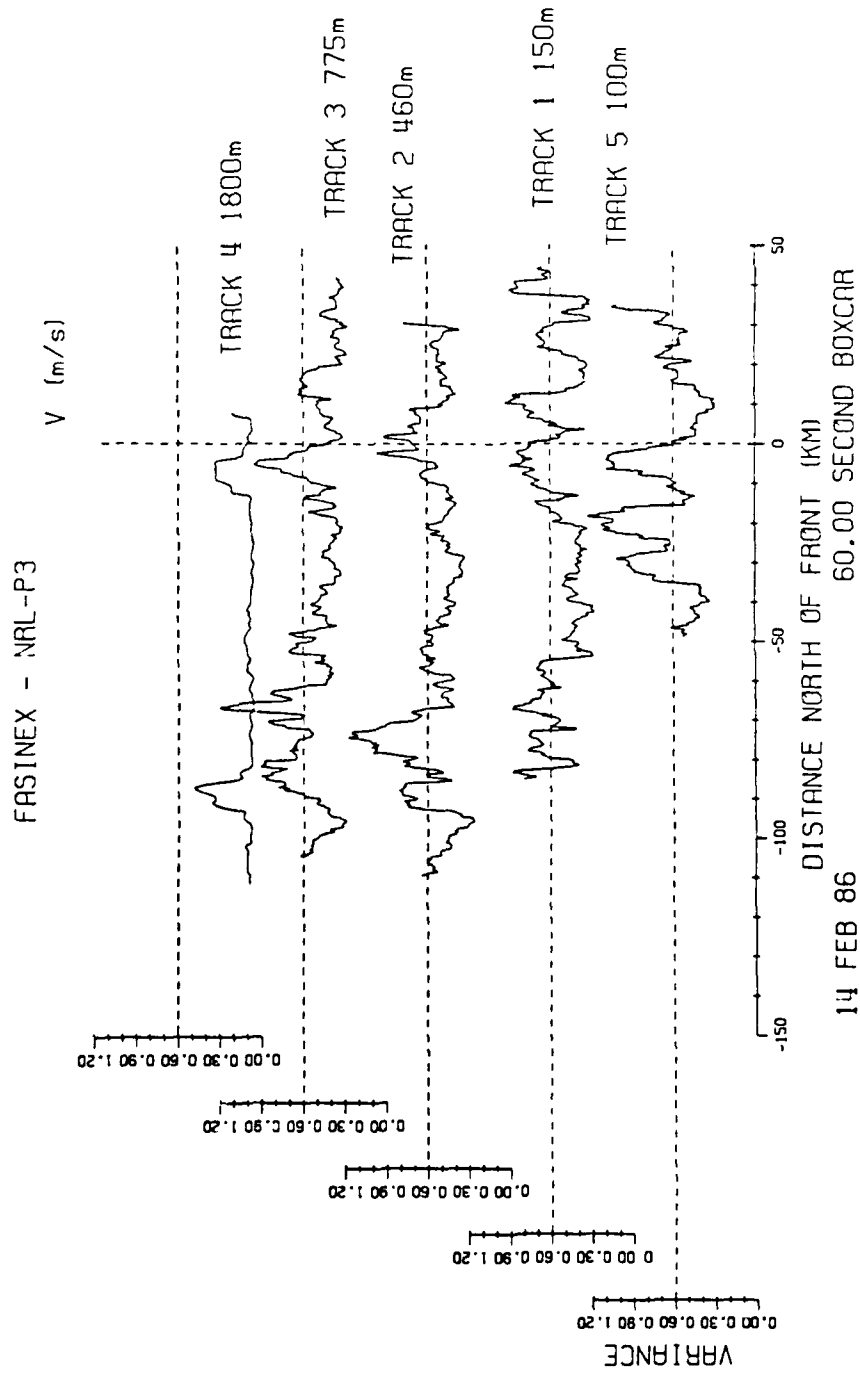


Figure 4.18 Boxcar Variance V Wind Component ( $m^2s^{-2}$ ) - 14 FEB 86

### 4.3.7 Vector Winds

The final figure from this day is for the vector winds plotted along each flight track. This figure has been withheld until now because it is felt that the lack of the Schuler correction for the horizontal wind field might lead to less reliable results. Since the Schuler period is roughly 84 minutes, the amount of power which makes it into a 60 second boxcar is quite small. Thus this problem is not as important for the turbulent quantities of the wind components than it is for the mean components which are used for the wind vectors.

Figure 4.19 shows the vector winds from the NRL-P3 on the 14th. The various legs represent an increase in altitude as we go across the figure from right to left. The most obvious feature in this figure is the large shear between the highest level flown within the BL and the 1800 m level flown above the BL. Less obvious are the subtle changes that occur from one level to the next, and those which occur across the front at any one level. Farthest to the right is the figure for track 5 (100 m). We should remind ourselves, as we look at this figure, that this is one of the last flight legs of the day, and there could be a change in the synoptic or mesoscale conditions from the time that track 1 (150 m) was flown to the time that track 5 (100 m) was flown. What is most obvious about track 5 is the more easterly nature of the wind. Tracks 1 through 3 each show a veering, or slight rotation of the wind in a clockwise sense with height. It is not clear as to the cause behind this wind

shift. That is to say, is this a measurement of the shear in the BL or are we seeing a slow and steady rotation of the wind on a synoptic scale. The evidence presented in this figure suggests that the synoptic turning of the wind is the best explanation as track 5 further supports the clockwise rotation of the winds as time progressed on this day. This synoptic change was also documented by the ship reports which were in the experiment area (Fellbaum et al., 1988).

If we look for changes along any one flight leg then we should be seeing mainly the effect of the change in the SST on the flow characteristics of the wind. Both tracks 1 and 2 show a noticeable change in the wind in the vicinity of the front. Track 1 shows a region just north of the front in which the wind first slows and turns slightly northward and then accelerates sharply across the front. As we continue further to the south the conditions appear to oscillate back and forth slowly but remain mainly between the conditions immediately on each side of the front. Track 2 (460 m) shows some similar features to track 1, however the same trend appears to have a longer period and there is a lag from track 1 to track 2. This lag is what one might expect between the two flight levels which are separated by over 300 m in altitude if the forcing for these changes occurs at the surface.

Track 3 shows oscillations similar to those seen at the lower levels, especially track 2, although it is difficult to determine if the features are connected to the front directly, indirectly or are independent of the surface layer altogether.

WIND VECTORS  
VMEAN= 4.38 M/S 43.58 DEG, VMAX= 8.89 M/S, MAX DEV=11.483 M/S  
FASINEX - NRL-P3  
14 FEB 86  
60.00 SECOND BOXCAR

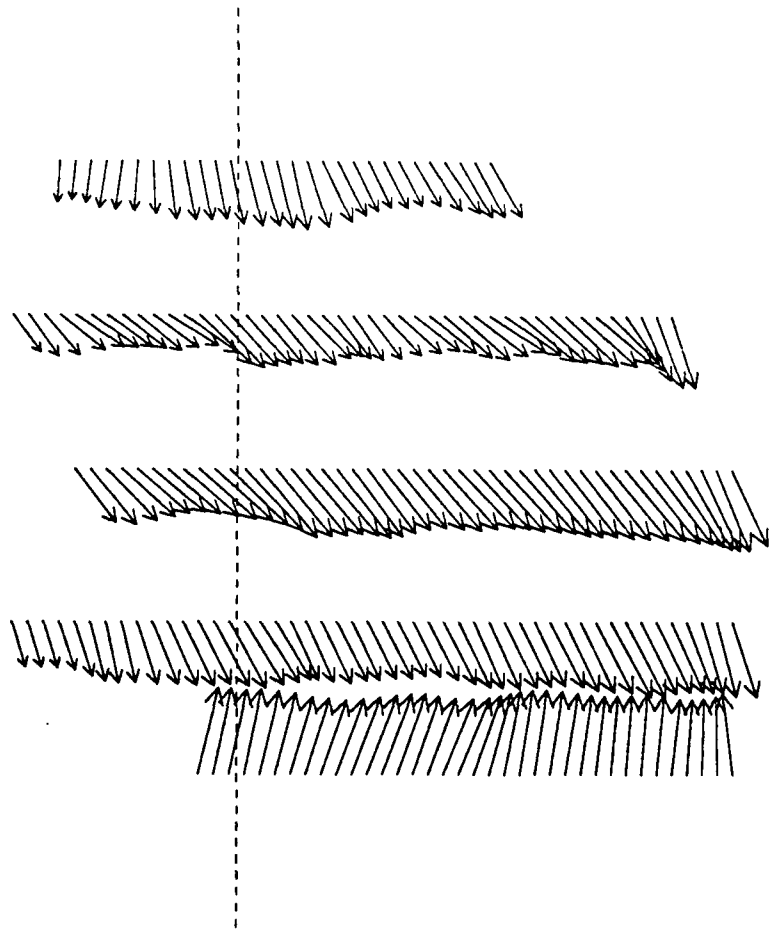


Figure 4.19 Vector Winds - 14 FEB 86  
(Left to Right) Track 4 (1800 m); Track 3 (775 m); Track 2 (460 m); Track 1 (150 m); Track 5 (100 m)

#### 4.4 Summary for February 14

We can summarize the results of this first case by saying that the change in SST has a pronounced effect on some aspects of the MABL. First, to begin our summary we remind the reader that the synoptic conditions for this day showed a strengthening sub-tropical high and a BL depth which generally was less than ~1300 m with the cold side being slightly shallower at just over 1000 m.

We found a remarkable resemblance between the SST and potential temperature records. The features most visible at the lowest levels became somewhat washed out as the altitude was increased; this is in agreement with the effects of turbulent mixing in the BL. The vertical heat flux showed two elevated regions, both associated with warm water, which were fairly well maintained throughout the BL and showed evidence of penetration into the inversion layer. Over the warm water we found that  $W$  and  $\theta$  are very much in phase at the lowest levels and then nearly out of phase in the middle of the BL. The vertical momentum flux, in contrast, showed that  $U$  and  $W$  are nearly in quadrature, though there was some variation in the relationship between the two. Also found were two regions of negative stress which were present at two flight levels. One region, at the lowest levels, was persistent for a period of over two hours. The other region, which was located

on consecutive flight tracks was well lined up despite the vertical separation of ~300 m between the flight tracks. The PHASE calculations in these two regions indicated that U and W were within  $\sim\pm 45^\circ$  of each other.

An inspection of the three wind component variances shows that the turbulent kinetic energy is contributed to somewhat equally by all three components. That is, the turbulence on this day shows some degree of three dimensional isotropy.

In general we find that the most prominent features which can be connected to the front tend to have only a slight, or non-existent, lag as the altitude increases. It is apparent that those features which establish themselves in the vicinity of the front are quite deep and persistent in time. Other results from this day are in general agreement with the type of vertical structure we would expect in the BL, among these are the variations in the VAR of W, and the vertical momentum and heat fluxes.

## Chapter 5

### Case two: 16 February, 1986

#### 5.1 Synoptic Forcing in the Region

A summary of the synoptic conditions, as presented by Fellbaum et al. (1988), for the 15th and 16th of February 1986 is contained in the following paragraphs. The synoptic maps from the 14th through the 16th are included in Appendix B for reference.

The 15th was predominantly influenced by the sub-tropical high, which had begun to develop on the 14th, continuing to move to the northeast, thus causing the wind to shift to the southeast.

By 1600 GMT the region was feeling the effects of a surface low pressure system associated with a deepening upper level trough at the 500 mb level. A frontal passage was recorded at approximately 2350 GMT on the 15th, as determined by the shift of the winds to the northwest.

The 16th was also a time of increasing surface pressure and decreasing winds after the frontal passage. The cold air mass created an air-sea temperature difference

of  $-1^{\circ}\text{C}$  to  $-3^{\circ}\text{C}$ , meaning the water temperature exceeded the air temperature. The wind shifted to the northeast at 1600 GMT as high pressure again began to dominate the synoptic conditions. Some rain showers were recorded until 0100 GMT while the cloud cover was dominated by a mostly low level stratus and stratocumulus deck.

The boundary layer returned to a well mixed structure with an inversion again at 1500 m by 0700 GMT on the 16th as the high pressure system began to move into the region. By 1800 GMT the high pressure system had moved into the region and had strengthened to a central pressure of about 1026 mb as plotted by NMC.

## 5.2 The Vertical Structure

### 5.2.1 The North Side

The boundary layer depth on the 16th is available from profiles by both the NRL-P3 and the NCAR Electra. The profiles shown are from two different points in the day, one of which was late in the day after having flown the entire flight pattern, approximately 20:20 GMT. All of the meteorological variables show the top of the MABL to be at about 1500 m. An inspection of another series of profiles from before the flight box, at approximately 15:08 GMT, shows a much less defined top

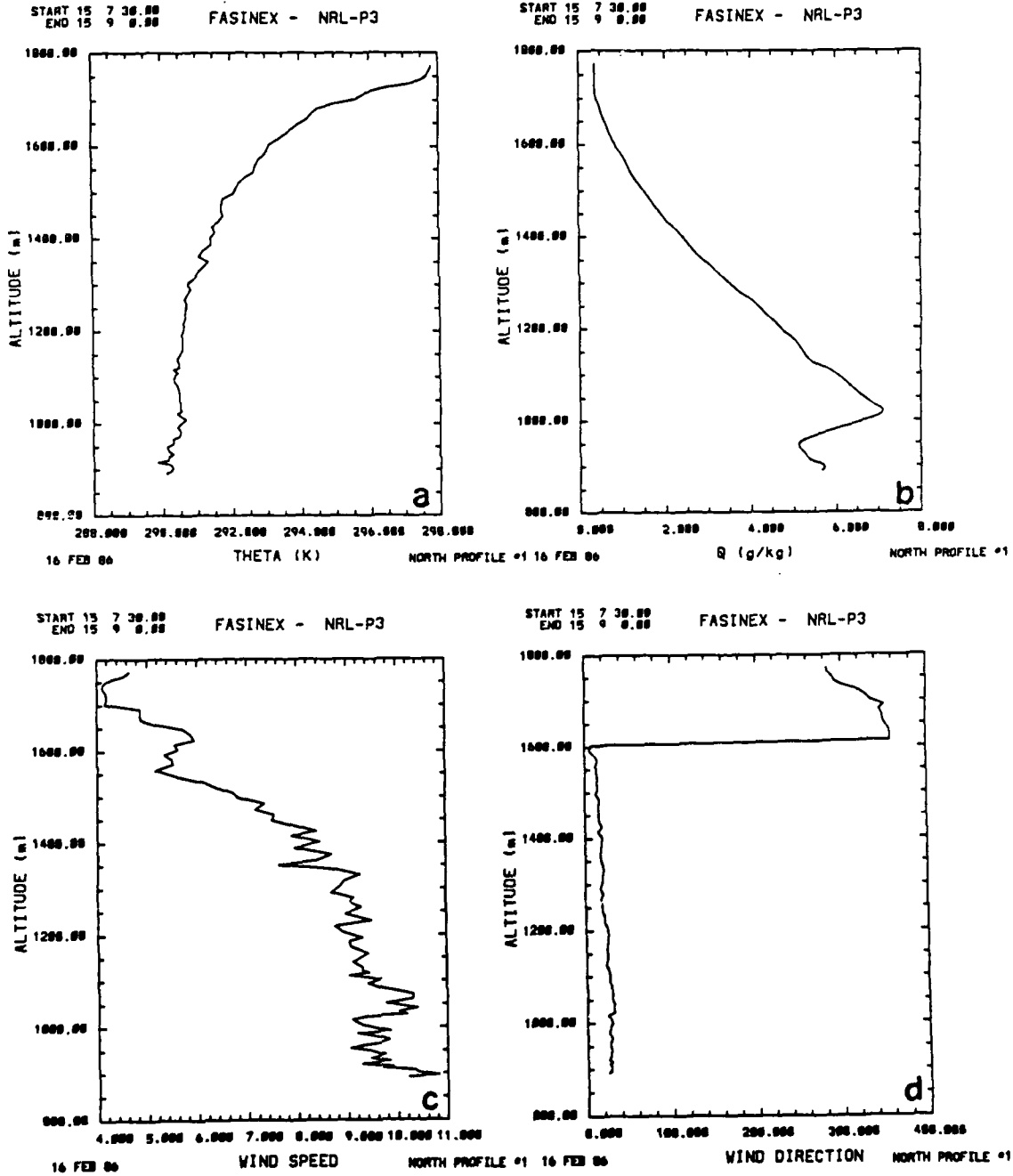


Figure 5.1 (a-h) North Profiles - 16 FEB 86

(a) Potential temperature (K); (b) Specific Humidity (g/kg); (c) Wind Speed (m/s); (d) Wind Direction

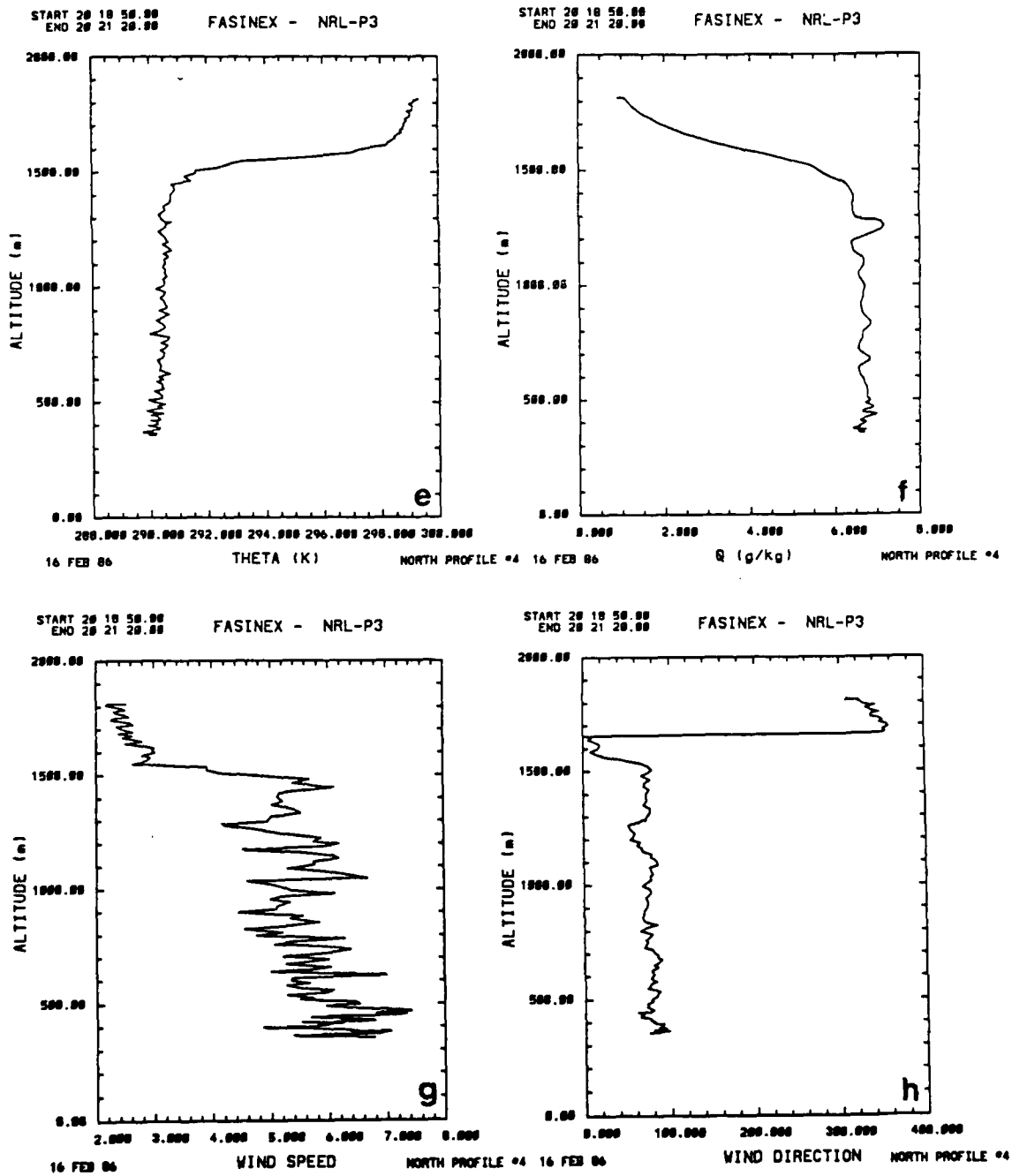


Figure 5.1 (a-h) North Profiles - 16 FEB 86 (cont.)  
(e) Potential temperature (K); (f) Specific Humidity (g/kg); (g) Wind Speed (m/s); (h) Wind Direction

of the MABL located between 1000 and 1400 m, depending on which variable is being inspected. We see in these profiles that the boundary layer becomes more uniformly mixed later in the day compared to the earlier profiles. Figure 5.1 (a-h) shows a sequence of profiles from the north side of the front on the 16th which is similar to those which were shown before for the 14th.

### **5.2.2 The South Side**

The boundary layer conditions for the south side of the front on the 16th is not available from the NRL-P3 data set because all of the profiles from the NRL-P3 for this day are located on the north side of the front. The boundary layer conditions will be determined from the NCAR Electra data set.

An inspection of the figure for theta (fig. 5.2a) shows the MABL is very well mixed up through 1500 m. Between 1500 m and about 1700 m the BL is not as well mixed. Above 1700 m we see the expected temperature profile for the lower troposphere with a lapse rate of about  $7^{\circ} \text{ C km}^{-1}$ . Figure 5.2b shows the specific humidity for the south profile. Again we see that things are quite well mixed up through 1500 m with a transition region from there to about 1700 m. An inspection of the plots of wind speed and direction (fig. 5.2c and 5.2d, respectively) shows good agreement with what is seen in the previous plots. Both of the latter plots show evidence that the top of the BL can be defined to be in the vicinity of 1600 m as this level seems to

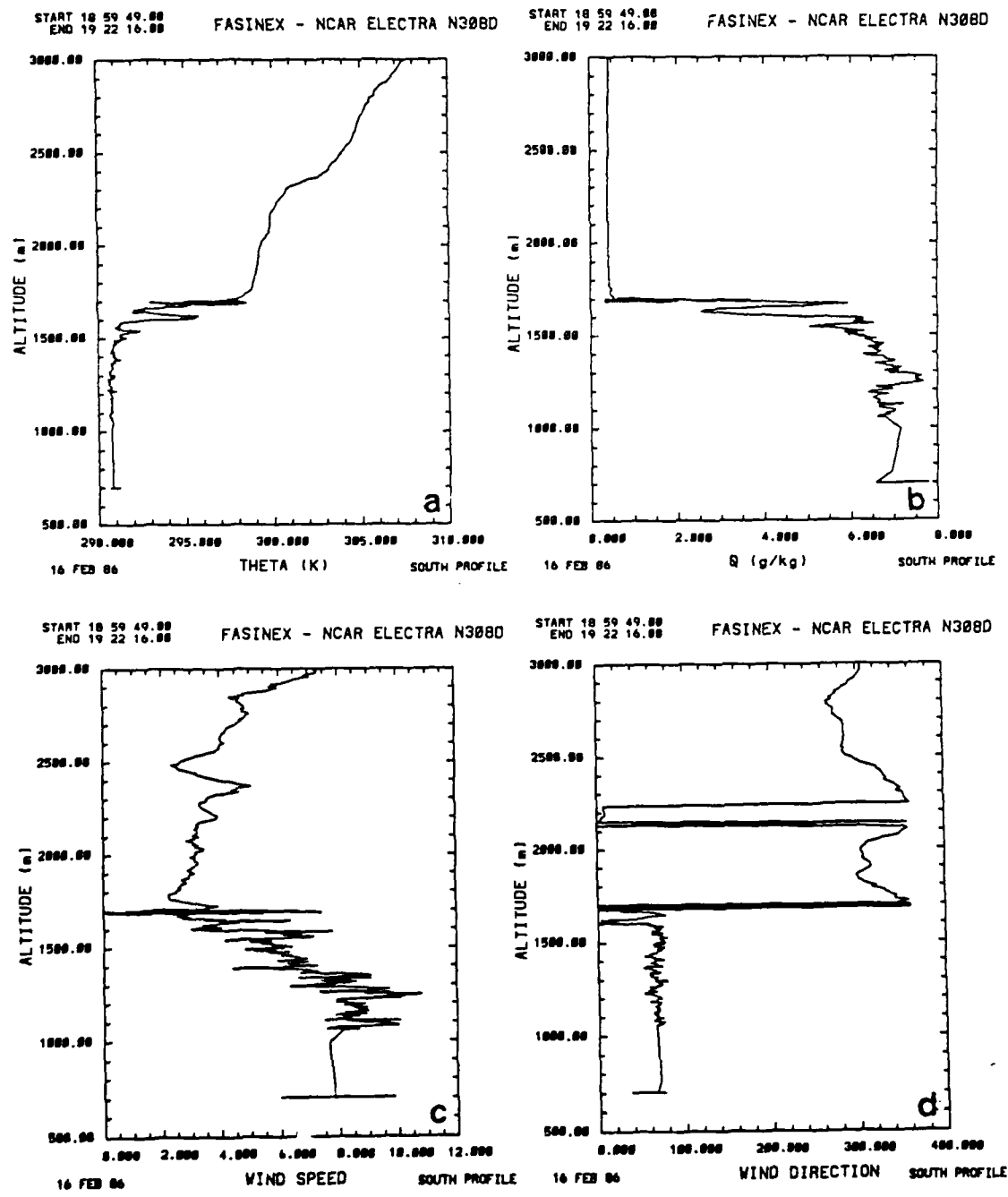


Figure 5.2 (a-d) South Profiles - 16 FEB 86  
(a) Potential temperature (K); (b) Specific Humidity (g/kg); (c) Wind Speed (m/s); (d) Wind Direction

be a region of strong shear.

In summary, we find that the boundary layer is found to be somewhat deeper on the warm side of the front for both the 14th and the 16th. Both days showed the BL depth over the warm water to be deeper by a few hundred meters. It is suggested that the increased surface heating that occurs over the warm water helps to deepen the mixed layer.

### **5.3 Results from Boxcar Statistics**

As we discuss the second of the two north wind cases for this paper we will follow the same format as for the first case insofar as possible. Hopefully this will aid in the comparison of the two cases as we proceed.

The flight tracks for this day are somewhat different than for the 14th. On this day the two aircraft flew the FASINEX box simultaneously. The Electra flew at 35 m while the NRL-P3 flew at 945 m. Upon completion of the original flight box the NRL-P3 flew the first half of another box at a level of 100 m. We will be examining legs 2-3 and 4-1 in this part of the study as these are the cross frontal legs for which we have the three levels. As a reminder, leg 4-1 is the eastern most leg of the box; leg 2-3 is located about 60 km west of leg 4-1 just to the west of the center of the FASINEX flight box (refer to fig 2.1).

FASINEX -- NCAR ELECTRA and NRL-P3

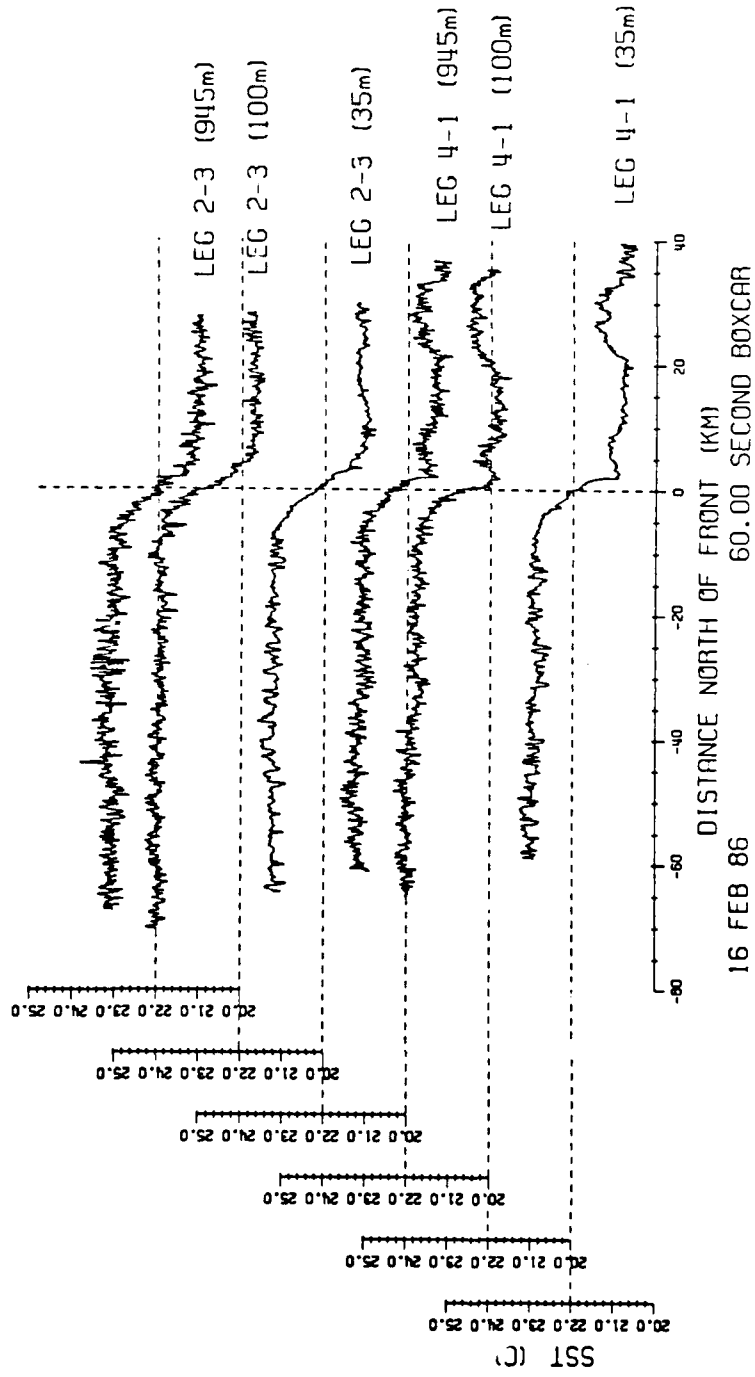


Figure 5.3 SST (°C) from 16 FEB 86

As we examine the SST record for this day (fig 5.3) we see that there is exceptional agreement for the SST features as measured over either of the flight tracks. There are some differences between leg 2-3 and leg 4-1. The most obvious difference between the SST records is the existence of a warm pool ~20-35 km north of the front on leg 4-1, which has also been documented by Stage et al. (1990). This pool of warm water is very persistent and is visible from each of the flight levels. The other difference between the two legs is the slope of the transition region. Leg 2-3 shows a more gradual, linear transition than is exhibited for leg 4-1. The SST shows about a 2° C jump over an average span of about 10 km.

### **5.3.1 Boxcar Means for Potential Temperature**

The figure for the potential temperature, theta, shows some interesting features (fig 5.4, dashed reference line at 290 K). Theta appears generally as a ramp function for each leg at each level, with some distinctions. At 35 m both legs show an increase north of the front, a nearly level zone over the front (within +/- 15 km), and a ramp-like increase further to the south. The warming in advance of the front for leg 4-1, located between 20-30 km north of the front, is most likely due to the warm pool on this leg (Stage et al., 1990). The SST for leg 2-3 shows only a slight indication of a warm region to the north of the front, though the air moving into this region appears to have been modified north of the front as can be seen north of ~15

km. It is also not clear why there is only a slight adjustment made directly over the front, especially at this low level. At 100 m there is a lag in the increase of about 15 km for leg 4-1 when compared to the 35 m flight level. The shape of leg 4-1 (100 m) is somewhat similar to the same leg at 35 m, with the transition between the previously described features being more gradual at the higher level. For leg 2-3 (100 m) the two legs have a somewhat different appearance; there is only a very slight increase to the north of the front at 100 m while there is a sharp increase beginning ~10 km to the south of the front. This is quite different from the 35 m level which shows the large increase beginning ~20 km south of the front. Perhaps the large time difference between these two levels is somehow responsible for the differences in these curves. Even at 945 m the presence of the front is noticeable. Leg 4-1 (945 m) shows a sharp increase in temperature from the beginning of the leg to a local maxima at ~10 km north of the front, corresponding to about a 10 km lag when compared to the southern edge of the warm pool. In contrast to leg 4-1, leg 2-3 (945 m) shows a nearly identical shape to the 35 m level for the same leg. In both cases, the temperature at 945 m is slightly cooler than the other levels, while the 100 m level is the warmest of the three. Also worth noting is that in all cases leg 4-1 is warmer than the corresponding level for leg 2-3.

The 16th shows a significant difference in the response of the atmosphere to the warm water when compared to the 14th. On the 14th the increase in temperature

FASINEX - NCAR ELECTRA and NRL-P3  
THETA (K)

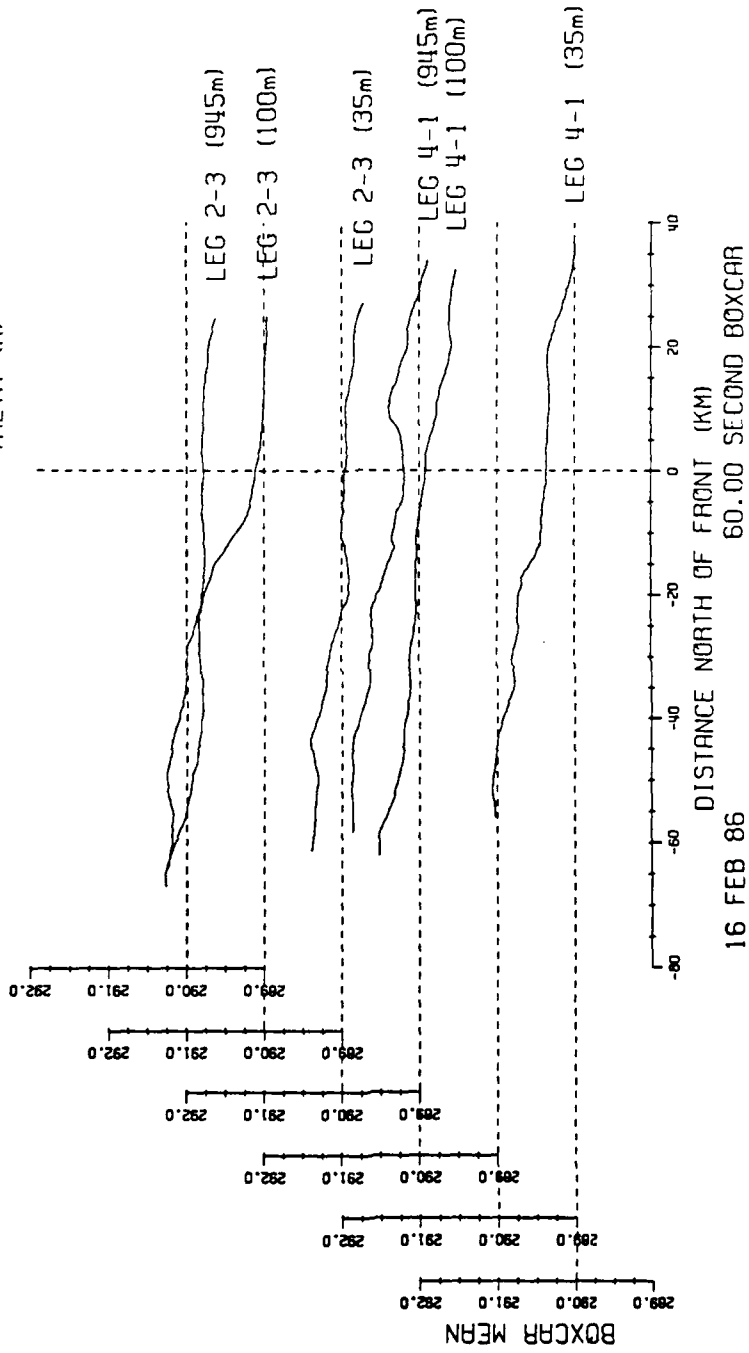


Figure 5.4 Potential temperature (K) - 16 FEB 86

was very rapid in response to the underlying warm water. On this day there appears to be somewhat of a delay between the point where the air first passes over the warm water and when the temperature shows a pronounced increase as was most notable for leg 2-3. Leg 4-1 showed a fairly rapid response to the warm pool but was equally slow in responding to the SST front. At this point, the reader is reminded that the air-sea temperature difference was less on the 16th ( $\sim -1$  to  $-3$  C) than was found for the 14th ( $\sim -2$  to  $-6$  C). This decrease in the difference in temperatures indicates that the air mass was slightly warmer on the 16th resulting in a less dramatic response to the change in the underlying SST.

### 5.3.2 The Vertical Heat Flux

Turning our attention to the vertical heat flux we begin with a look at the COV for  $W$  and  $\theta$  (fig 5.5, dashed reference line at 0). The COV at 35 m shows a significant increase in the presence of warm water. Even some of the smallest features in the SST make themselves seen in the COV. For leg 4-1 the increase first occurs to the north, over the warm pool in the region between 20 and 40 km. The heat flux then decreases slightly for about the next 10 km towards the south at which point it begins to increase again. South of the front the COV remains higher than over the cold water. Leg 2-3 also shows a sharp increase at the front, after which the COV remains elevated. For both legs the south average has a heat flux of  $\sim 35-40$

$\text{Wm}^{-2}$  which is ~50% greater than the north side average.

At 100 m we see many of the same features as at 35 m. This is especially true for leg 2-3 where there is a pronounced increase in the heat flux beginning at the front and continuing for about 20 km to the south. Both lower levels then show a region ~15 km wide in which the heat flux decreases from its elevated value. South of this the heat flux again increases slightly. The connections between the two lowest levels for leg 4-1 are not quite as obvious. In general, leg 4-1's (100 m) heat flux for the entire leg is much less than that of leg 2-3 at the 100 m level. North of the front leg 4-1 has a nearly zero heat flux when compared to the lower level for both legs. There is a slight indication of a series of increases corresponding to the increases at 35 m with about a 5-7 km lag at 100 m. These increases are not as obvious as at 35 m and may not be physically connected. In contrast, leg 2-3 shows a relatively strong heat flux of about  $30 \text{ Wm}^{-2}$  for the entire leg and closely resembles leg 2-3 at 35 m. There appears to be little or no lag between the two levels.

At 945 m the heat flux is very slight, averaging nearly two orders of magnitude less than the surface layer. At this altitude the heat flux is expected to be quite small thus these small values are reasonable. Despite this, the overall shape for leg 2-3 (945 m) closely resembles both of the lower levels. In contrast it is difficult to conclusively connect any of the features seen on leg 4-1 at 945 m to the lower levels. The COR of W and theta for this day (fig 5.6, dashed reference line at 0)

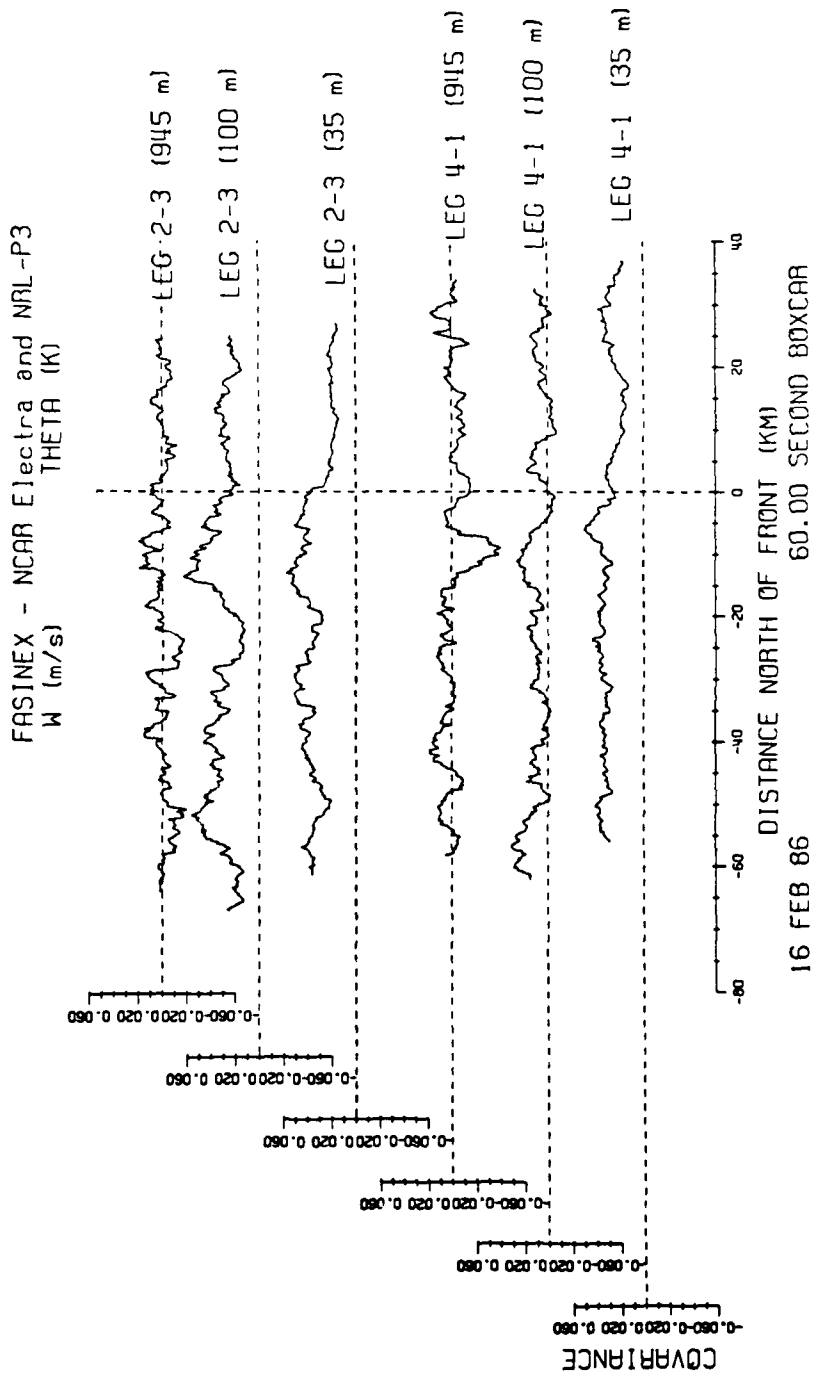


Figure 5.5 Boxcar Covariance (W-Theta) (Kms<sup>2</sup>) - 16 FEB 86

shows essentially the same features as the COV. The COR at 35 m is quite high, for turbulence data, with average values of nearly 0.6 for both legs. Leg 2-3 at 100 m continues to show the two variables to be well correlated with an average value of  $\sim 0.35$ . In contrast, leg 4-1 at 100 m has an average COR of only  $\sim 0.115$ . At 945 m both legs show a COR which varies greatly though averages nearly zero. In all cases the COR increased over the warm water. This statement is true even at 945 m though the values tend to be much smaller than at the lower levels.

The COH (fig 5.7, dashed reference line at 0.4) is highest at 35 m, averaging nearly 0.6 for both legs. This value is essentially the same value as the COR and indicates that there is little contribution to the COH from the quadrature. Despite the high values it is difficult to find any changes that can clearly be attributed to the front, though both legs show an increase north of the front. The similarity between leg 4-1, where we know there is a warm pool of water, and leg 2-3 are remarkable and further suggest the presence of warm water to the north of leg 2-3. Both legs do show an average increase over the warm water south of the front of about 5%. The COH for leg 4-1 at 100 m ( $\sim 0.16$ ) is much lower than leg 2-3 at 100 m ( $\sim 0.38$ ). At 945 m the COH varies greatly for leg 4-1 with a higher average than for the 100 m level, while leg 2-3 at 945 m shows a decrease to a value about half of the 100 m level for that leg.

For the coherence it is difficult to make any indisputable connections to the

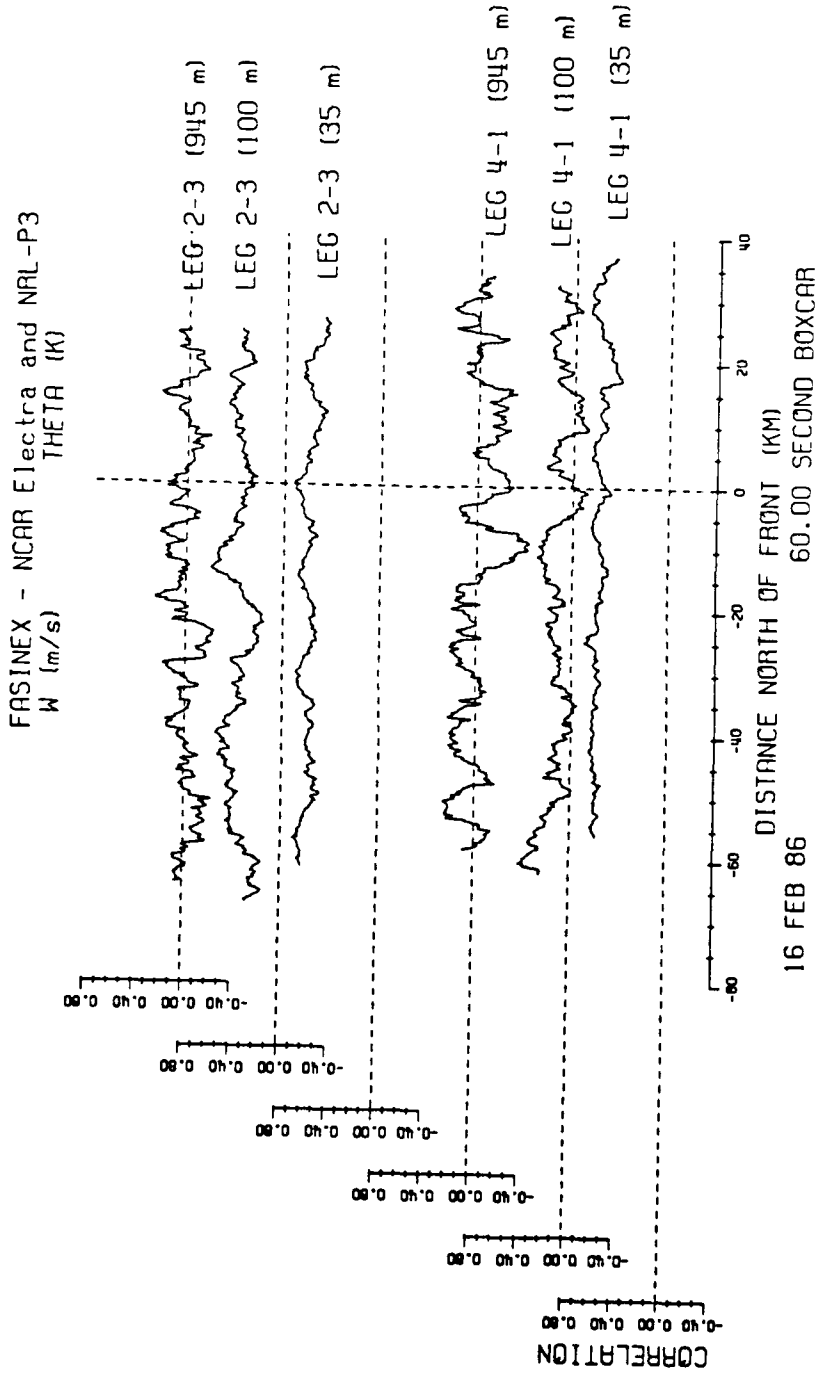


Figure 5.6 Boxcar Correlation (W-Theta) - 16 FEB 86

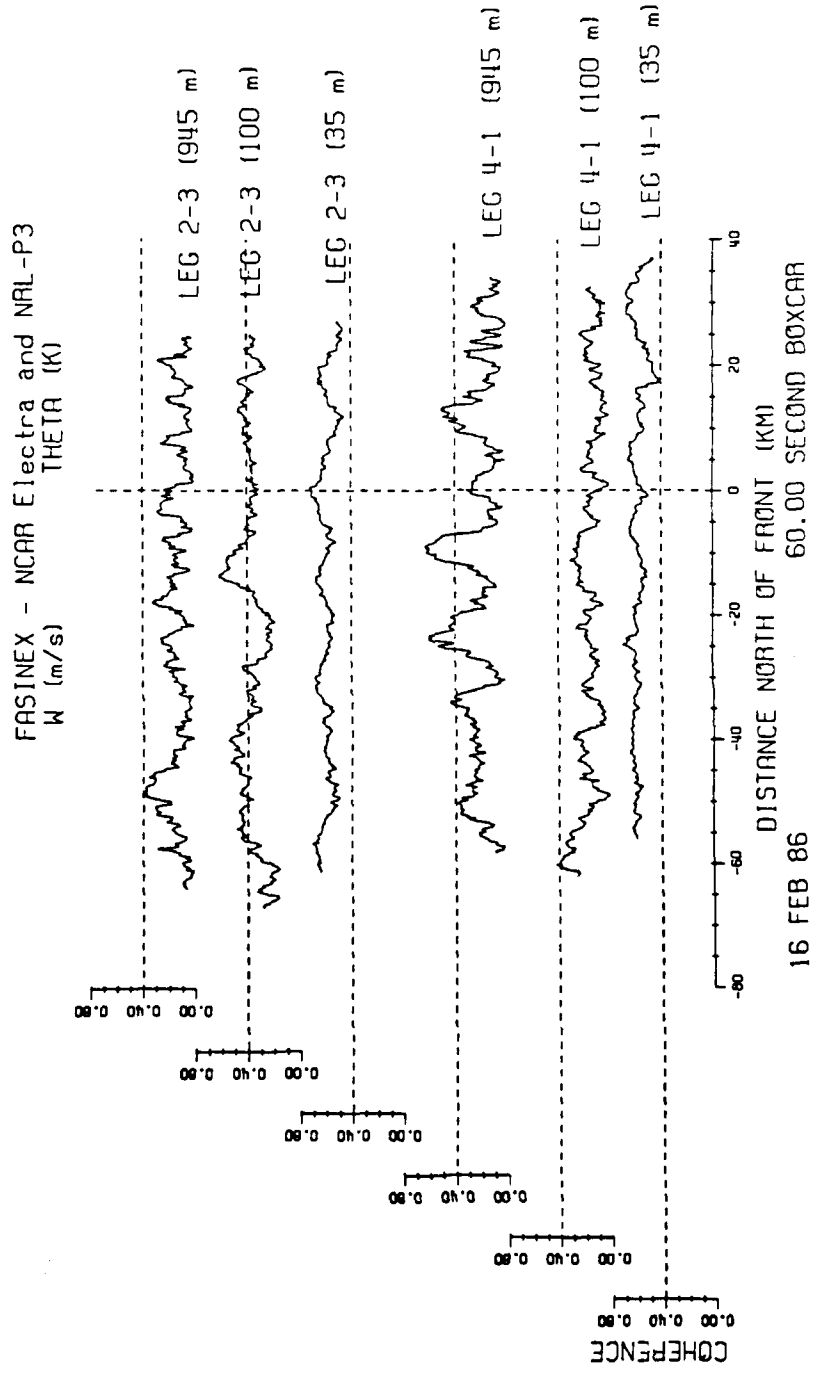


Figure 5.7 Boxcar Coherence (W-Theta) - 16 FEB 86

front or any clear connections from one level to the next.

The PHASE relationship is given in figures 5.8 (dashed reference line at 0) and 5.9 (a-1). Again we see that  $W$  and  $\theta$  are almost exactly in phase at 35 m (fig 5.9a-d). This represents a very efficient transport of heat away from the surface. There is obviously no significant change in the PHASE across the front. At 100 m the picture is not quite as clear. Leg 2-3 (100 m) again shows a strong in phase relationship of  $\pm 30^\circ$  with little change across the front, but leg 4-1 (100 m) does not show the same type of relationship. The PHASE for this leg varies much more, especially north of the front. North of the front there are a fair number of occurrences in the vicinity of  $180^\circ$ , this is the cause of the discontinuities seen in figure 5.8. It is not a case of the COH going to zero as we have seen previously. South of the front the distribution of the PHASE is much greater than for leg 2-3 at 100 m. There is at least one additional mode in the vicinity of  $280^\circ$  ( $-90^\circ$ ) and some indication of another mode between  $300^\circ$  and  $330^\circ$ .

At 945 m there is a distinct difference between both the two legs and the lower levels. Leg 4-1 shows a strong preference for a PHASE between  $30^\circ$  and  $150^\circ$ , especially south of the front. North of the front leg 4-1 (945 m) shows a complicated multi-mode situation. Most notable is the exclusion of the  $110^\circ$  PHASE with strong peaks at both  $90^\circ$  and  $120^\circ$ , where the reader is reminded that for this case  $W$  is leading  $\theta$  while traveling from south to north. There is another promi-

nent peak at the 200-215° PHASE relationship. Leg 2-3 shows a more uniform distribution at all angles south of the front while north of the front the pattern is very complicated. Both legs show a difference across the front but the legs tend to be more different from each other than alike. It is not clear why these differences exist.

There are many differences between the heat flux for this day when compared to the 14th. For one thing we do not see the same kind of deep, organized convective regions in the vicinity of the front on the 16th that we saw on the 14th. Both days were under the influence of high pressure with an 18Z central pressure of 1026 mb as analyzed by NMC though the high was centered more to the north on the 16th.

Besides the sharp contrast between the two days there are some significant differences between the two sets of legs for the 16th. At times leg 2-3 and leg 4-1 show more differences than they do similarities. The reasons behind these differences are not apparent but the two legs are separated by about 60 km and this may indicate that there are many processes in the vicinity of the front which have scales that are significantly smaller than this. Also it is not clear why the two lower levels for leg 2-3 show a fair amount of similarity, given their 2.5 hour separation, while leg 4-1 seems to show little similarity at these two levels.

FASINEX - NCAR Electra and NRL-P3  
W (m/s)  
THETA (K)

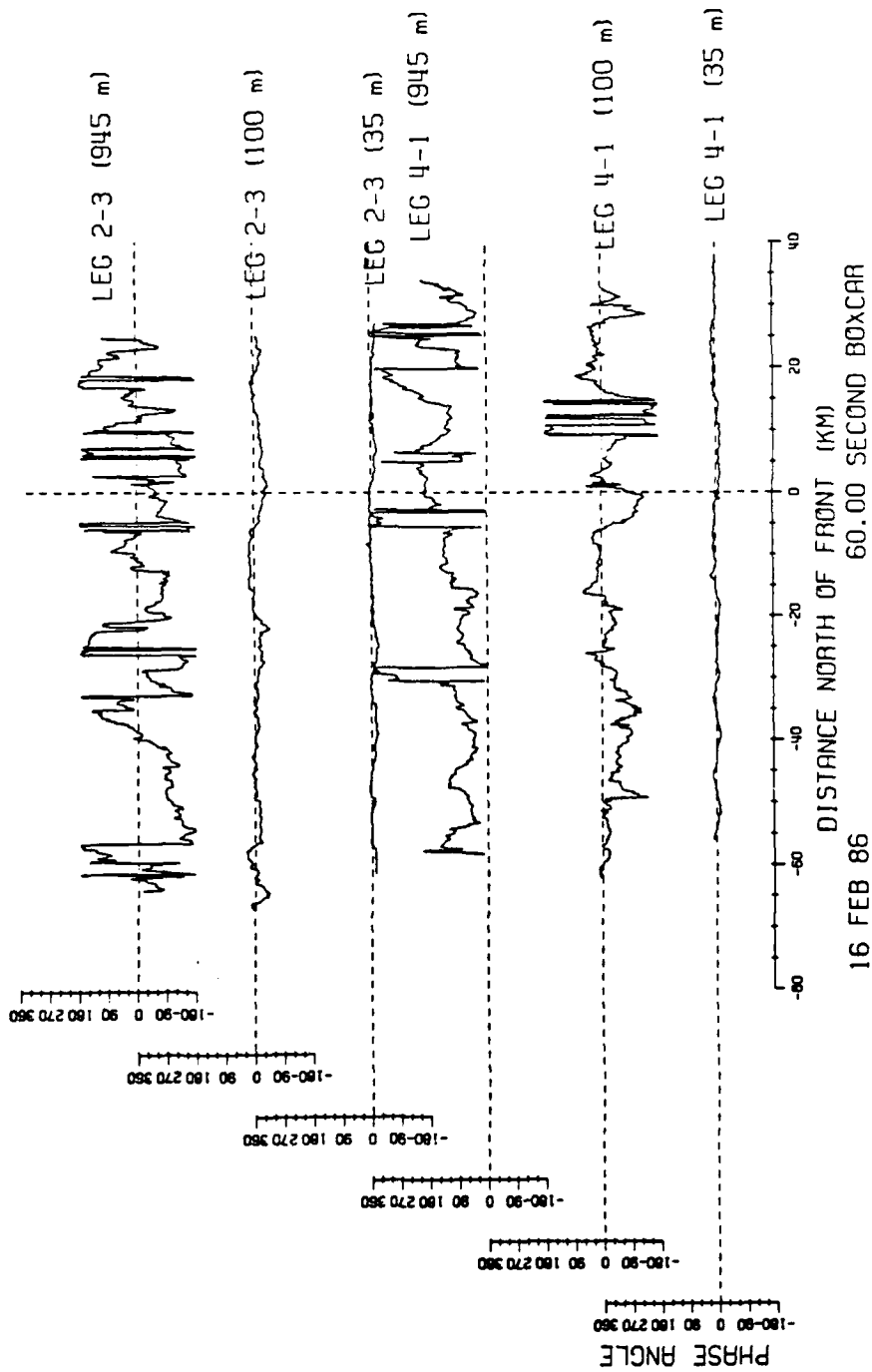
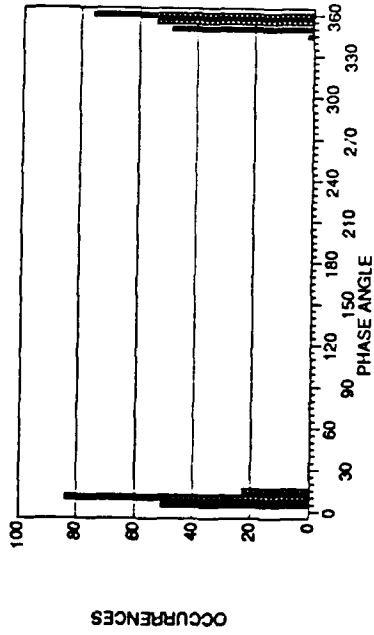


Figure 5.8 Boxcar Phase Angle (W-Theta) - 16 FEB 86

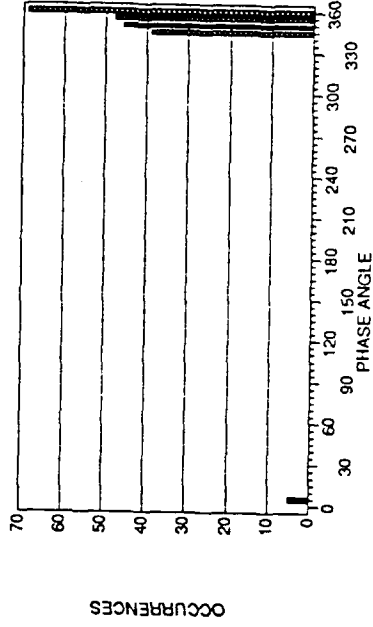
<WT> 16 FEB 86 - NCAR ELECTRA

LEG 4-1 (35 m) North Side



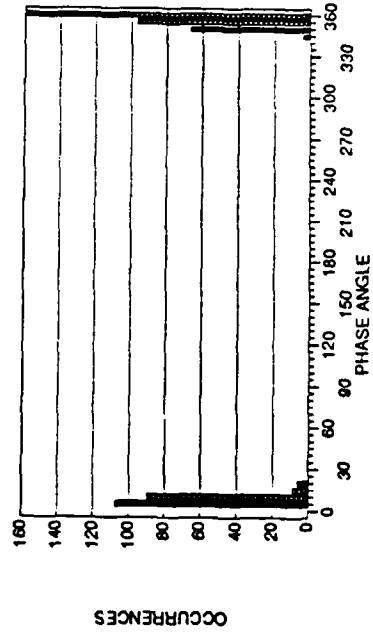
<WT> 16 FEB 86 - NCAR ELECTRA

LEG 2-3 (35 m) North Side



<WT> 16 FEB 86 - NCAR ELECTRA

LEG 4-1 (35 m) South Side



<WT> 16 FEB 86 - NCAR ELECTRA

LEG 2-3 (35 m) South Side

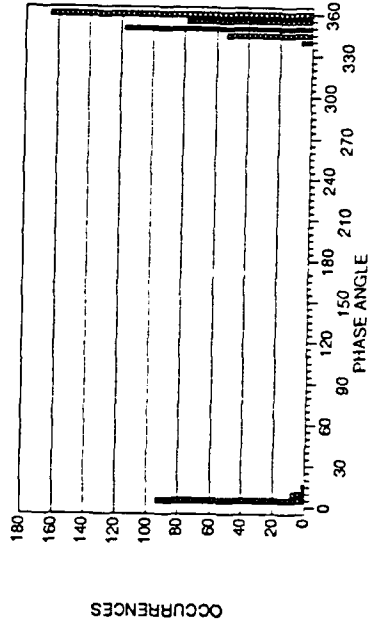
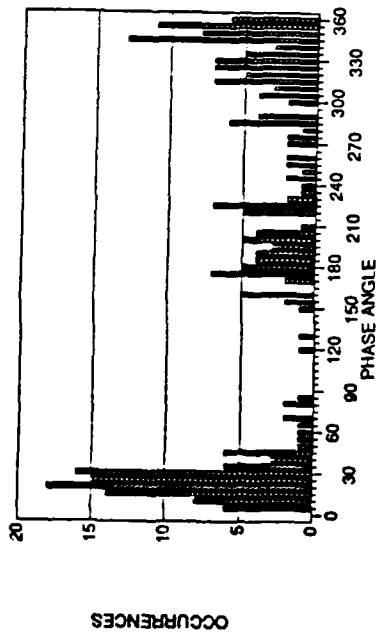


Figure 5.9 Phase Angle PDF for (W-Theta) - 16 FEB 86  
(a) Leg 4-1 (35m) North Side; (b) Leg 4-1 (35m) South Side; (c) Leg 2-3 (35m) North Side; (d) Leg 2-3 (35m) South Side

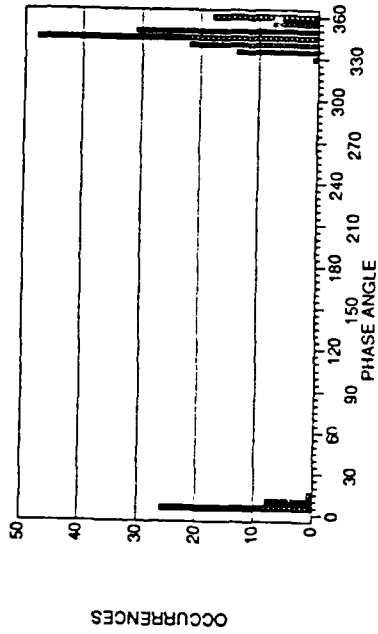
<WT> 16 FEB 86 - NRL-P3

LEG 4-1 (100 m) North Side



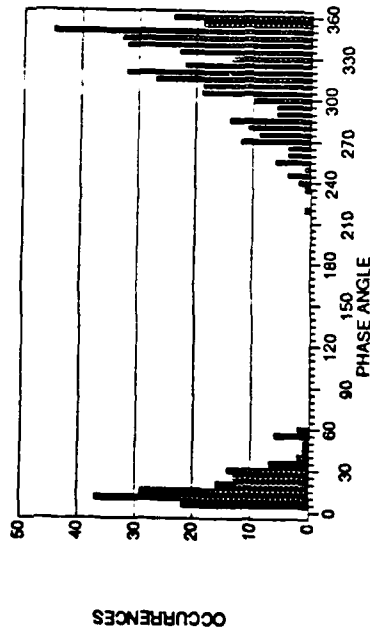
<WT> 16 FEB 86 - NRL-P3

LEG 2-3 (100 m) North Side



<WT> 16 FEB 86 - NRL-P3

LEG 4-1 (100 m) South Side



<WT> 16 FEB 86 - NRL-P3

LEG 2-3 (100 m) South Side

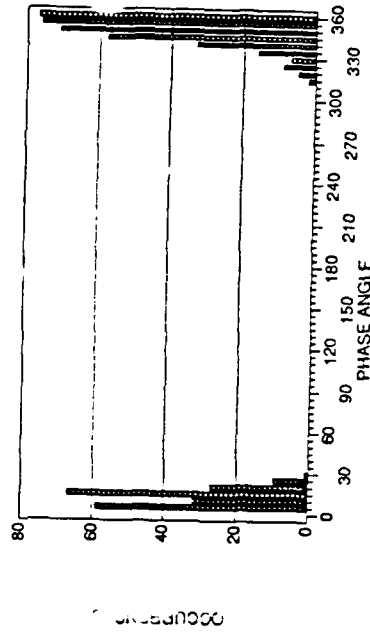
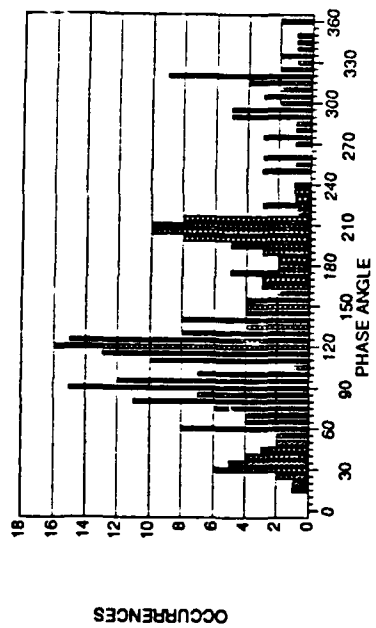


Figure 5.9 Phase Angle PDF for (W-Theta) - 16 FEB 86 (cont.)  
(e) Leg 4-1 (100m) North Side; (f) Leg 4-1 (100m) South Side; (g) Leg 2-3 (100m) North Side; (h) Leg 2-3 (100m) South Side

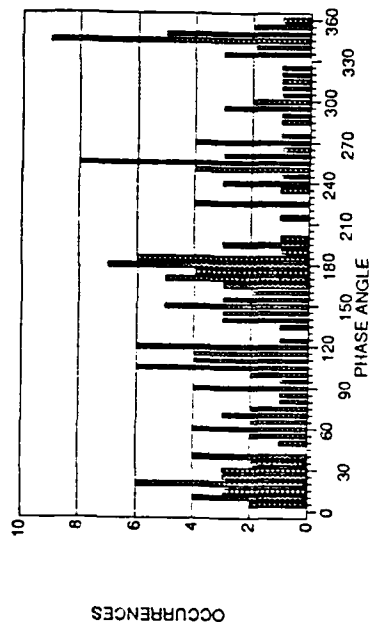
<WT> 16 FEB 86 - NRL-P3

LEG 4-1 (945 m) North Side



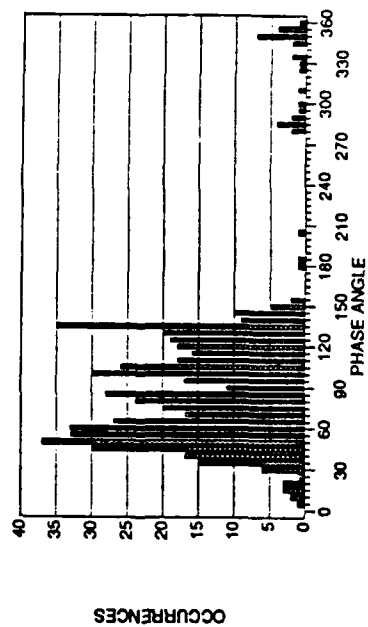
<WT> 16 FEB 86 - NRL-P3

LEG 2-3 (945 m) North Side



<WT> 16 FEB 86 - NRL-P3

LEG 4-1 (945 m) South Side



<WT> 16 FEB 86 - NRL-P3

LEG 2-3 (945 m) South Side

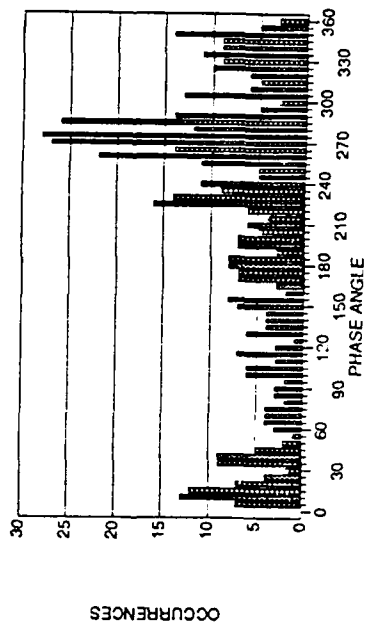


Figure 5.9 Phase Angle PDF for (W-Theta) - 16 FEB 86 (cont.)  
(i) Leg 4-1 (945m) North Side; (j) Leg 4-1 (945m) South Side; (k) Leg 2-3 (945m) North Side; (l) Leg 2-3 (945m) South Side

### 5.3.3 Boxcar Variance for Potential Temperature

We now turn to the variance estimates for theta from the 16th (fig 5.10, dashed reference line at 0.015). At the lowest level, 35 m, we see that the VAR is closely tied to the SST. Leg 4-1 (35 m) has a pronounced increase over the warm pool of water and then decreases for a short span, ~15 km, in advance of the front. As the warm water is crossed the variance again increases and remains elevated for the remainder of the leg. Leg 2-3 (35 m) shows a very similar nature, though there is a region ~20 km south of the front in which the variance decreases for a 10 km stretch.

At 100 m there is very little change across the front for leg 4-1. In contrast, leg 2-3 (100 m) shows a noticeable increase, beginning slightly ahead of the front. This feature is difficult to explain given the data available. Again it is felt that there must be some process north (and slightly east) of this leg causing these effects. For both legs at 100 m the variance is greater than at either the lower (35 m) or higher (100 m) levels for the same leg.

The two lower levels for leg 2-3 (35 m and 100 m) show some similar features. Both levels show a local maximum beginning at (35 m) or just north (100 m) of the front, reaching a peak value ~10 km south of the front and followed by a decrease further to the south. It is not clear if these features are actually related to each other as the length of the individual elements are different from one level to the

next.

At 945 m leg 2-3 shows only a very slight indication that there might be a connection with the lower levels with the same kind of local maximum as just described above. Beyond comparing individual wiggles of the curves there are essentially no other apparent connections that can be made to the lower levels for either of the legs.

Comparing the overall changes from one level to the next we see that the VAR for theta has its lowest values at the 35 m level, the highest values at the 100 m level and values comparable to the 35 m level, though slightly higher, at 945 m.

Again we find that we do not see the same kind of vertical connections on this day that we saw on the 14th. It is also important to point out that the variance of theta on the 16th had, on the average, values lower than that which were found for the 14th (see figure 4.10); again, this difference is likely due to the decreased air-sea temperature difference. Also, there appear to be two different regimes from leg 4-1 to leg 2-3 which may be related to the presence of the warm pool found on leg 4-1 though the 60 km horizontal separation between the legs makes this conclusion difficult to support.

FASINEX - NCAR Electra and NRL-P3  
THETA (K)

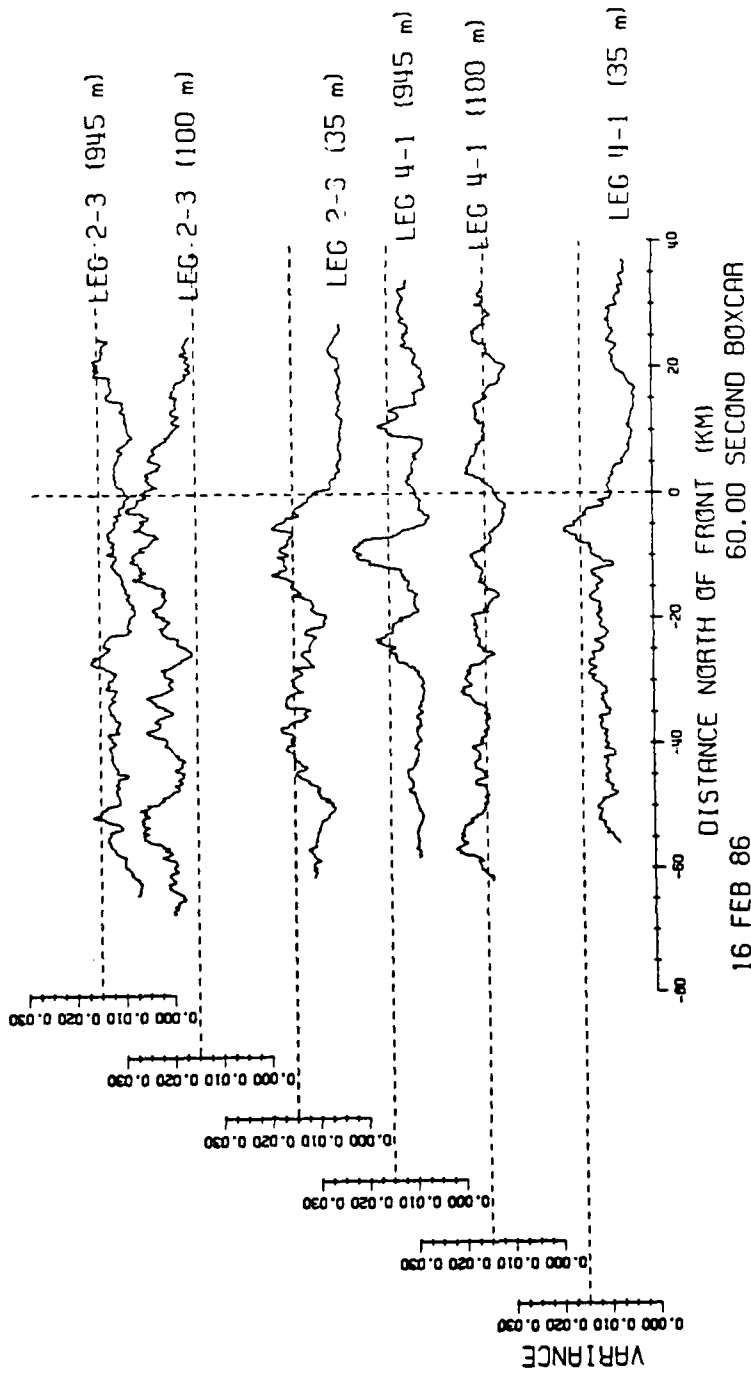


Figure 5.10 Boxcar Variance Theta ( $K^2$ ) - 16 FEB 86

#### **5.3.4 Boxcar Variance for Vertical Velocity**

The next topic to be covered is the VAR for W for this day, shown in figure 5.11 (dashed reference line at 0.4). Again we see that the two sequences for each of the legs are different from each other as much as they are alike. There are, however, some similarities at the 35 m flight level. Leg 4-1 (35 m) shows a sharp increase over the warm pool (~20-35 km) of twice the value just to the south of the warm pool. Following the elevated region there is a rapid decrease to a local minimum. South of the warm pool and the local minimum the VAR continues to increase slowly across the front and continues at a slightly elevated value to a point ~30 km south of the front where it again decreases suddenly. This sudden decrease corresponds to a slightly cooler region in the SST. Leg 2-3 (35 m) begins to increase right at the front and continues to increase for about 15 km south of the front. The variance then remains elevated, at a value of about twice the cold water side, again to a point about 30 km south of the front. It is believed that this 30 km wide region is one of enhanced convection and represents a secondary circulation established in the presence of the front (Stage and Herbster, 1989). The region to the south of this circulation cell, denoted by the decrease in variance, is believed to be the downwind edge of the secondary circulation. On leg 2-3 at 100 m we see the same structure as at the 35 m level, though the decrease in variance to the south of the front is found to occur at about -25 km. This is quite a good agreement with the lower level consider-

ing the temporal spacing of greater than 2.5 hours between the two flight levels. At 945 m we see a region of decreased variance at approximately the same location.

Leg 4-1 at 100 m has more features in common with the 945 m level than with the 35 m level. Many of the small scale changes in the variance at the 100 m level are visible in the 945 m, beginning with the slight increase just north of the front at about 10 km for 100 m and 5 km for 945 m. The widths of the individual elements vary slightly between the two levels without any systematic behavior, but one can connect the edges of essentially each of the larger features at the 100 m level with a similar feature at 945 m. This suggests some level of organized circulation within the BL given the time separation between the legs. It is difficult to say that the same type of connections exist for leg 2-3 since the two curves have such distinctly different amplitudes.

Comparing the variance overall from one level to the next we find that the variance increases with increasing altitude for both legs. This is in agreement with what we saw for the 14th as the top level of 945 m is at about  $0.6 Z_i$ . Since the other two levels are so low in the BL we would expect to find the 945 m level to have the highest variance for W. In general the effect of underlying warm water shows an increase in the VAR of W, though the increases on the 16th are not nearly as pronounced as they were for the 14th, this is in agreement with the decreased temperature difference between the air and sea surface. Overall, as was found for the vari-

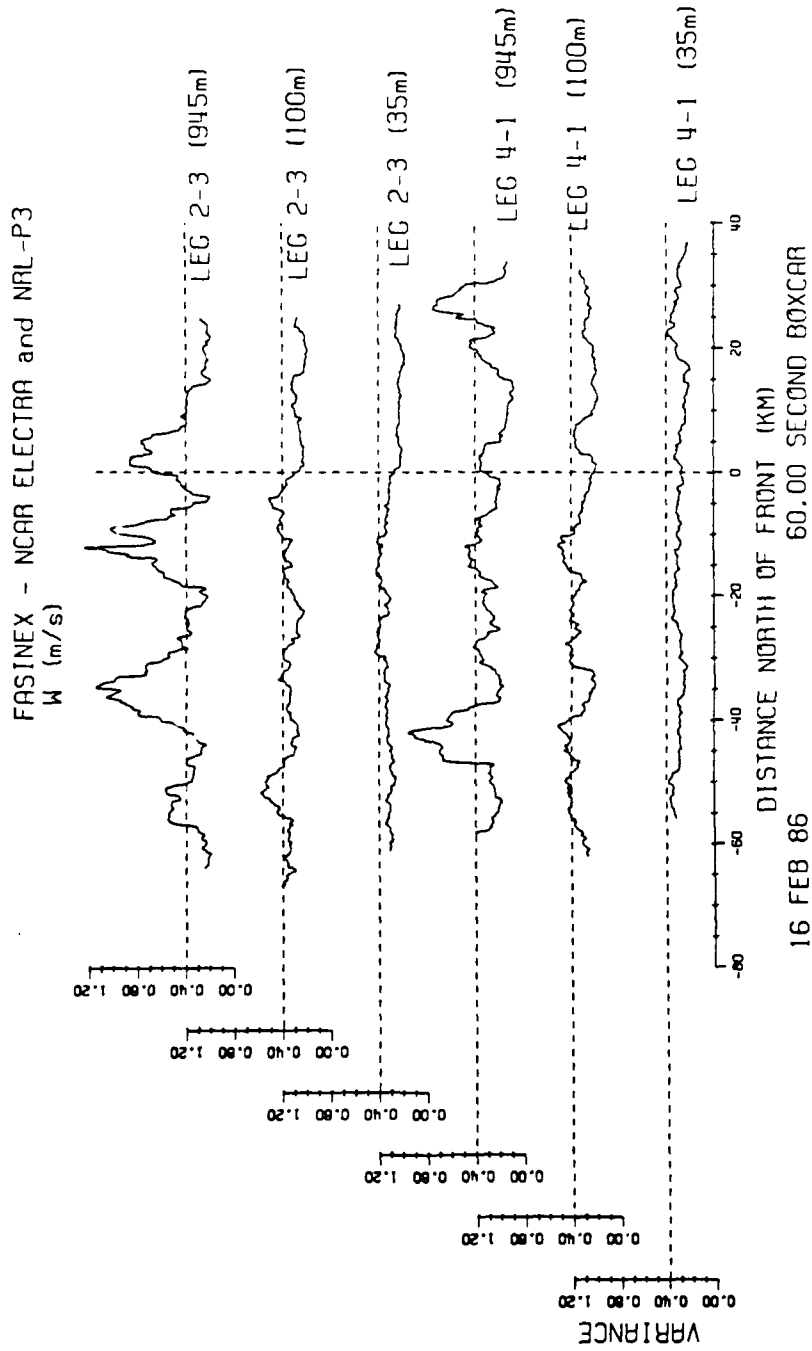


Figure 5.11 Boxcar Variance Vertical Velocity ( $m^2s^{-2}$ ) - 16 FEB 86

ance of theta, the variance for W is lower on the 16th than it is on the 14th. Finally, unlike what was found on the 14th, we do not find that the peaks in heat flux, variance of theta and variance of W occur in all the same areas, this agrees with the interpretation that the convection is not as well organized on the 16th.

### 5.3.5 The Vertical Momentum Flux

The COV for U and W on the 16th shows better agreement between the legs than has been seen for many of the other statistics we have looked at for this day as seen in figure 5.12 (dashed reference line at 0). To start with, both 35 m legs show the stress to be positive for the duration of the entire leg. Leg 4-1 has a region of increased stress right at the front. The stress gradually decreases towards the south to a point about 15 km south of the front where the stress is nearly zero. Leg 2-3 (35 m) shows only a slight change across the front, has a more pronounced region of high stress located about 15 km south of the front but also has a region where the stress goes to zero, this time at about 20 km south of the front.

The comparison of the 35 m level to the 100 m level shows generally good agreement between them. Leg 2-3 clearly shows the same region of high stress to the south of the front, though the width of the element is slightly less for leg 2-3(100 m). The connection between the two lowest levels is not quite as clear for leg 4-1, though if we begin at the south end there is a region, about 5-7 km wide, of slightly

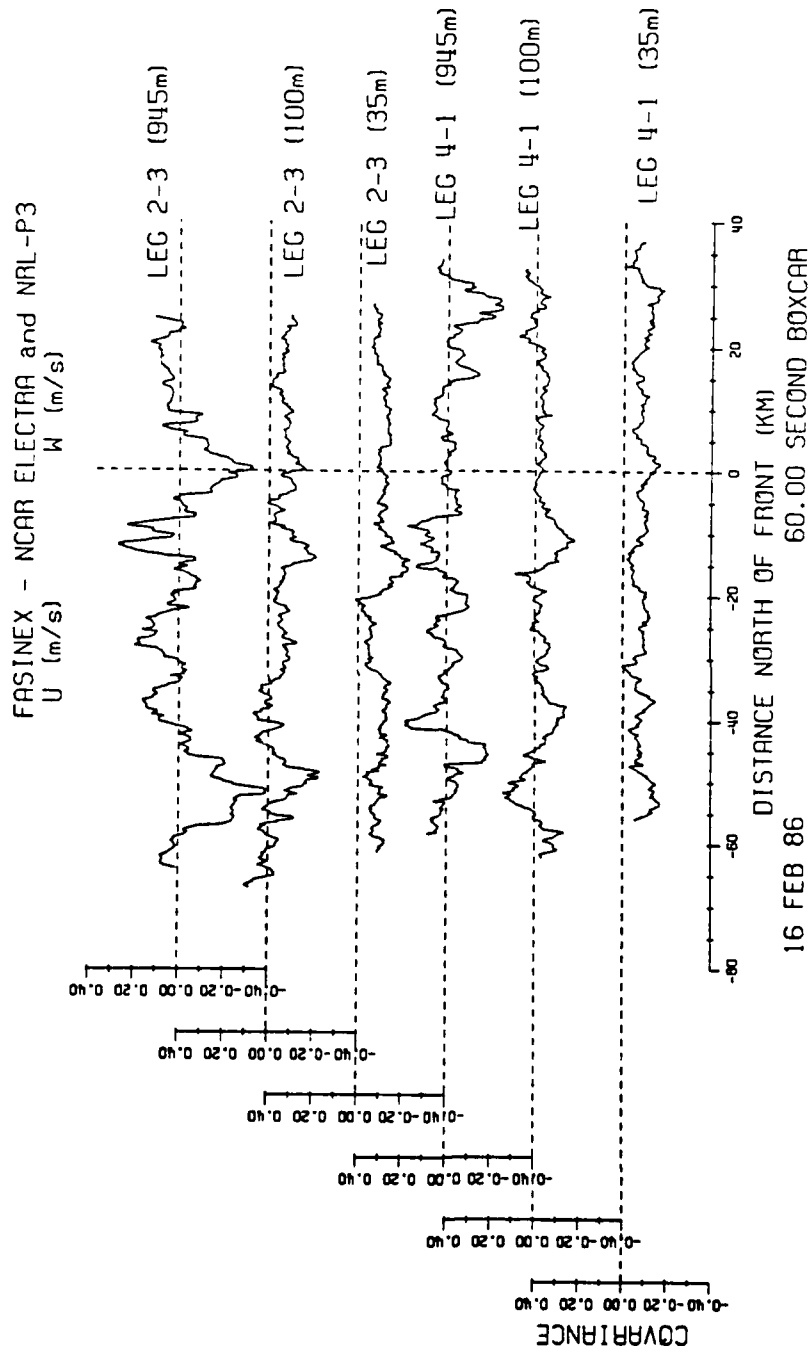


Figure 5.12 Boxcar Covariance (U-W) ( $m^2s^{-2}$ ) - 16 FEB 86

increased stress about 35 km south of the front. Moving towards the north the stress is somewhat less at 100 m but has the same general structure as at 35 m up to about 20 km south of the front. At this point there is a pronounced increase in the stress at 100 m while the increase at 35 m is only slight. However, this region at 100 m corresponds spatially to the same feature seen at both the lower levels (35 m and 100 m) of leg 2-3. Both legs at 100 m show a few, relatively small regions well south of the front (~35-45 km) in which the stress becomes negative, these might be associated with the secondary circulation believed to be over the front.

At 945 m the most prominent features which we are able to connect to the lower levels are the regions of strong negative stress. In many cases, these regions of negative stress are directly over regions of high (positive) stress at the 100 m level.

Again the COR (fig 5.13, dashed reference line at 0) agrees well with the COV. At the 35 m level the COR ranged from -0.35-0.0, remaining negative for essentially the entire time. At 100 m the COR is closer to zero and does contain some regions of positive values associated with those regions of negative stress mentioned above. At 945 m the COR varies greatly but averages out to the lowest of the three levels. For both sets of legs the average value for the COR over the whole leg decreases with increasing altitude.

The COH of U and W from the 16th (fig 5.14, dashed reference line at 0.4)

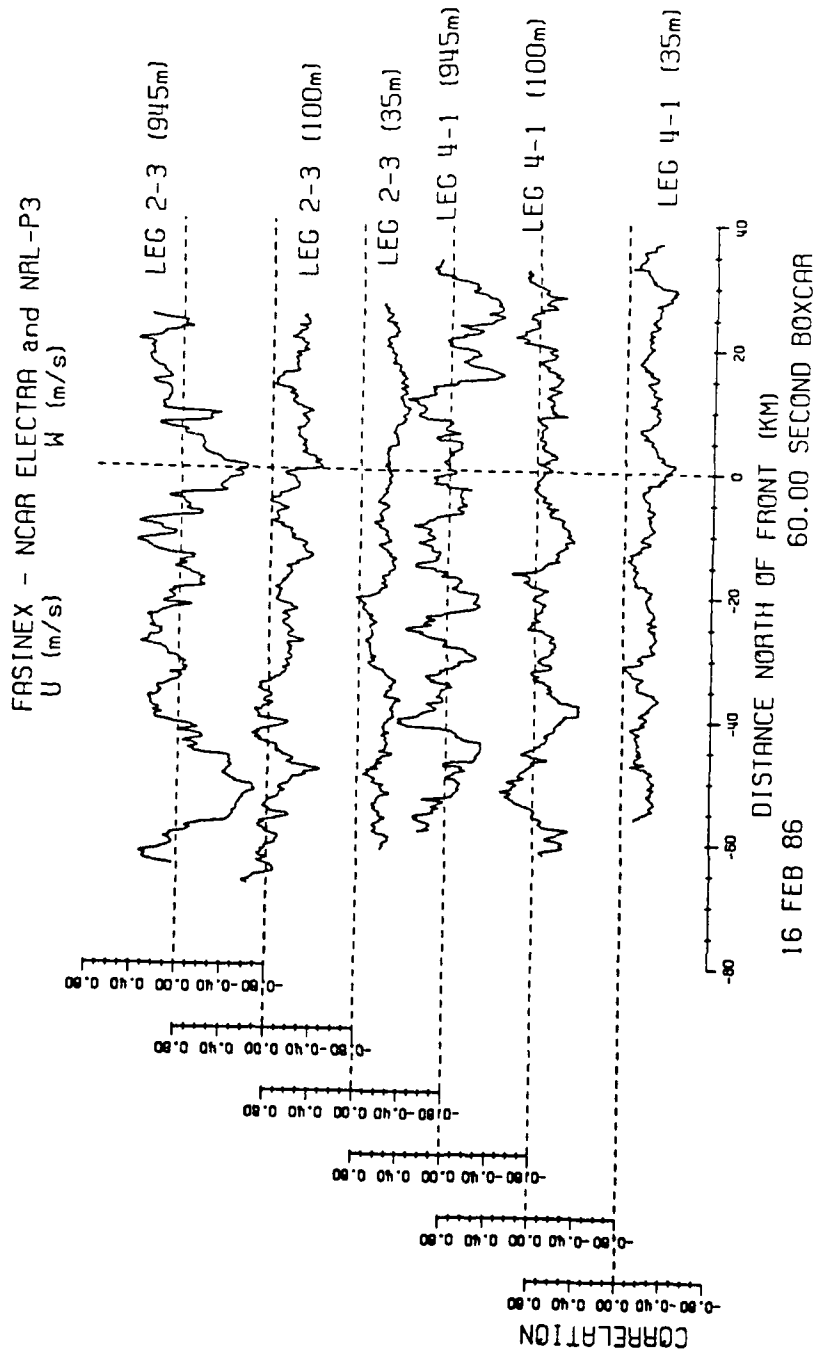


Figure 5.13 Boxcar Correlation (U-W) - 16 FEB 86

shows some larger scale features which suggest a link between the various levels. The most prominent of these features can be seen at the 100 m and 945 m levels of leg 4-1. Both of these levels show a region of relatively low coherence, just north of the front for the 945 m level and beginning essentially at the front at 100 m. Both levels then show a steady and fairly rapid increase over approximately the next 10 km. To the south of this peak both levels show a broad region about 30 km wide in which the coherence slowly decreases and then increases, in an area that suggests it is associated with the secondary circulation previously discussed. Connections from these levels down to the 35 m level are not very clear.

For leg 2-3 there are only subtle connections between the levels though there is a slight similarity between the 35 m and 100 m levels for the region beginning at the front and extending south about 30 km. Within this region both legs show a slight decrease/increase/decrease and increase again with a periodicity of about 15 km. Again the 30 km region to the south of the front appears to have some significance though it is not clear how this pattern relates to that which was seen for the other leg.

For both legs at 35 m the COH drops by about 10% over the warm water compared to the cold side, though the transition is somewhat gradual. At the higher levels the difference between the two sides is generally less.

The results of the PHASE estimates are given in figures 5.15 (dashed refer-

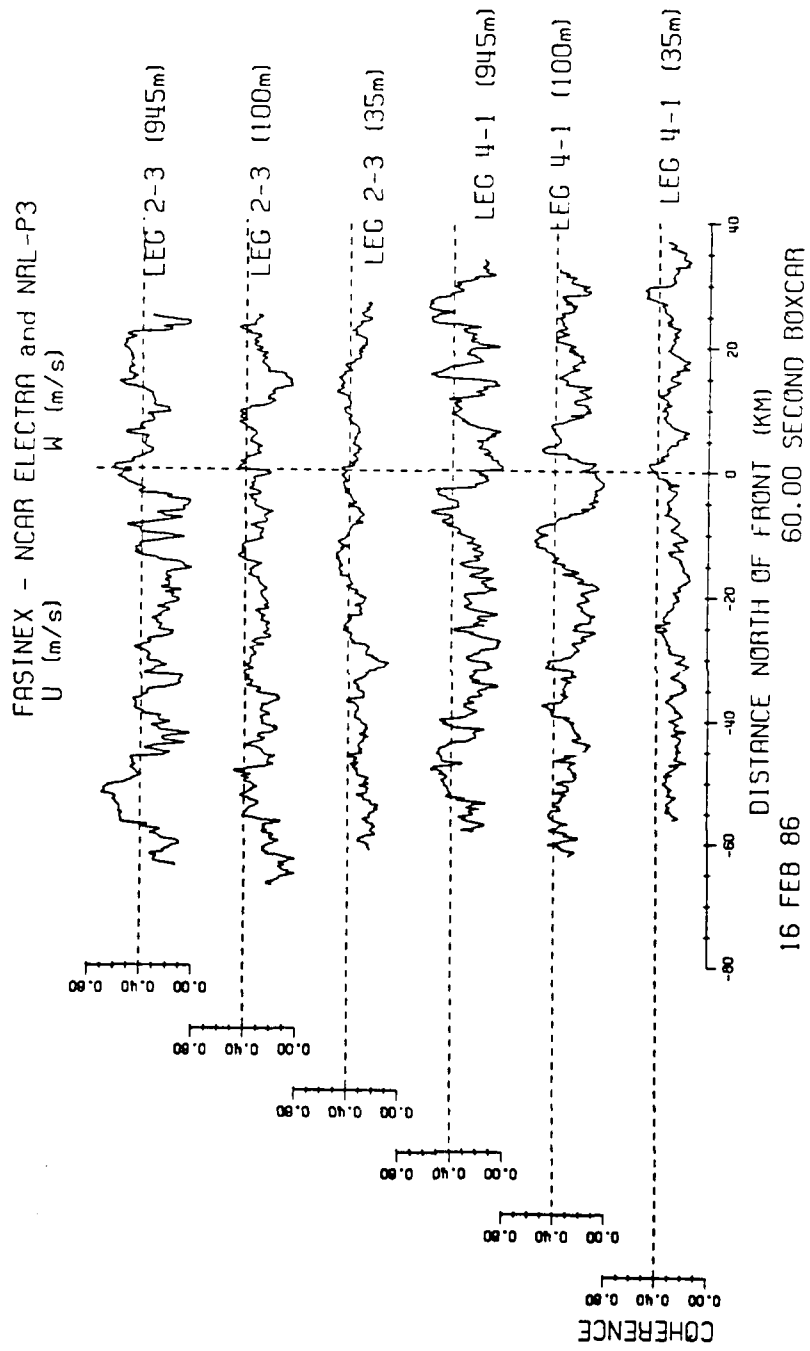


Figure 5.14 Boxcar Coherence (U-W) - 16 FEB 86

ence line at 90) and 5.16(a-1) as before. From figure 5.15 we see that the PHASE relationship is relatively steady at the lowest level for both legs and becomes more erratic as the altitude increases. From figure 5.16(a-d) we see that the PHASE estimates at 35 m show U to lead W by roughly  $150^\circ$  while traveling from south to north. North of the front the spread of the PHASE is quite small. In contrast, south of the front we find that the PHASE becomes a little more complicated. Both legs show a somewhat normal distribution between  $\sim 100$ - $160^\circ$ . Leg 2-3 shows some evidence that there are two preferred regions, one around  $120^\circ$  and the other around  $160^\circ$ .

At 100 m the PHASE relationship is slightly closer to  $\sim 90^\circ$  (U leading W) for both legs south of the front. The difference from the north to south sides is only slight for leg 4-1 while leg 2-3 shows that U and W are more nearly in quadrature to the south of the front, with values only between  $130^\circ$ - $240^\circ$  north of the front. Again we find that the regions in which the stress was negative at the 100 m level show a tendency for the phase angle to approach  $45^\circ$ . This can be seen on leg 4-1 (100 m) at  $\sim 45$ - $55$  km south of the front and on leg 2-3 at  $\sim 38$ - $45$  km south of the front.

Again at the upper level we find that the PHASE tends to have fewer preferred values, though there are some features worth pointing out. For leg 4-1 (945 m) there are no occurrences north of the front between  $60^\circ$  and  $120^\circ$ . There are however quite a few occurrences in the  $200$ - $260^\circ$  range. South of the front the range

FASINEX - NCAR ELECTRA and NRL-P3

U (m/s)

W (m/s)

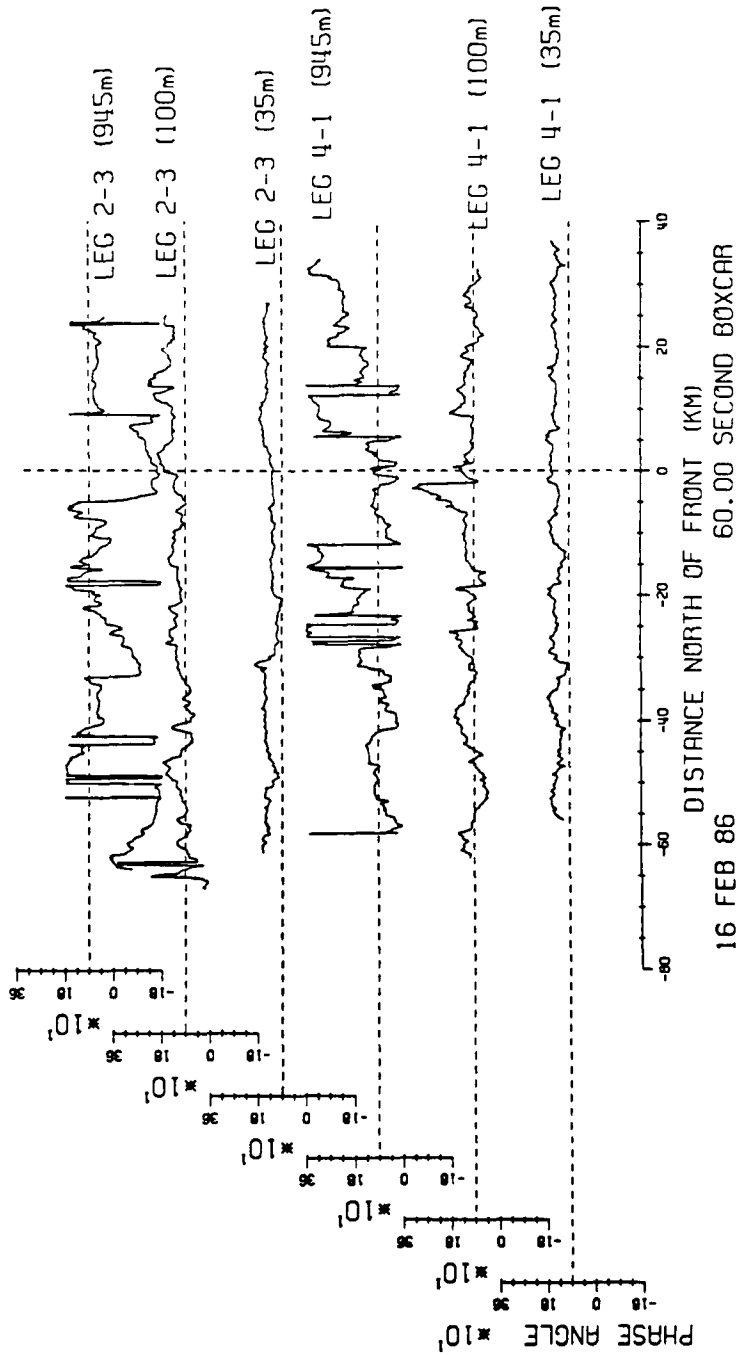
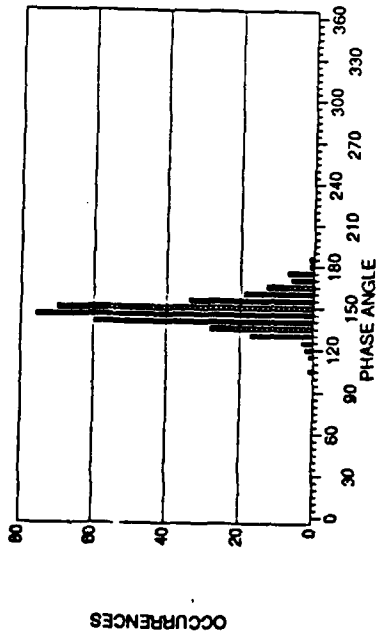


Figure 5.15 Boxcar Phase Angle (U-W) - 16 FEB 86

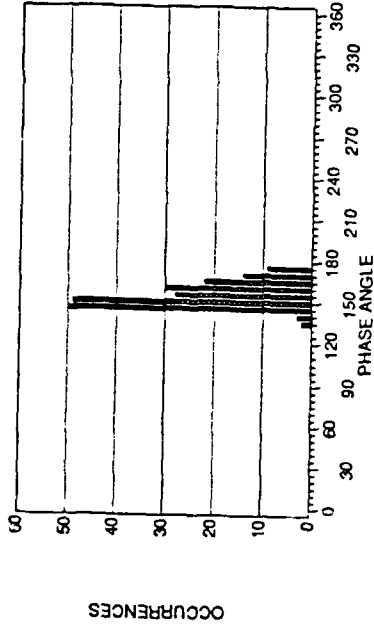
<UW> 16 FEB 86 NCAR ELECTRA

LEG 4-1 (35 m) North Side



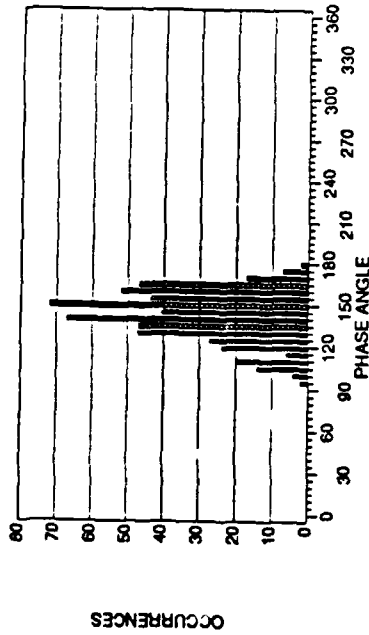
<UW> 16 FEB 86 NCAR ELECTRA

LEG 2-3 (35 m) North Side



<UW> 16 FEB 86 NCAR ELECTRA

LEG 4-1 (35 m) South Side



<UW> 16 FEB 86 NCAR ELECTRA

LEG 2-3 (35 m) South Side

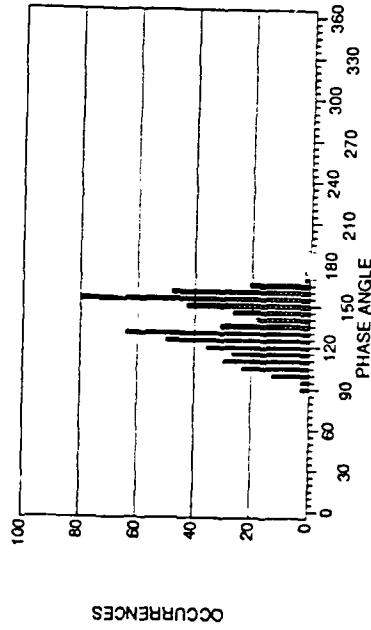


Figure 5.16 Phase Angle PDF for (U-W) - 16 FEB 86  
(a) Leg 4-1 (35m) North Side; (b) Leg 4-1 (35m) South Side; (c) Leg 2-3 (35m) North Side; (d) Leg 2-3 (35m) South Side

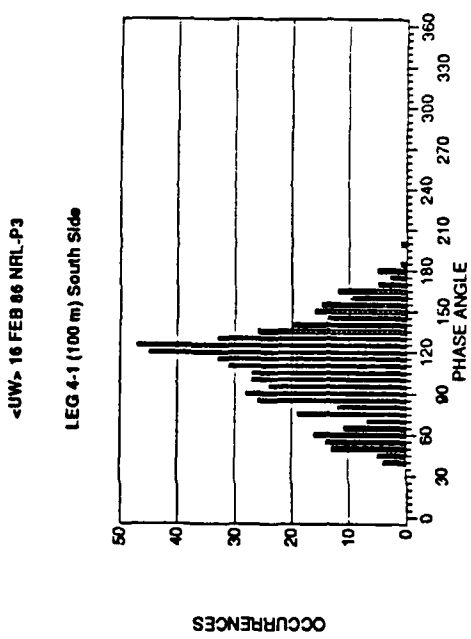
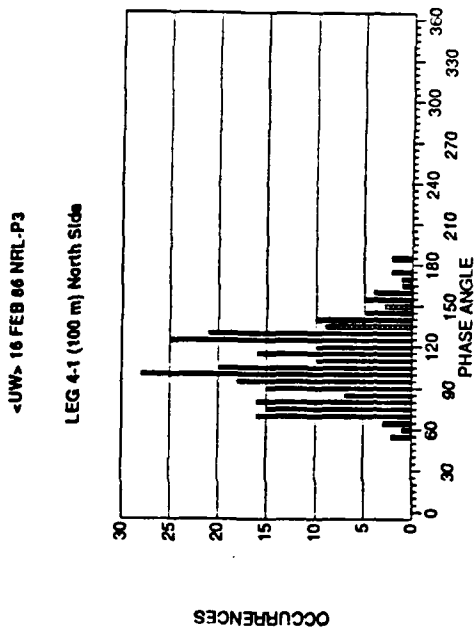
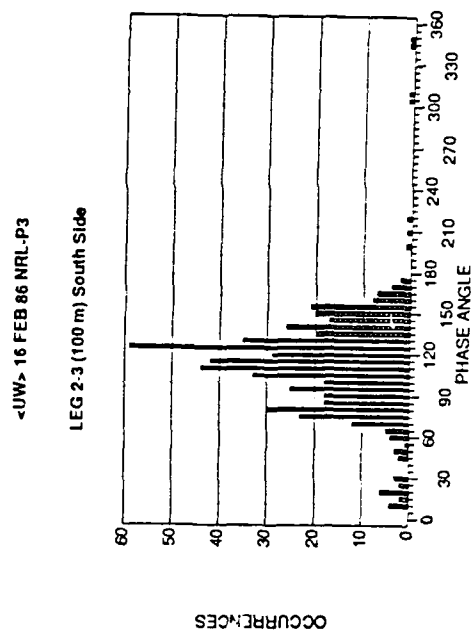
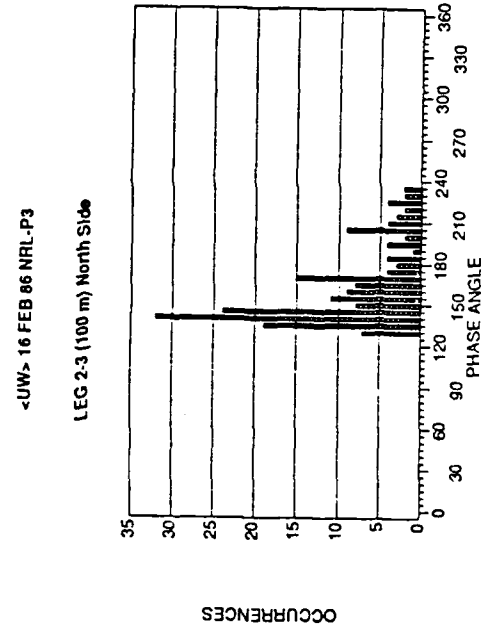
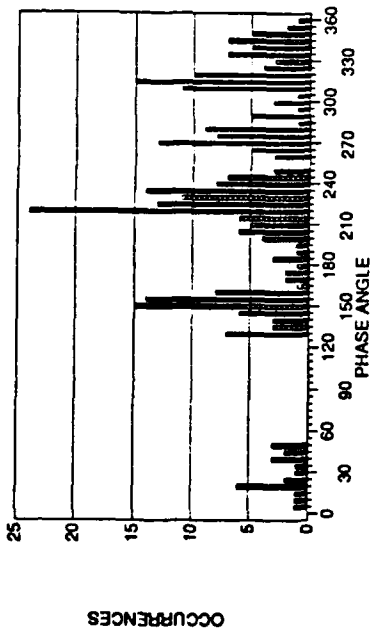


Figure 5.16 Phase Angle PDF for (U-W) - 16 FEB 86 (cont.)  
(e) Leg 4-1 (100m) North Side; (f) Leg 4-1 (100m) South Side; (g) Leg 2-3 (100m) North Side; (h) Leg 2-3 (100m) South Side

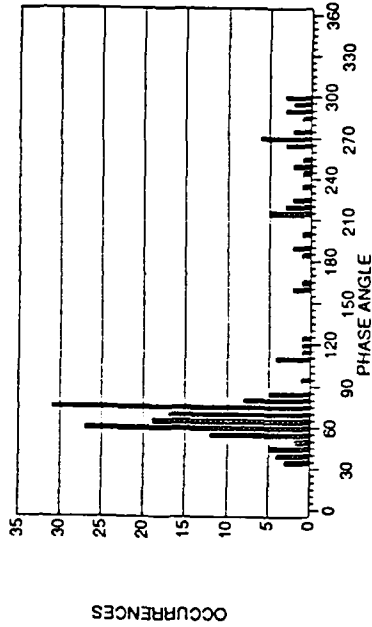
<UW> 16 FEB 86 NRL-P3

LEG 4-1 (945 m) North Side



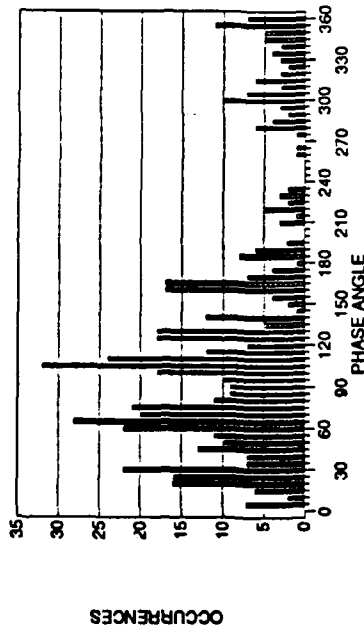
<UW> 16 FEB 86 NRL-P3

LEG 2-3 (945 m) North Side



<UW> 16 FEB 86 NRL-P3

LEG 4-1 (945 m) South Side



<UW> 16 FEB 86 NRL-P3

LEG 2-3 (945 m) South Side

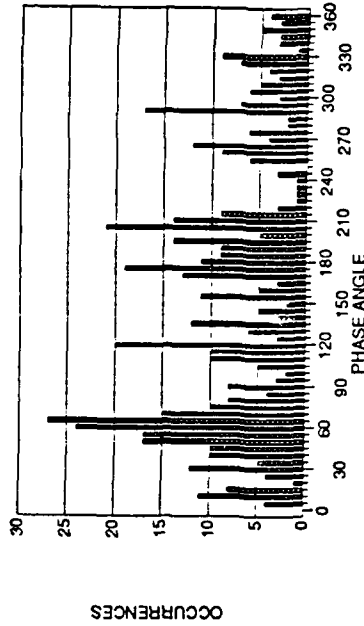


Figure 5.16 Phase Angle PDF for (U-W) - 16 FEB 86 (cont.)

(i) Leg 4-1 (945m) North Side; (j) Leg 4-1 (945m) South Side; (k) Leg 2-3 (945m) North Side; (l) Leg 2-3 (945m) South Side

of 60-120° is well populated while 200-280° is relatively sparse. What makes this interesting is the nearly 180° relationship between the two sparse regions. Leg 2-3, unfortunately, does not show the same type of distribution so it is difficult to say if this is a physical feature or simply coincidence. Leg 2-3 at 945 m shows U tending to lead W by 30-90° north of the front and a more uniform distribution to the south with some preference towards the same region.

### 5.3.6 The Horizontal Velocity Variances

The next topic of interest is the horizontal TKE, which can be inferred from the VAR of U and VAR of V (figures 5.17-18, dashed reference line at 0.3). Again both figures are plotted on the same scale for easy comparison between the two variables. The first point to be made about these two figures is that again, as for the 14th, the amplitudes of both variables are comparable. This is especially true for the two levels above the 35 m flight level. At 35 m the VAR of V is slightly more energetic than the VAR of U. Leg 2-3 shows a general increase in TKE beginning slightly north of the front and continuing for about 20 km to the south of the front. A comparison of the horizontal velocity variances with the vertical velocity variance (figure 5.11) shows that the turbulence is not a three dimensionally isotropic as was found on the 14th. Aside from these general observations it is difficult to make any other clear connections to the front.

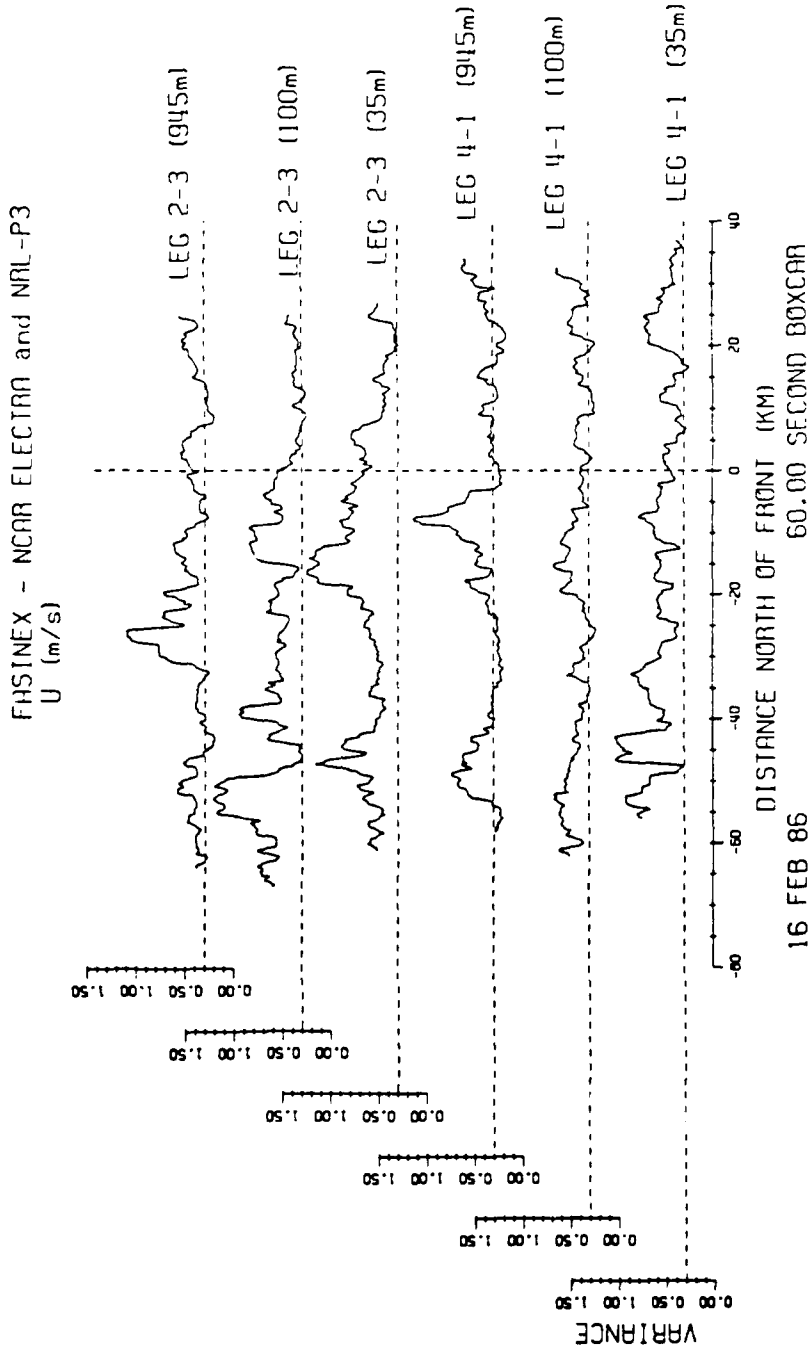


Figure 5.17 Boxcar Variance U Wind Component ( $m^2s^{-2}$ ) - 16 FEB 86



### 5.3.7 Vector Winds

We conclude our analysis with a figure showing the vector winds for the 16th (fig 5.19, dashed reference line represents the front). Figure 5.19 is laid out such that there are pairs of legs at the same level side-by-side. Beginning at the far right is leg 4-1 for 35 m, the eastern most leg, just to the left is leg 2-3 also at 35 m. This pattern is repeated for the 100 m and 945 m levels.

At 35 m we see the first indication that legs 4-1 and 2-3 are being influenced differently, remembering that there is a pool of warm water to the north-east of leg 4-1 which is not visible for leg 2-3. At the most northern end of leg 4-1 the direction of the wind is close to the same as that of leg 2-3. As the effect of the warm water on leg 4-1 is felt, the wind begins to turn clockwise, towards the east. At the front we find the wind for leg 2-3 is approximately 10 degrees more northerly than for leg 4-1. The adjustment made at the front for leg 4-1 is less drastic than for leg 2-3 (~2 deg vs. ~5 deg). Also the wind continues to turn towards the east for the rest of leg 4-1 while leg 2-3 returns to a more NNE flow. Other work (Stage et al., 1990) has shown that there is a region in which the flow field changes from convergence to divergence about half way along the part of the leg which is to the south of the front. This interpretation has been reinforced by the existence of the southern edge of a cloudy region associated with the flow. Along leg 4-1 this region is one of conver-

↑ WIND VECTORS  
VMEAN= 7.70 M/S 45.81 DEG, VMAX= 9.34 M/S, MAX DEV= 3.341 M/S  
FASINEX - NCAR ELECTRA N308D  
16 FEB 86 60.00 SECOND BOXCAR

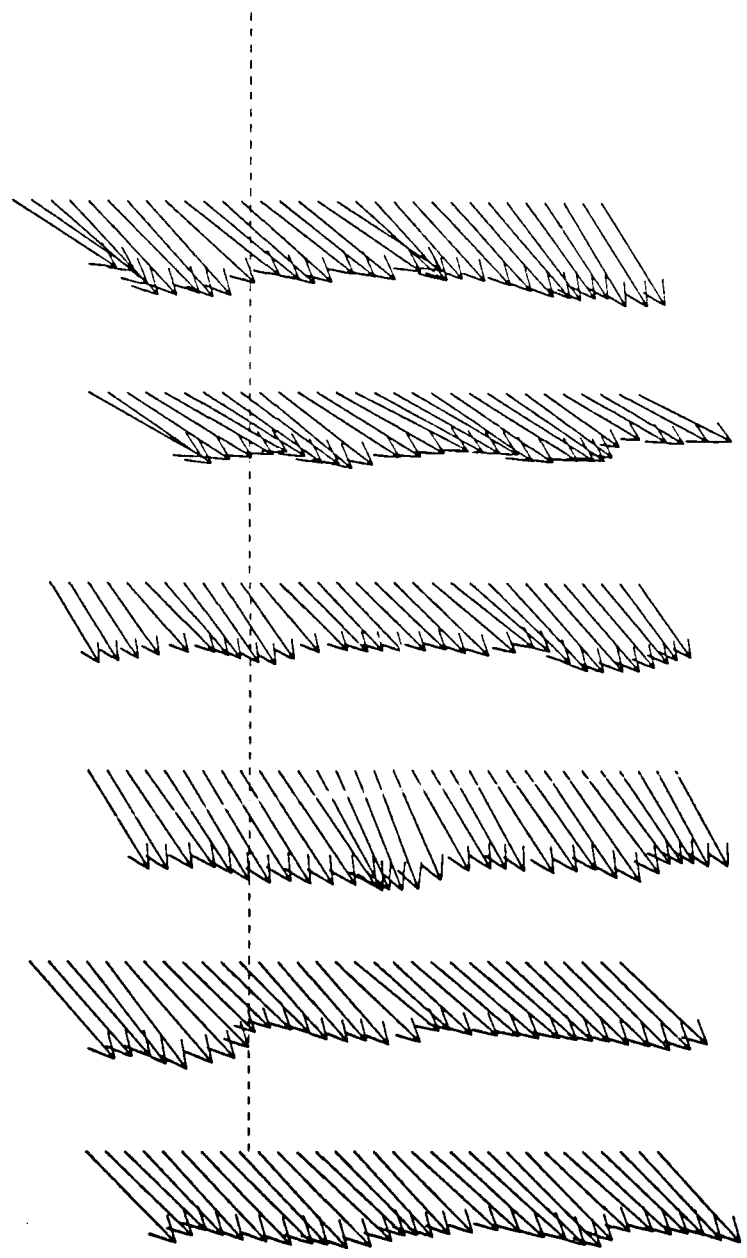


Figure 5.19 Vector Winds - 16 FEB 86  
(Left to right: Leg 2-3, Leg 4-1 @ 945 m; Leg 2-3, Leg 4-1 @ 100 m; Leg 2-3, Leg 4-1 @ 35 m)

gence and is evidenced by the cloud coverage continuing well to the south of the leg.

The next level, 100 m, shows less of an influence by the front than is seen at the lowest level. The change across the front is slight while there appears to be some transition occurring south of the front at about 5-10 km. There is a slight veering of the wind from the 35 m level to the 100 m level.

At 945 m it is unlikely that any of the features that we see are well connected to the front as is suggested by leg 2-3 which shows little change for the duration for the leg.

The reader is reminded that only the two 35 m legs have had the wind field corrected for the Schuler oscillation and any conclusions made from the NRL-P3 wind field (100 m and 945 m) are tenuous at best.

#### **5.4 Summary for February 14 and 16**

We will now try to summarize what we have seen in the two north wind cases which have been discussed. There were many differences in the characteristics of the turbulence between the two days, despite the fact that both days were under the influence of ~1024-1026 mb high pressure systems centered in the same general location. Both days showed the BL to be a few hundred meters deeper over the south side of the front when compared to the north side.

Both days showed well defined SST fronts, though the "front" was much more complicated on the 14th with a large warm pool to the north of the warm water defined as the front. A similar warm pool feature was seen for the easternmost leg on the 16th. The air flow for both days was out of the northeast though there was some synoptic change in the wind field noticed on the 14th. It is assumed that the air had been flowing over relatively homogeneous conditions in advance of the warm water, either associated with the warm pool or the front itself.

As the air moved across the warm water the potential temperature went up quite rapidly, more so for the 14th than 16th. This temperature change was evident well into the upper BL and often had an associated lag towards the south (downstream) as the altitude increased. Associated with this increase in temperature was a general increase in the vertical heat flux. In general the heat flux was strong at the lower levels and decreased into the middle of the BL where it changed sign. On the 14th there were two regions of organized convection which extended vertically, with little or no lag, throughout the entire BL. One of these convective plumes left a signature into the inversion layer at 1800 m while the plume located slightly to the north of the front may or may not have penetrated the inversion as the data are inconclusive and quite sparse over the cold water. On the 16th the convection appeared to be somewhat less organized though there was evidence of a secondary circulation established within the BL beginning at the front and extending for about

30 km to the south. The phase relationship between  $W$  and  $\theta$  was found to be quite narrow with the two variables closely in phase at the lower levels. The phase relationship was observed to become more organized over the warmer water. In general the phase angle had a broader distribution as altitude was increased.

The vertical profiles for the variances of  $\theta$  and  $W$  showed good agreement with previous BL experiments. The maximum values for these statistics were found in the middle of the BL to about 30-60% of the depth of the inversion layer. Both the variance of  $\theta$  and  $W$  showed pronounced increases over the warm water. This was particularly true at the lowest levels, but the variance of  $\theta$  was seen to increase throughout the BL to the south of the front.

The vertical momentum flux was shown to have a somewhat more complicated vertical structure. On the 14th there were three distinct regimes; (1) the surface layer which was characterized of high stress, (2) the middle BL which showed an increased stress over the front, though a slight lag between the levels was noted, and (3) above the BL where the flux was essentially zero. There were areas of negative stress found on both days and there was a tendency towards a phase relationship of  $\sim +45^\circ$  or  $\sim -25^\circ$  in these regions. On the 14th these regions of negative stress were shown to have both some vertical structure and temporal persistence. There was a slight horizontal consistency shown for these negative stress regions on the 16th, though the legs themselves were separated by a relatively large distance and

closer legs were not available at the 100 m flight level where the negative stress regions were found.

The variances of U and V were compared for each of the days. It was noted that for both days the amplitude of the two statistics were quite similar though the VAR of V tended to be larger than the VAR of U at the lowest levels. The two variances were most comparable in the middle of the BL. A further inspection of all three velocity variances showed that the turbulence was more nearly three dimensionally isotropic on the 14th than it was on the 16th. This turbulent structure suggests that the convection on the 14th was stronger than the convection on the 16th.

In an effort to further understand the degree of convectivity on the two days, an estimate of the scaling parameter  $Z_i/L$  was made, where  $Z_i$  refers to the height of the inversion and L refers to the Monin-Obukhov length. Because the values for the surface heat flux were not available for calculating the Obukhov length, the 100 m values were used. Values for  $Z_i/L$  ranged from -36 to -116 over the cold and warm water respectively on the 14th. The values found for the 16th were -22 to -69 for the cold and warm sides of the front, respectively. While both days presented values which indicate the boundary layer was somewhat unstable, the differences between the two days is not great enough to state definitively that one day was much more convective than the other. These numbers do agree with the previously stated

premise that the convection was more energetic on the 14th than on the 16th.

Finally an estimate of the vector winds was evaluated to determine the effect that the warm water had on the flow field. The lowest levels showed some indication of convergent and divergent regions though the bulk of the wind measurements could not be properly corrected for the Schuler oscillation and must not be given too much confidence.

Contrasting the two days we find that the 14th offered more opportunity to connect one level to the next, primarily the result of more vertical resolution in the data. Also the horizontal spacing of the data on the 14th was much smaller (~10 km) compared to the horizontal spacing for the 16th (60 km). At times it appeared that the two legs at any one level on the 16th were experiencing different turbulent conditions as was evident in the frequently different vertical structures seen on the two different legs from this day.

## Chapter 6

### Summary and Conclusions

FASINEX was the first experiment specifically designed to evaluate the response of the atmosphere in the vicinity of an inhomogeneous SST. The results of FASINEX have been fruitful, both in the acquisition of the data by a diverse group of multi-disciplinary investigators, and in the development of new analysis techniques such as the technique used by Crescenti (1988) and this study along with other significant works (Friehe et al, 1990; Stage et al, 1990; Fellbaum et al, 1988; Rogers, 1989 and Khalsa and Greenhut, 1989).

This study is the first effort to use the FASINEX data obtained from the NRL-P3 to investigate the vertical structure of the atmosphere across the SST front. The data were obtained from two of the aircraft, the NCAR Electra and NRL-P3, which participated in the intensive phase of the experiment. The two data sets are in general quite similar to each other though there are significant differences as were pointed out. Each aircraft possessed the necessary equipment to measure the turbulent properties of the atmospheric velocities. Both aircraft were also equipped to measure the turbulent fluctuations in the ambient temperature. There were some

aspects of the NRL-P3 data set which limited its use in comparison to the Electra's data set, but despite these shortcomings the results from the two aircraft compare quite well against each other.

For this study, two FASINEX flight days in which the synoptic forcing was quite similar were chosen. The two days chosen were the 14th and 16th of February, 1986, in which the overall conditions were influenced by two different high pressure systems to the north and west of the research area. This synoptic structure established a generally northerly wind in which the air traveled over a region of relatively uniform cold water and then passed over warm water south of the SST front. There were differences in the large scale features between the two days. The air-sea temperature difference was found to be slightly greater on the 14th with the SST  $2\text{ C}^\circ$  -  $6\text{ C}^\circ$  warmer than the air. In contrast, the SST on the 16th was only  $1\text{ C}^\circ$  to  $3\text{ C}^\circ$  warmer.

The two days for the study offered two different flight plans which allowed for the investigation of many of the same aspects of the MABL structure. The two flight plans, being somewhat different from each other, also enabled us to investigate some different aspects of the boundary layer for these days. The first of the two days, February 14th, was distinguished by the participation of just one aircraft, the NRL-P3, following a flight plan which allowed for the investigation of the vertical structure of the boundary layer across the front at four different levels, and one level

above the BL, all of which were within the same horizontal domain. The 16th was marked by the use of both aircraft in a flight pattern that allowed for both the horizontal and vertical measurement of the MABL. Each of the two flight plans presented some strengths and weaknesses. The vertical stack from the 14th allowed us to see the different levels of the atmosphere over one particular region, but the close horizontal spacing and significant separation in time between the various levels was not able to properly address questions about the shape and size of the features found on the various legs or about the possible connections between the processes occurring on the various flight levels. The FASINEX flight box from the 16th allowed for a horizontal inspection of the frontal zone, but the vertical distance between the two aircraft on the initial flight box was too great to be sure of the connections between the two levels, while the temporal separation between the two, closer spaced, lower levels presented a similar problem. Given the choice of these two flight plans, the plan used on the 14th appears to offer the best perspective of the vertical structure of the boundary layer.

The structure of the SST front was found to be generally quite uniform in a nearly east-west manner. There was evidence, however, that the structure can be significantly more complicated as the presence of a warm pool of water to the north of the front was found on the 14th and on the easternmost leg on the 16th.

The results from the ascent/descent profiles north and south of the front

showed that the boundary layer was deeper over the warm water by about 200 m for both days. This feature has been verified by other investigators from FASINEX (Stage et al., 1990; Friche et al. 1990).

A relatively new technique was used to estimate the mean and turbulent characteristics of the meteorological variables. The linearly detrended moving boxcar average technique, developed by Crescenti (1988) and used by Stage and Crescenti (1989), Stage and Herbster (1989) and Stage et al. (1990), has shown that a 6km average is quite good for both the determination of a specific spatial average, equivalent to the boxcar length, and for the removal of the highest frequency information which otherwise might hide some of broader details of the statistics. The moving boxcar method gives results equivalent to breaking the data into segments equal to the boxcar length. This was the primary result of the work prior to this project which was presented by Crescenti (1988). In addition to the basic boxcar technique developed by Crescenti, the Hilbert transform was used to obtain estimates of the quadrature, quadrature correlation, coherence and phase angle between pairs of the various meteorological variables. This technique is modeled after the coherence and phase calculations which are traditionally used in the spectral domain. The use of the Hilbert transform for calculations in this manner is new and gives good results.

The results of the boxcar technique showed that the potential temperature of

the atmosphere displayed a pronounced increase over the warm water at all levels in the MABL. This increase in temperature was found to occur over a slightly broader region as one increased the altitude of the flight track. The temperature increase also tended to shift towards the south, (downstream direction) as the altitude increased. It was observed that theta adjusted to the warm SST at a slower rate on the 16th, when the air-sea temperature difference was slightly less. However, the effect of the warm water was seen at all levels.

An estimate of the convectiveness on the two days was made using the scaling parameter  $Z_i/L$ , where  $Z_i$  refers to the height of the inversion and  $L$  refers to the Monin-Obukhov length. Values for  $Z_i/L$  ranged from -36 to -116 over the cold and warm water respectively on the 14th. The values found for the 16th were -22 to -69 for the cold and warm sides of the front, respectively. The difference between the values on the two days is not enough to make a clear distinction between the two days it does appear that the boundary layer is somewhat more convective on the 14th than on the 16th. This is evident in the way that the convection penetrates to a deeper level on the 14th, while showing less of a downstream lag in the jump in the potential temperature at the same time than was found on the 16th.

It was found that the heat flux in the surface layer (lowest 100 m or so) increased sharply over the warm water. The vertical velocity and potential temperature fluctuations were found to be well correlated and very closely in phase with

each other, especially over the warm water. As the flight level was increased the relationship between these two variables became somewhat less organized and the heat flux changed sign in the upper half of the boundary layer. There were distinct differences in the heat flux for the two days. This was most pronounced for a pair of organized convective cells, which penetrated the entire boundary layer, associated with warm water in the vicinity of the front on the 14th. This type of organized convection was not found for the 16th. Both days had the largest values for the heat flux over the warm water at the lowest levels. In the middle of the boundary layer, as compared to the lower levels, there was a broader distribution in the phase angle, with a shift towards a  $0^\circ$  relationship in regions of increased heat flux and over the warm water in general. Elevated regions of heat flux, in most cases, were due to similar increases in both variances of  $W$  and  $\theta$ . The flight plan for the 14th, with its nearly vertical stack, did not offer a clear picture of the convective regions. For example, it is not possible to determine if the convection was limited to a plume-like structure, or if the convection was present in a sheet-like manner paralleling the front.

The vertical momentum transfer, or stress, showed a nearly quadrature relationship between the horizontal and vertical velocity fluctuations as is expected. The structure in the phase relationship between these two variables was found to be significantly more complicated than that which was found for the heat flux. In

general, regions of negative stress found in the lower levels of the boundary layer were found in conjunction with regions which had about a  $45^\circ$  phase relationship between the variables. On both days, regions of increased positive stress were found in the vicinity of ~30-40 km south of the front. These features were most prominent in the lower levels of the boundary layer (for both days) and were accompanied by regions of negative stress in the upper boundary layer (most notably on the 16th). The limited coverage of the data, both temporally and spatially, make it impossible to arrive at a precise interpretation of the dynamical processes involved in these areas, though evidence of a secondary circulation is suggested (Stage et al., 1990; Stage and Herbster, 1989). From these limited observations we are unable to determine if these are merely stochastic occurrences or actual structures in the boundary layer.

The variances of the meteorological variables were, in general, found to increase across the front while moving from the cold to warm side. This was particularly evident in the vertical velocity and temperature fields. Both of these variables showed a vertical structure which was in generally good agreement with previous boundary layer experiments. The maximum values for both of these statistics were found in the middle of the boundary layer in the region of 30-60% of the depth of the inversion layer. The boxcar variances of the along-wind and cross-wind velocity components were found to be of comparable magnitudes, indicating some degree of

horizontal isotropy. Comparison with the vertical velocity boxcar variances suggest that on the 14th there was some degree of three dimensional isotropy. Again this is in agreement with the premise that the 14th was a more convective environment as the more active turbulence would be more nearly isotropic in all dimensions.

The work presented in this study only begins to explore the complicated vertical structure of the atmosphere in the presence of an inhomogeneous SST. There is sound evidence that the entire boundary layer is modified by the increased SST for the specific case where the wind is blowing from north to south. The technique used in this study appears to show a very realistic picture of the changes in the MABL in the vicinity of the front and has been verified against model output for the lowest level of 35 m which was investigated in this study (Stage et al., 1990).

As these data sets were analyzed it became obvious that a multi-disciplinary investigation of the boundary layer has specific goals which each investigator would like to see met, thus resulting in a compromise in the data acquisition techniques. This type of forced compromise resulted in the aircraft flight tracks being designed to inspect a variety of processes at one time and therefore often left any one investigator's goals only partially met. This was the case for the 16th of February. Other measurements from those discussed in this study were obtained at the 945 m flight level for the NRL-P3. This was the reason that the aircraft first flew at this high level in the boundary layer. The 100 m flight level was flown after the Electra

exited from the experiment area. We can only speculate how the data set might have differed if there had been better vertical resolution of the boundary layer, either through a different choice of flight levels or, if funds and equipment had permitted, an increased number of levels flown simultaneously by more aircraft.

One suggestion for future studies would be the inclusion of multiple aircraft in a flight pattern similar to that which was used on the 14th. The use of multiple aircraft would allow for either simultaneous horizontal or vertical sampling of the boundary layer. The ideal situation would involve as many as four aircraft to sample both horizontally and vertically at the same time. Also, the regions of negative stress are features which are interesting and suggest the need for further investigations in boundary layer processes so that we might further understand what is happening.

There is a large volume of data which has yet to be analyzed from the NRL-P3 flights alone. Many investigators have been reluctant to use the NRL-P3 data because of the deficiencies mentioned in this study. However, the results from this work show that there may be a significant amount of information lost if this trend continues. Due to the logistics of funding and scheduling of the various aircraft which participated in FASINEX there are more flight days for the NRL-P3 than for the better equipped Electra. Typically the flight tracks for the NRL-P3 were more varied than were the tracks flown by the Electra and consequently there is a potential

wealth of information about the vertical structure of the MABL under different synoptic conditions contained in the other NRL-P3 flight days.

Overall the data from FASINEX have proven to be exceptional for both meteorologists and oceanographers. Much of the data still need to be analyzed in detail with some of the techniques which have been developed thus far. The results published by FASINEX investigators in the scientific literature have been quite extensive though the potential has only partially been tapped with the existing data.

## Appendix A

### Table A.1

#### Summary of NRL-P3 Flights

<u>Flt.</u> No.	<u>Date</u>	<u>Start (GMT)</u> hh mm ss	<u>Stop (GMT)</u> hh mm ss	<u>Duration</u> hh mm ss
1	10 FEB 86	15 56 10	22 14 54	06 18 44
2	14 FEB 86	13 39 26	20 21 02	06 41 36
3	16 FEB 86	13 41 51	21 29 27	07 47 36
4	17 FEB 86	13 44 02	19 53 58	06 09 56
5	18 FEB 86	13 46 26	20 36 58	06 50 32
6	25 FEB 86	13 58 12	16 56 40	02 58 28
7	26 FEB 86	16 56 26	22 47 30	05 51 04
8	01 MAR 86	13 03 06	21 29 58	08 26 52
9	03 MAR 86	13 27 39	21 13 27	07 45 48
10	05 MAR 86	12 31 37	21 04 13	08 32 36
11	07 MAR 86	13 27 46	21 10 29	07 42 43
12	09 MAR 86	12 37 24	20 43 56	08 06 32

**Table A.2**  
**NRL-P3 Flight Legs**  
**14 FEB 86**

<u>Track</u>	<u>Start</u>	<u>Stop</u>	<u>Start</u>		<u>Stop</u>		<u>Alt.</u>
	<u>Time (GMT)</u>		<u>Lat</u>	<u>Long</u>	<u>Lat</u>	<u>Long</u>	
	hh mm ss	hh mm ss	deg	deg	deg	deg	m
1	16 07 35	16 26 40	27.26	-69.99	28.49	-69.98	150
2	16 34 00	16 52 45	28.42	-70.01	27.09	-70.03	460
3	17 00 00	17 20 10	27.11	-70.03	28.50	-70.02	775
4	17 40 45	17 55 50	28.22	-70.01	27.07	-70.03	1800
5	18 12 00	18 24 20	27.65	-70.04	28.47	-70.04	100
6	18 26 00	18 38 00	28.48	-69.95	27.69	-69.65	500

Tracks 1-5 are roughly co-linear in a North-South direction, track 6 is oriented approximately NW-SE.

**Table A.3**  
**NRL-P3 Flight Legs**  
**16 FEB 86**

<u>Leg</u>	<u>Start</u>		<u>Stop</u>		<u>Start</u>		<u>Stop</u>	
	<u>Time (GMT)</u>		<u>Lat</u>	<u>Long</u>	<u>Lat</u>	<u>Long</u>	<u>Lat</u>	<u>Long</u>
	hh mm ss	hh mm ss	deg	deg	deg	deg	deg	deg
<b>FASINEX Flight Box @ 945 m.</b>								
Leg 1-2	16 00 45	16 10 10	28.45	-69.55	28.44	-70.16		
Leg 2-3	16 17 40	16 32 25	28.40	-70.16	27.54	-70.15		
Leg 3-4	16 40 00	16 50 45	27.54	-70.16	27.54	-69.54		
Leg 4-1	16 55 45	17 13 05	27.54	-69.55	28.42	-69.55		
Leg 1-5	17 19 35	17 24 30	28.44	-69.56	28.44	-69.88		
Leg 5-6	17 31 25	17 47 30	28.43	-69.86	27.54	-69.86		
Leg 6-7	17 53 50	18 03 00	27.54	-69.86	27.54	-70.45		
Leg 7-8	18 10 15	18 27 35	27.55	-70.46	28.44	-70.46		
Leg 8-1	18 33 30	18 49 10	28.44	-70.45	28.43	-69.54		
<b>(Partial) FASINEX Flight Box @ 100 m.</b>								
Leg 1-2	18 55 05	19 00 30	28.43	-69.78	28.43	-70.16		
Leg 2-3	19 07 35	19 22 10	28.42	-70.17	27.53	-70.17		
Leg 3-4	19 25 55	19 36 00	27.52	-70.17	27.52	-69.55		
Leg 4-1	19 40 15	19 56 25	27.52	-69.55	28.43	-69.54		

**Table A.4**  
**NRL-P3 Profile Times**  
**14 FEB 86**

<u>Alt. Range</u> meters	<u>Start</u>	<u>Stop</u>	<u>Start</u>		<u>Stop</u>	
	<u>Time (GMT)</u> hh mm ss	hh mm ss	<u>Lat</u> deg	<u>Long</u> deg	<u>Lat</u> deg	<u>Long</u> deg
N 150-475	16 26 40	16 27 40	28.49	-69.98	28.55	-69.98
S 450-775	16 52 50	16 53 45	27.08	-70.03	27.02	-70.03
N 775-1800	17 28 00	17 29 45	28.56	-69.91	28.48	-69.94
S 1800-100	17 56 25	18 01 00	27.04	-70.04	26.94	-69.99
N 100-500	18 24 20	18 25 25	28.47	-70.04	28.51	-69.98
S 500-100	18 38 40	18 40 50	27.64	-69.65	27.49	-69.63
S 100-775	18 51 50	18 53 00	27.47	-69.65	27.47	-69.73
N 775-1800	19 13 25	19 14 45	28.52	-68.69	28.58	-68.62

N= North side of front profile.

S= South side of front profile.

Ranges are in meters.

**Table A.5**  
**NRL-P3 Profile Times**  
**16 FEB 86**

<u>Alt. Range</u> meters	<u>Start</u>	<u>Stop</u>	<u>Start</u>		<u>Stop</u>	
	<u>Time (GMT)</u> hh mm ss	hh mm ss	<u>Lat</u> deg	<u>Long</u> deg	<u>Lat</u> deg	<u>Long</u> deg
N 1800-900	15 07 30	15 09 00	28.75	-69.10	28.69	-69.19
N 900-100	18 49 30	18 52 30	28.43	-69.52	28.48	-69.61
N 100-300	20 04 50	20 05 40	28.46	-69.61	28.48	-69.61
N 350-1800	20 18 50	20 21 20	28.91	-68.93	29.01	-68.78

N= North side of front profile.

S= South side of front profile.

Ranges are in meters.

**Table A.6**  
**NRL-P3 SST Frontal Offsets**  
**14 FEB 86**

<u>Flight Leg</u>	<u>Frontal Offset</u>
Track 1 (150 m)	88.6 km
Track 2 (460 m)	113.5 km
Track 3 (775 m)	108.5 km
Track 4 (1800 m)	115.7 km
Track 5 (100 m)	52.7 km

**Table A.7**  
**NRL-P3 SST Frontal Offsets**  
**16 FEB 86**

<u>Flight Leg</u>	<u>Frontal Offset</u>
Leg 4-1 (945 m)	61.0 km
Leg 5-6 (945 m)	66.3 km
Leg 2-3 (945 m)	67.3 km
Leg 7-8 (945 m)	66.2 km
Leg 4-1 (100 m)	65.2 km
Leg 2-3 (100 m)	70.5 km

**Table A.8**  
**NCAR Electra SST Frontal Offsets**  
**16 FEB 86**

<u>Flight Leg</u>	<u>Frontal Offset</u>
Leg 4-1	58.9 km
Leg 5-6	62.9 km
Leg 2-3	64.6 km
Leg 7-8	66.6 km

**Table A.9**  
**NCAR Electra SST Frontal Offsets**  
**17 FEB 86**

<u>Flight Leg</u>	<u>Frontal Offset</u>
Leg 4-1	45.2 km
Leg 5-6	60.6 km
Leg 2-3	55.7 km
Leg 7-8	55.0 km

**Table A.10**  
**NCAR Electra SST Frontal Offsets**  
**18 FEB 86**

<u>Flight Leg</u>	<u>Frontal Offset</u>
Leg 4-1	60.0 km
Leg 5-6	62.3 km
Leg 2-3	53.0 km
Leg 7-8	23.4 km

**Appendix B**  
**Synoptic Maps**

The maps reproduced on the following pages of this appendix are from Fellbaum et al. and are used by permission.

For continuity each page contains the maps from one day, beginning with the 14th of February, 1986 and ending with the 16th of February, 1986.

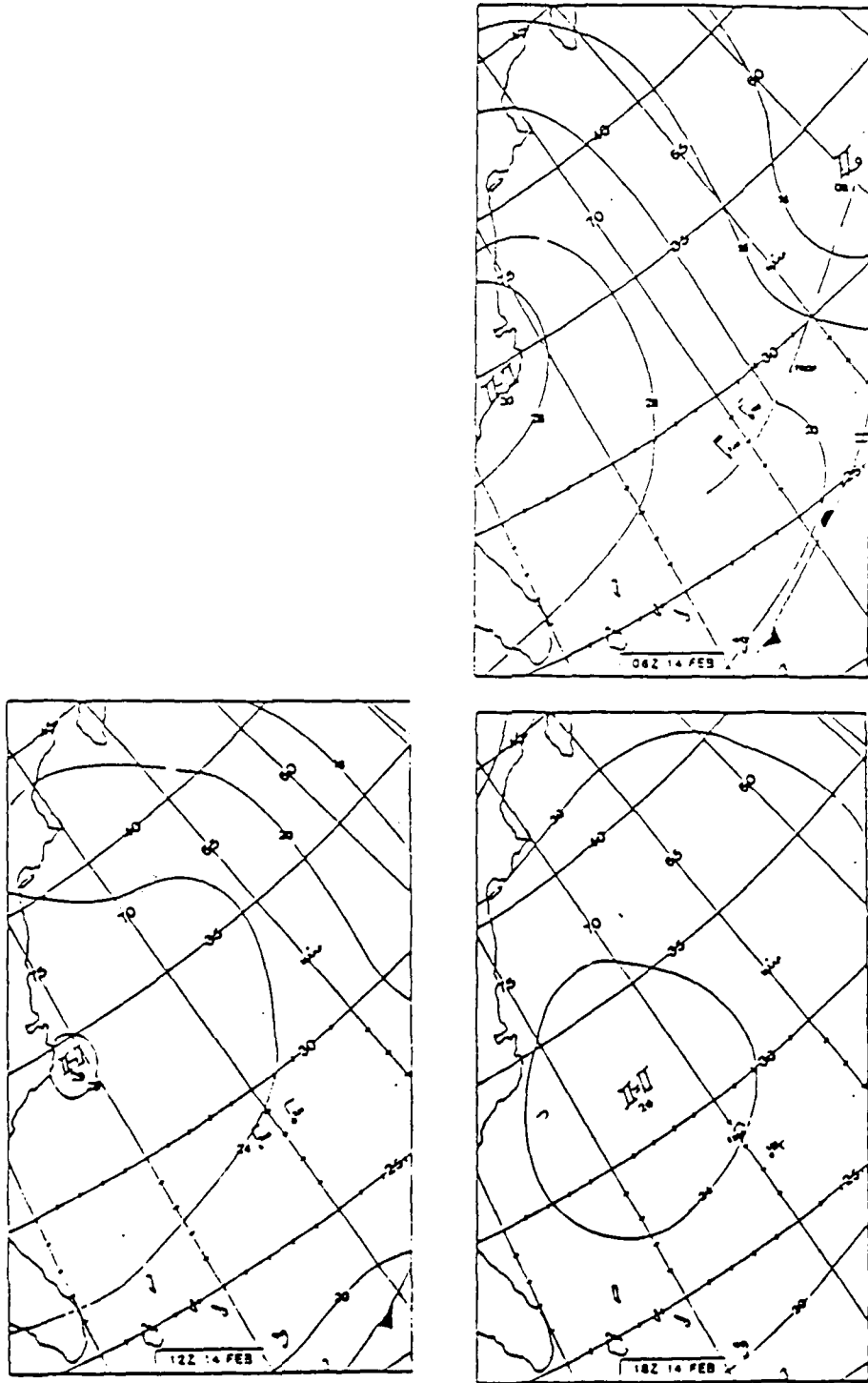


Figure B.1 NMC Surface weather maps for 14 FEB 86; (a) 06Z; (b) 12Z; (c) 18Z

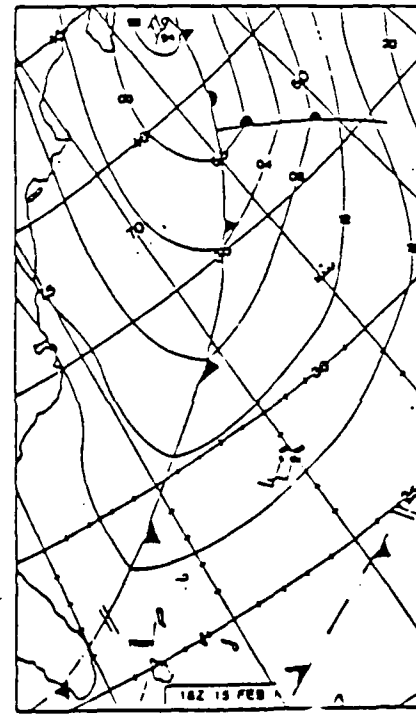
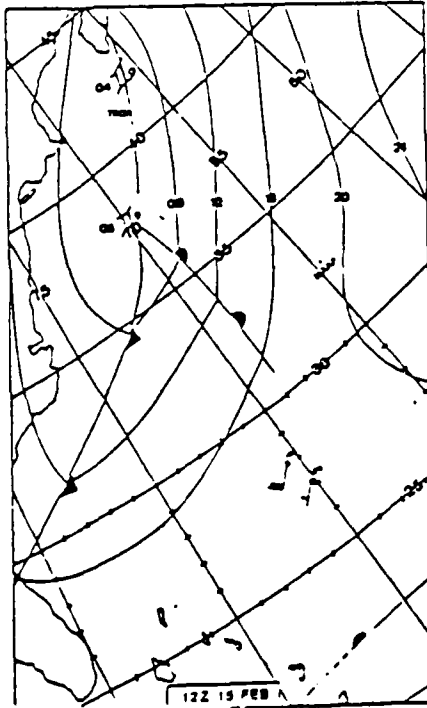
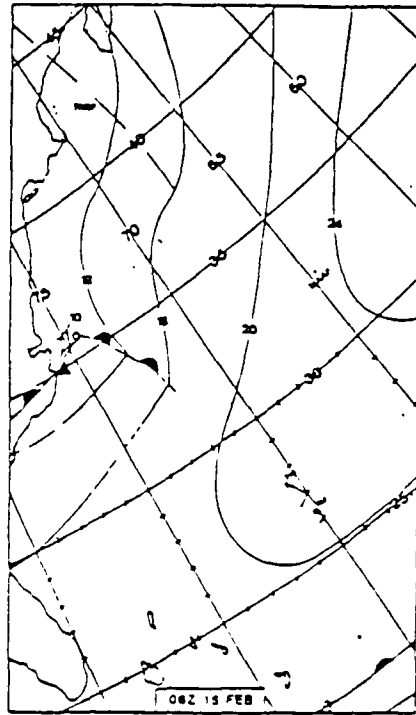
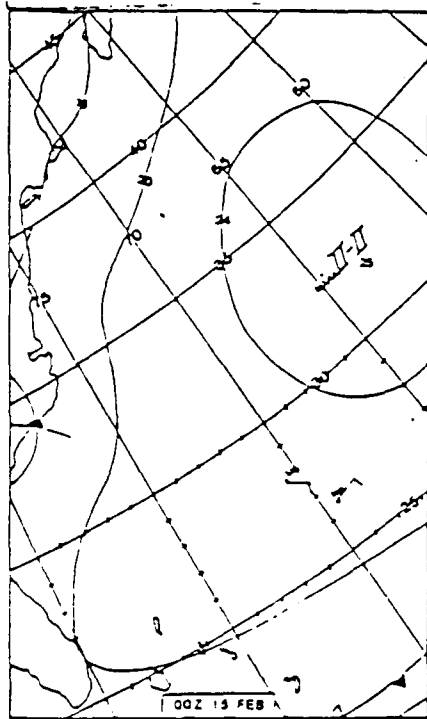


Figure B.2 NMC Surface weather maps for 15 FEB 86; (a) 00Z; (b) 06Z; (c) 12Z; (d) 18Z

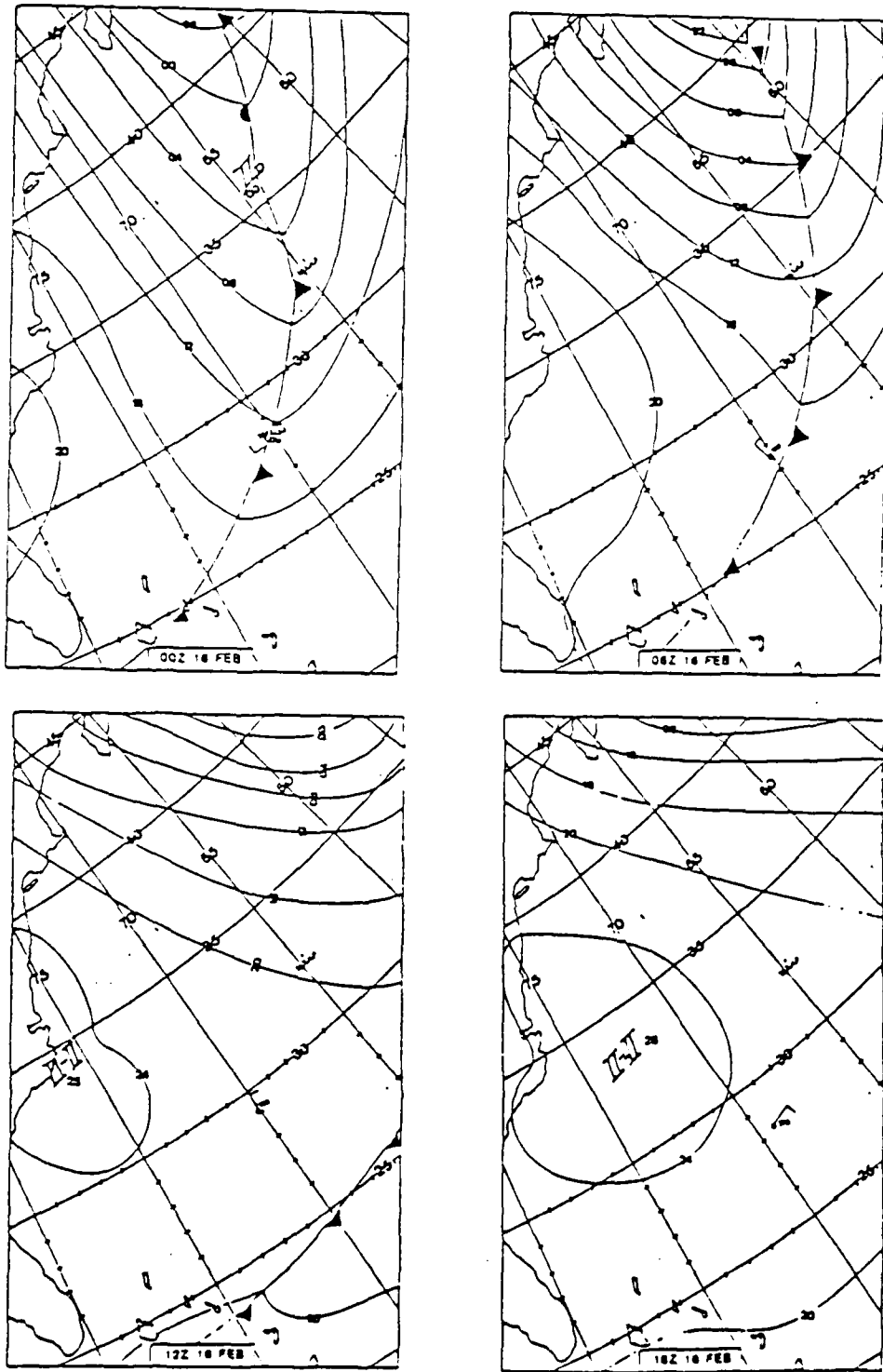


Figure B.3 NMC Surface weather maps for 16 FEB 86; (a) 00Z; (b) 06Z; (c) 12Z; (d) 18Z

## References

- Bendat, J.S., and A.G. Piersol, 1986: Random Data. John Wiley and Sons, New York, 566 p.
- Bowman, M.J., 1978a: Introduction and Historical Perspective. Oceanic Fronts in Coastal Processes. Springer-Verlag, New York, 2-5.
- Bowman, M.J., 1978a: Proceedings of the Workshop. Oceanic Fronts in Coastal Processes. Springer-Verlag, New York, 6-13.
- Broxmeyer, C., 1964: Inertial Navigation Systems. McGraw Hill, New York, 254 p.
- Burroughs, W.J., 1978: On running means and meteorological cycles. Weather, 33: 101-109.
- Businger, J.A., and H. Charnock, 1983: Boundary layer structure in relation to larger-scale flow: Some remarks on the JASIN observations. Philosophical Transactions of the Royal Society of London, Series A, 308: 445-449.
- Crescenti, G.H, 1988: Turbulent Variances and Covariances in the Marine Atmospheric Boundary Layer Over the FASINEX Front. M.S. Thesis, Department

of Meteorology, Florida State University, 167pp.

Cromwell, T., and J.C. Reid, 1956: A study of oceanic fronts. Tellus, 8: 94-101

Fellbaum, S.R., and S.H. Borrmann, P.A. Boyle, K.L. Davidson, W.G. Large, T. Neta, and C.A. Vaucher, 1988: Frontal Air-Sea Interaction Experiment (FASINEX) Shipboard Meteorology Data and Weather Atlas, Naval Post-graduate School, Monterey California, available through the Office of Naval Research, Arlington, Virginia, 22217, NPS-63-88-002.

Freiberger, W., and U. Grenander, 1965: On the formulation of statistical meteorology. Review of the International Statistical Institute, 33, 59-86.

Friehe, C.A., W.J. Shaw, D.P. Rogers, K.L. Davidson, W.G. Large, S.A. Stage, G.H. Crescenti and F. Li, 1990: Air-sea fluxes and surface-layer turbulence around a sea surface temperature front. Journal of Geophysical Research , To be published.

Griffith, K., 1986: Data Quality Report, NCAR Electra N308D. NCAR Research Aviation Facility, FASINEX #6-881, 19 p.

Guymer, T.H., J.A. Businger, K.B. Katsaros, W.J. Shaw, P.K. Taylor, W.G. Large, and R.E. Payne, 1983: Boundary layer structure in relation to larger-scale flow: Some remarks on the JASIN observations. Philosophical Transactions of the Royal Society of London, Series A, 308: 253-273.

- Halliwell, G., and P. Cornillon, 1987: Five-Day Maps of AVHRR/2 Sea Surface Temperature Fields and Wind Stress Analysis During FASINEX. Graduate School of Oceanography, University of Rhode Island, Technical Report No. 87-5, 67 p.
- Hennemuth, B., 1978: Statistical description of anisotropic and inhomogeneous turbulence. Boundary Layer Meteorology, 15: 489-506.
- Hsu, S.A., 1984a: Effect of cold air advection on internal boundary layer development over warm ocean currents. Dynamics of Atmospheres and Oceans, 8: 307-319.
- Hsu, S.A., 1984b: Sea breeze like winds across the North Wall of the Gulf Stream: An analytical Model. Journal of Geophysical Research, 89: 2025-2028.
- Hsu, S.A., R. Fett, and P.E. LaViolette, 1985: Variations in atmospheric mixing height across oceanic thermal fronts. Journal of Geophysical Research, 90: 3211-3224.
- Ishida, H., 1986: Mesoscale spatial and temporal variability of meteorological observations from an array of buoys in JASIN - 1978. Boundary Layer Meteorology, 37: 149-165.
- Khalsa, S.J.S. and G. K. Greenhut, 1989: Atmospheric turbulence structure in the vicinity of an oceanic temperature front., Journal of Geophysical Research, 94, 4913-4922.

- Lenschow, D.L., 1986: Aircraft measurements in the boundary layer. Probing the Atmospheric Boundary Layer. American Meteorological Society, Boston, 39- 55.
- Miller, E.R., and K.B. Friesen, 1985: Standard Output Data Products from NCAR Research Aviation Facility. NCAR Research Aviation Facility, Bulletin No. 9, 64 p.
- Lewis, P., 1960: The use of moving averages in the analysis of time series. Weather 15, 121-126.
- Lui, W.T., and K.B. Katsaros, 1984: Spatial variation on sea surface temperature and flux-related parameters measured from aircraft in the JASIN experiment. Journal of Geophysical Research, 89: 10641-10644.
- Nicholls, S., B. Brummer, F. Fiedler, A. Grant, T. Hauf, G. Jenkins, C. Readings, and W. Shaw, 1983: The structure of the turbulent atmospheric boundary layer. Philosophical Transactions of the Royal Society of London, Series A, 308: 291-309.
- Pollard, R.T., 1978: The Joint Air-Sea Interaction Experiment, JASIN 1978. Bulletin of the American Meteorological Society, 59: 1310-1318.
- Pollard, R.T., T.H. Guymer, and P.K. Taylor, 1983: Summary of the JASIN 1978 field experiment. Philosophical Transactions of the Royal Society of Lon-

don, Series A, 308: 221-230.

Panofsky, H.A., and J.A. Dutton, 1984: Atmospheric Turbulence. John Wiley & Sons, New York, 397 p.

Rogers, D.P., 1989: The Marine Boundary Layer in the Vicinity of an Ocean Front. Journal of the Atmospheric Sciences Vol 46, No. 13 2044-2062.

Schanot, A., 1987: An evaluation of the uses and limitations of a Lyman-alpha hygrometer as an operational airborne humidity sensor. Sixth Symposium on Meteorological Observations and Instrumentation, 12-16 January 1987. New Orleans, Louisiana, 257-260.

Shaw, W.J., and G.T. Vaucher, 1987: Correction of the Wind Field Measured by the NCAR Electra During FASINEX for Inertial Navigation System Drifts. Naval Postgraduate School, Monterey, California, NPS-63-87-008, 43 p.

Stage, S.A., and G.H. Crescenti, 1988: Determination of Turbulent Fluxes in a Non-Homogeneous Region. Paper presented at The Third Airborne Geoscience Workshop, February 21-24, 1989, La Jolla, California.

Stage, S.A., G.C. Crescenti, K. Davidson, C. Gautier, G. Greenhut, C.G. Herbster, K. Katsaros, S.J. Khalsa, R. Lind, D. Rogers, W.J. Shaw and M.K. Wai, 1990: Marine Atmospheric Boundary Layer Structure in the Vicinity of a Sea Surface Temperature Front. Journal of Geophysical Research. Currently under revision (authors listed alphabetically for now).

- Stage, S.A., and C.G. Herbster, 1989: Turbulent Statistics in the Vicinity of an SST Front: A North Wind Case, FASINEX February 16, 1986. Poster presented at the FIRE/ASTEX Workshop, Monterey, CA, July 10-14, 1989.
- Stage, S.A., and R.A. Weller, 1985: The Frontal Air-Sea Interaction Experiment (FASINEX); Part 1: Background and scientific objectives. Bulletin of the American Meteorological Society, 66: 1511-1520.
- Stage, S.A., and R.A. Weller, 1986: The Frontal Air-Sea Interaction Experiment (FASINEX); Part II: Experimental plan. Bulletin of the American Meteorological Society, 67: 16-20.
- Stull, R.B., 1988: An Introduction to Boundary Layer Meteorology. Kluwer Academic Publishers, Boston, 666 pp.
- Taylor, P.K., A.L.M. Grant, H. Gunther, and G. Olbruck, 1983: Mass, momentum, sensible heat and latent heat budgets for the lower atmosphere. Philosophical Transactions of the Royal Society of London, Series A, 308: 275-290.
- Tennekes, H., and J.L. Lumley, 1972: A First Course in Turbulence. MIT, Cambridge, 300 p.
- Voorhis, A.D., 1969: The horizontal extent and persistence of thermal fronts in the Sargasso Sea. Deep Sea Research, Supplement 16: 331-337.

Voorhis, A.D., and J.B. Hersey, 1964: Oceanic thermal fronts in the Sargasso Sea.

Journal of Geophysical Research, 69: 3809-3814.